

NEUTROPHIL DIVERSITY IN THE PATHOGENESIS OF
ISCHEMIC ACUTE KIDNEY INJURY

Seth Winfree

Submitted to the faculty of the University Graduate School
in partial fulfillment of the requirements
for the degree
Doctor of Philosophy
in the Department of Cellular and Integrative Physiology,
Indiana University

September 2020

Accepted by the Graduate Faculty of Indiana University, in partial fulfillment of the requirements for the degree of Doctor of Philosophy.

Doctoral Committee

Tarek M. El-Achkar, MD, Chair

Pierre C. Dagher, MD.

July 16, 2020

Richard N. Day, Ph.D.

James C. Williams Jr., Ph.D.

© 2020
Seth Winfree

Seth Winfree

NEUTROPHIL DIVERSITY IN THE PATHOGENESIS OF
ISCHEMIC ACUTE KIDNEY INJURY

Acute kidney injury (AKI) affects millions of patients worldwide yet has few treatment options. There is a critical need to identify novel interventions for AKI, especially approaches targeting cell types that are central to the disease, such as neutrophils. Neutrophils are professional phagocytic cells that respond early to tissue injury. In rodent models of *severe* ischemic-reperfusion-injury AKI, neutrophils transiently infiltrate the injured kidney, appearing within 6 hours, and are gone by 72 hours. These infiltrating neutrophils are considered proinflammatory and harmful to tissue repair and recovery of kidney function. However, neutrophils can exhibit atypical activity such as antigen presentation and have a central role in recovery from myocardial ischemic injury. Furthermore, little is known of neutrophil polarization, atypical activity, or neutrophil diversity in AKI. Lastly, the kidney generated and renal-protective immunomodulatory protein uromodulin (Tamm-Horsfall Protein, THP) regulates granulopoiesis. In the absence of uromodulin, there is a systemic increase in neutrophils and mouse kidneys are sensitive to injury in AKI. To elucidate neutrophil diversity in AKI and their sensitivity to uromodulin, I performed a series of single-cell sequencing experiments to generate transcriptional profiles of neutrophils from the blood and kidneys of wild-type and THP-knockout mice after renal ischemic-reperfusion-injury (IRI). Neutrophil diversity was detected following IRI of the mouse kidney in the blood and kidney. The distribution of subpopulations was sensitive to the kidney milieu. Within the kidney, this diversity and the transcriptional programs of neutrophil subpopulations was sensitive to the severity of ischemic injury. Lastly, *Cxcl3* was uniquely upregulated in specific neutrophils after severe ischemic injury. Using single-cell sequencing of uromodulin knock-out mice, I detected the upregulation of toll-like receptor pathways and complement cascades across

neutrophil subpopulations in a THP sensitive manner. Furthermore, CXCR2 ligand expression was a combination of moderate and severe injury in wild-type mice. This confirmed previously reported cytokine dysregulation in the uromodulin knock-out mouse after IRI and uncovers a novel role for *Cxcl3*. Thus, upon revisiting the well-studied neutrophil, I have uncovered novel neutrophil diversity that correlates with recovery of kidney function in AKI and suggests new roles for an old player.

Tarek M. El-Achkar, MD, Chair

Table of Contents

List of Tables	x
List of Figures	xi
List of Abbreviations	xiv
Introduction and Background	1
Acute kidney injury	1
Neutrophils and AKI	3
Ischemic injury models and neutrophil polarization	5
Neutrophil polarization following myocardial infarction.	6
Neutrophil polarization in areas of injury following stroke.	6
Polarized N2 neutrophils are found in AKI	6
The response of neutrophils is early and swift in ischemic AKI.	7
Neutrophils persist in depletion and inhibitory experiments	7
Chapter 1. The cellular map of 129Sv/Ev mouse kidney	9
Introduction	9
Results	10
Quality of single cell RNAseq and basic processing of datasets	10
The cellular composition of 129Sv/Ev mouse kidneys	11
Epithelial cells of the proximal tubule subsegments	12
Epithelial cells of the distal nephron	12
Endothelium and associated cells	12
Leukocytes	13
Isolation and CD45+ enrichment of immune cells	13
Monocytes and macrophages of the mouse kidney	14
Populations of neutrophils	15
Discussion	16

Methods.....	17
Animals and surgeries	17
Kidney dissociation and isolation of single cells	17
Kidney dissociation and enrichment of CD45+ leukocytes	18
Flow cytometry of immune cells isolated by differential centrifugation.....	19
Staining of tissue sections	20
Confocal large-scale imaging of tissue.....	20
Single cell 3' RNA-seq	20
Analysis of scRNA-seq sequence data	21
Analysis of expression matrices.....	22
Combined dataset of cells from single cell isolation protocols.....	22
Data availability.....	22
Chapter 2. Neutrophil diversity and cellular census of kidneys after ischemic injury	37
Introduction.....	37
Results	39
Quality of RNA libraries during ischemic injury.....	39
Tubular epithelium expression of injury markers increases following ischemia	40
Functional changes in the epithelium induced by injury.....	41
Endothelium.....	41
Sub-segments of the nephron.....	41
Injury induced expansion of immune cells.....	42
Injury expands neutrophil subtypes in a severity of injury dependent manner	43
The kidney affects neutrophil subtype proportions and transcriptional programs....	44
Recruitment of neutrophils to the injured kidney via the CXCR2 axis.....	46
Neutrophils in AKI share markers with neutrophils in cancer.....	47
Discussion	47

Methods.....	51
Animal handling and surgeries.....	51
Isolation of single cells from injured kidneys	51
Isolation of immune cells from blood for scRNASeq.....	52
Generation of figures.	53
Data availability.....	53
Chapter 3. Uromodulin dependent change in neutrophil transcriptomes	79
Introduction.....	79
Results	80
Validation of THP ^{-/-} and effects of gene knockout	80
Neighboring gene regulation in the THP ^{-/-} mouse	80
Functional differences of kidney epithelium in THP ^{-/-} mice	81
Changes in kidney epithelium during injury in THP ^{-/-} mice	81
Monocyte/macrophages distribution in THP ^{-/-} mice is altered.....	82
Neutrophil distribution in THP ^{-/-} mice is like wild-type mice with moderate injury	82
Neutrophils in THP ^{-/-} mice are uniquely primed for tissue damage	83
Injury in THP ^{-/-} mice expands specific neutrophil subtypes	83
Toll-like receptor signaling and complement cascade pathways after injury in THP ^{-/-} mice.....	84
CXCR2 axis is dysregulated in THP ^{-/-} mice versus wild-type mice	84
Discussion	85
Methods.....	87
Animal handling and surgeries.....	87
Isolation of single cells from injured kidneys	87
Isolation of immune cells from blood for scRNASeq.....	87

Data availability.....	88
Chapter 4. Animal use and experimentation	101
Animal protocols	101
Protocol 1. Ischemia reperfusion injury surgery.....	101
Protocol 2: Sham surgery	102
Animal use.....	102
Justification.....	102
Veterinary care	103
Limiting discomfort of animals.....	103
Euthanasia.....	103
Summary and Conclusions.....	105
Future directions.....	106
Appendices	109
Appendix A	109
References.....	112
Curriculum vitae	

List of Tables

Table 2.1. Working Neutrophil Definitions	73
Table 2.2. Pathways upregulated by neutrophil clusters within the blood or kidney with 22-minute IRI.....	74
Table 2.3. Pathways upregulated by neutrophil clusters within the blood or kidney with 30-minute IRI.....	75
Table 2.4. Pathways differentially upregulated by cluster in the kidney between ischemic injuries	76
Table 2.5. Pathways differentially upregulated by cluster when in the blood versus the kidney with 22-minute IRI	77
Table 2.6. Pathways differentially upregulated by cluster when in the blood versus the kidney with 30-minute IRI	78
Table 3.1. Exemplar ReactomePA pathways in THP ^{-/-} mice.....	97
Table 3.2. Pathways upregulated in neutrophils from THP ^{-/-} versus wild-type kidneys after a sham surgery	98
Table 3.3. Pathways upregulated by neutrophil cluster in the blood or kidney with 22-minute IRI in THP ^{-/-} mice	99
Table 3.4. Pathways differentially upregulated by cluster when in the blood versus the kidney with 22-minute IRI in THP ^{-/-} mice.....	100

List of Figures

Figure 1.1. Initial quality control metrics.....	23
Figure 1.2. Detecting the variable genes for use in calculating principal components....	24
Figure 1.3. Elbow plot of principal components.....	25
Figure 1.4. Clustering and dimensionality reduction of kidney scRNASeq data.....	26
Figure 1.5. Identifying cell types in whole kidney using published markers.....	28
Figure 1.6. Identification of granular cells of the juxtaglomerular apparatus.....	29
Figure 1.7. Differential centrifugation for isolation of immune cells from whole kidneys.....	30
Figure 1.8. Clustering and dimensionality reduction of CD45+ enriched scRNASeq data.....	31
Figure 1.9. Identifying cell types in the CD45+ enrichment isolation using published markers	32
Figure 1.10. Subdividing monocytes/macrophages into resident and infiltrating populations.....	33
Figure 1.11. Four neutrophil subtypes identified in wild-type mice after sham surgery.....	35
Figure 1.12. Markers of neutrophil subpopulations identified in wild-type mice after a Sham surgery.....	36
Figure 2.1. Morphological indications of kidney injury.....	54
Figure 2.2. Quality control metrics in injured tissue.....	55
Figure 2.3. UMAP plot of all cells from whole kidney.....	56
Figure 2.4. Injury and apoptosis marker expression in the kidney following ischemic injury.....	57
Figure 2.5. ReactomePA analysis of endothelium.....	58
Figure 2.6. ReactomePA analysis of proximal tubule subsegments.....	59

Figure 2.7. ReactomePA analysis of loop of Henle and distal convoluted tubule.....	60
Figure 2.8. ReactomePA analysis of connecting tubules and collecting duct principal cells.....	61
Figure 2.9. ReactomePA analysis of collecting intercalating cells A.....	62
Figure 2.10. UMAP projection of classified immune cells from sham and injury surgeries.....	63
Figure 2.11. Distribution of immune cells in response to ischemia reperfusion injury....	64
Figure 2.12. UMAP of neutrophils isolated from kidneys after sham and injury.....	65
Figure 2.13. Markers of neutrophil subpopulations.....	66
Figure 2.14. Distribution of neutrophil subpopulations is sensitive to compartment and severity of injury.....	67
Figure 2.15. Expression analysis of CXCR2 ligands.....	68
Figure 2.16. Injury affects <i>Cxcl3</i> and <i>Cxcl2</i> expression by neutrophil clusters.....	70
Figure 2.17. Neutrophils from a breast cancer metastasis model mirror population identified in AKI.....	71
Figure 3.1. THP transcript is not detected in the THP ^{-/-} mouse.....	89
Figure 3.2. Exploring polar effects in the THP ^{-/-} mouse.....	90
Figure 3.3. The distribution of immune cells is sensitive to the presence of THP.....	91
Figure 3.4. The distribution of neutrophils is modulated by THP.....	92
Figure 3.5. Injury in THP ^{-/-} mice affects the distribution of neutrophils.....	93
Figure 3.6. Distribution of neutrophil subpopulations is sensitive to the compartment in THP ^{-/-} mice.....	94
Figure 3.7. CXCR2 signaling in the THP ^{-/-} mouse after ischemic kidney injury.....	95
Figure A.1. Model of cytokine activity on neutrophils with moderate injury.....	109

Figure A.2. Model of cytokine activity on neutrophils with severe injury.....110

Figure A.3. Model of cytokine activity on neutrophils with moderate injury
in THP-/- mice.....111

List of Abbreviations

AKI	acute kidney injury
B	B-cell
CD	collecting duct
CD-PC	principal cell of the collecting duct
CD-ICa	intercalating cell a of the collecting duct
CD-ICb	intercalating cell b of the collecting duct
CNT	connecting tubules
DAPI	4',6-diamidino-2-phenylindole
DCT	distal convoluted tubule
Endo.	endothelium
Eryt.	erythrocyte
FACS	fluorescence activated cell sorting
Gran. cells	granular cells of the JGA
IRI	ischemia reperfusion injury
JGA	juxtaglomerular apparatus
LOH	loop of Henle
M Φ	macrophage
NK	natural killer cell
Neut.	neutrophil
PT-S(1-3)	proximal tubules segment 1-3
T	T-cell
THP	Tamm-Horsfall protein
tSNE	t-distributed stochastic neighborhood embedding
UMAP	uniform manifold approximation and projection
WT	wild-type

Introduction and Background

The nature and behavior of neutrophils are central to the pathogenesis of AKI. Neutrophil plasticity exists in several diseases and pathologies. There are examples of neutrophil plasticity and diversity in infection, autoimmunity, sterile inflammation, and cancer. Some of the best characterized examples are in cancer where specific classes of tumors are more likely to support pro-tumorigenic neutrophils. The plasticity of neutrophils in cancer has extended to the description of antigen presenting neutrophils *ex vivo*. In AKI there has been only a limited description of diverse types of neutrophils. In combination with high-resolution and high throughput transcriptomics the stage is set for uncovering novel cell types across the kidney parenchyma and immune cells such as neutrophils. With this high-resolution data, the mechanisms behind injury and disease may become apparent.

Acute kidney injury

Worldwide, there are an estimated 13 million cases of acute kidney injury (AKI) annually(1). In the United States there are an estimated 1.2 million cases annually or about twenty percent of adult patients(2-7). AKI is estimated to have an economic cost of five to nine billion dollars annually(4). Comorbidities and risk factors such as stroke, heart disease, diabetes and chronic kidney disease, major surgery, cancer treatment and common drugs exacerbate AKI(3, 8, 9). Thus, AKI is a public health problem.

Mechanistically, AKI causes include, drug induced nephrotoxicity and/or ischemia. Drug induce nephrotoxicity can lead to tissue damage included interstitial nephritis, tubular necrosis, glomerular injury, and changes in hemodynamics. Common drugs that can cause AKI include non-steroidal anti-inflammatory drugs, angiotensin-converting enzyme

inhibitors, angiotensin receptor binders and chemotherapies for solid tumors such as cisplatin(10-12).

Systemic, kidney and urinary tract pathologies can lead to AKI (10). Typically, AKI occurs over a period of few days and includes a rapid drop in kidney function and blood filtration. This can be measured by the accumulation of creatinine, a byproduct of muscle metabolism of creatine, in the serum and reduced urine volume. AKI is defined clinically as an increase in serum creatinine above 0.3 mg/dL or 1.5x increase in serum creatinine levels above baseline within days and a drop of urine output to less than 0.5ml/kg over 6 hours(3, 13). The goal in treating AKI is to return the kidney to normal function as measured minimally by urine output and serum creatinine levels. Intervention are limited to removing or replacing nephrotoxic drugs, maintaining blood volume and urine output while also providing supportive care(14, 15). Thus, there is a need for novel interventions and therapeutic strategies to reduce the burden of AKI.

The etiologies for ischemic AKI can be grouped into three categories based on their origin: systemic, kidney and urinary tract(16). Respectively, blood volume loss and ischemia from surgery or organ failure, occlusion of the urinary tract by kidney stones or cancer and ischemia and/or inflammation at the kidney can all lead to AKI. In the kidney, inflammation is often localized to specific segments of the nephron-the filtering unit of the kidney(3, 16-19). This includes inflammation associated with glomeruli, vasculature, renal tubules and the interstitium, respectively: glomerulonephritis, vasculitis and tubulointerstitial nephritis. The inflammation can be an allergic reaction or nephrotoxicity. Non-steroidal anti-inflammatory drugs can be especially harmful with a “two-hit mechanism”, decreasing renal flow at the glomeruli and causing nephrotoxicity and tubular necrosis. Ischemic injury also leads to tubular necrosis in the kidney and subsequent sterile tissue inflammation(16). In total, the breadth and the mechanistic diversity in AKI is challenging.

Because ischemic injury is the leading cause of AKI(20), these works focus on ischemia and reperfusion injury (IRI) of the mouse kidney to model AKI(21). As one might expect the amount of ischemia, time or degree (e.g. one or two kidneys) affects the degree of injury and AKI. Specifically, In IRI, the injury time and the time after injury, reperfusion, can be varied. During reperfusion there are three phases of on-going damage, recovery and repair depending upon the degree of injury(16). One the earliest cell-types to arrive, by 6 hours, peak at 24 hours and leave by 72 hours, are neutrophils.

Neutrophils and AKI

Neutrophils make-up as much as 70% of the circulating white blood cells. Their lifecycle maybe as short as hours or as long as days. Neutrophil behaviors are diverse and include variable times in circulation, specific association with endothelial cells, regulated migration out of circulation and into tissue or margination, reverse migration to lymphoid tissue and the bone marrow (BM) and transcriptional plasticity(22-25).

Neutrophils are granulocytes formed in the BM niche during granulopoiesis. Granulocytes are myeloid cells that share a common progenitor with mononuclear phagocytic cells such as monocytes, macrophages and dendritic cells. Classically, granulocytes were identified by the presence of pigment reactive granules in their cytoplasm and their distinct nuclear morphology. Their differentiation is tightly regulated by the activity of transcription factors including CCAAT/enhancer-binding proteins, PU.1 and GATA-1. During neutrophil maturation CXCL12 expressed on the cell surface interacting with CXCR4 to retain them in the BM. Neutrophils leave the BM in a naïve state after the upregulation of CXCR2 on their cell surface and an increase in CXCL2 supplants CXCL12 interaction with CXCR4. Dendritic cells further modulate the distribution of neutrophils between the BM, circulation and margination into tissues through granulocyte colony stimulating factor (G-CSF) and the cytokines CXCL1, CCL2

and CXCL10. In addition, the pro-inflammatory cytokines such as IL-1 β , TNF α , and the growth factors G-CSF and granulocyte/macrophage colony stimulating factor (GM-CSF) can also drive granulopoiesis and neutrophil production and maturation. IL-17 originating in sites of inflammation may drive G-CSF and further granulopoiesis. These proinflammatory cytokines also shift the neutrophil from a “resting” or naïve state to a primed state whereby neutrophils may be recruited to sites of tissue damage, infection or on-going inflammation(26, 27).

Once out of the BM, neutrophils are found in three basic locations: circulation, marginating under non-injury conditions and infiltrating tissue during injury. Marginated pools of neutrophils are found in the lung, spleen and liver. Neutrophil margination in the lung is driven by CXCL12 from endothelial cells and the neutrophil age dependent increase in surface expression of CXCR4. During tissue injury neutrophils transition from circulatory pools to the tissue, in five distinct steps: rolling, adhesion, crawling, extravasation and migration within the tissue(28).

Classically, neutrophils in circulation are thought of as early “hunter-killers” with specific transcriptional responses and self-destructive responses such as efferocytosis and NETosis (neutrophil extracellular trap-osis)(22, 29, 30). In this model of neutrophil behavior, often in the context of infection, neutrophils are drawn to the site of infection via cytokines and pathogen associate molecular patterns (PAMPs). Once at the site of infection the neutrophils generate ROS, degranulate releasing cytotoxic antimicrobial proteins and peptides and phagocytosis pathogens. Once the “killing” capacity of the neutrophils is reached they undergo apoptosis and are phagocytosed or efferocytosed by macrophages. Neutrophil extracellular traps are the most severe example of a neutrophil’s self-destructive potential(31). In NETosis PAD4 citrullinates histones driving DNA decondensation. The decondensing DNA breaks out of the nucleus and spills out of the cell. This net of DNA is thought to trap pathogens and limit infection. In AKI, this is

considered a deleterious process as inhibiting PAD4 or treatment with DNase improves renal function after IRI(31-33). Presumably, this is because tissue damage is limited, minimizing fibrosis and loss of functional nephrons. Although these classic behaviors dominate our model of neutrophils, growing evidence suggests that *neutrophils are more nuanced and exhibit phenotypic plasticity and heterogeneity or, at the least, significant transcriptional activity in response to infection and tissue injury.*

There are several striking examples of neutrophil phenotypic heterogeneity and plasticity(22). One of the best characterized examples of phenotypic heterogeneity in neutrophils is found in cancer(34-38). Tumor associated neutrophils (TANs) have been classified as either N1 (anti-tumorigenic) or N2 (pro-tumorigenic) neutrophils. The cytokine and growth factor TGF β , is sufficient for a transition to the immunosuppressive N2(34). Strikingly, the N2 phenotype is often found at the center of the tumor-presumably where the TGF β concentration is highest(39). An important recent finding is that, *in vitro*, this transition involves transcriptional reprogramming, suggesting that the N2 is a bona fide type of neutrophil(36). Thus, neutrophil polarization occurs in response to specific cytokines and polarized N2 neutrophils localize within the core of the tumor and are pro-tumorigenic.

Ischemic injury models and neutrophil polarization

N1 and N2 polarized neutrophils also have roles in ischemic injury of several organs. This includes ischemic injury of the brain, heart and kidney. In brain and heart there appears to be a role in recovery and repair for neutrophil polarization. The role of neutrophil polarization in AKI is less clear.

Neutrophil polarization following myocardial infarction.

In myocardial infarction (MI) there is a clear temporal regulation of neutrophil polarization(40). In the days immediately after MI, in response to DAMPs, a proinflammatory milieu is formed occupied primarily by N1 neutrophils. By five days post MI the site of injury transitions to an anti-inflammatory milieu; IL1 β and TNF α drop and IL-10 increases with a concomitant increase in N2 and decrease in N1 neutrophils. This transition correlates with better outcomes and less long-term damage (thinning of the ventricle). It is unclear whether the polarization to an N2 phenotype occurs only at the site of injury. Although, the authors did not detect N2 neutrophils in circulation. The author's also present data suggesting the mannose receptor, CD206, also a marker for M2 macrophages, may be a marker for separating N2 from N1 neutrophils by flow cytometry.

Neutrophil polarization in areas of injury following stroke.

While investigating the mechanism behind the beneficial of a PPAR γ agonist in treating (a driver of M1 to M2 macrophages switches), Cuartero and colleagues discover a distinct polarization of neutrophils, based on the M2 markers CD206 and Ym1, by flow cytometry and immunofluorescence(41). In their model of stroke, permanent middle cerebral artery occlusion (pMCAO), ~30% of the infiltrating neutrophils are Ym1+ and CD206+. Importantly, there were nearly no N2 neutrophils by either marker in a sham treated group further supporting my *hypothesis that the milieu drives neutrophil polarization.*

Polarized N2 neutrophils are found in AKI.

In a 2018 study to understand the impact of cannabinoids on AKI, N2 neutrophils were found in the kidney after IRI using the putative N2 marker CD206(42, 43). In this

work the authors show that equal proportions of N1 and N2 neutrophils is required to minimize KIM-1+ tubular injury. Unique to this work is the detection of equal numbers of N1 and N2 neutrophils in the uninjured and injured milieu 24 hours after surgery. In other models of ischemic injury, myocardial infarction and stroke only ~20% of neutrophils were N2 polarized during the recovery phase(40, 41). Also contrary to the other ischemic injury models, the fraction of N2 neutrophils following a Sham surgery were high-they were nearly undetectable in stroke. This suggests either a unique milieu exists in the kidney or that the models of ischemic injury differ greatly. For instance, in these studies of AKI, they used a mouse model of moderate injury with an ischemic injury time of 20 minutes. The large fractions of N2 neutrophils in the sham surgery is perplexing. *It is unclear what role the severity of injury is playing in the degree of neutrophil polarization and neutrophil diversity in ischemic injury of the kidney, warranting further investigation.*

The response of neutrophils is early and swift in ischemic AKI.

In wild-type mouse models of ischemic AKI neutrophils are detected as early as *30 minutes* after injury(18, 44, 45). The peak of infiltration occurs between 24 and 48 hours and by 72 hours the infiltration has subsided. Recovery of kidney injury with moderate injury is seen by one-week post injury(46). Arguably the microenvironments formed by 24 hours is a direct consequence of *the conditions that have been developing for hours.*

Neutrophils persist in depletion and inhibitory experiments.

An important consideration, with respect to depletion and drug-based interventions is that often the improvement in kidney function is not necessarily in a kidney devoid of neutrophils. Although early works on ICAM-1 confirms the depletion with less than 100-200 neutrophils per mm³ in their experiments, it is unclear whether this was based on

cortical or medullary assessments(47). Furthermore, other experimental interventions, inhibitory or chemokine depletions, often have residual neutrophil levels not investigated(32, 45, 48). Could these interventions bias the kidney milieu to a reparative neutrophil? *This suggests a high-resolution assessment of the types of neutrophils is needed.*

Chapter 1. The cellular map of 129Sv/Ev mouse kidney

Introduction

Identification of critical cellular players involved in diseases, especially those as complicated in their etiology as acute kidney injury (AKI) is difficult with directed approaches, such as antibody based multiplexing techniques used in immunofluorescence and flow cytometry. Although the depth of these approaches has improved greatly over the last decade now permitting up to 30 markers, they are still based on the assumptions made about specific markers for cell subtypes and confined by identification through gating strategies. Methods that combine a regional isolation of tissue structures, such as laser microdissection, with RNASeq enhance the depth of the cellular players involved in disease while maintaining tissue context but compromise the breadth of cell-types by assaying regions containing many cells(49, 50). Importantly, the context of a cell is critical for understanding the biology and physiology of an organ—especially an organ as structurally diverse as the kidney. Single cell RNASeq, provides the best breadth and depth for cell identification at the cost of this contextual metadata(51).

Single cell RNASeq has been used previously to identify cell types in the mouse kidney(52, 53). In these publications a major limitation has been the recovery of leukocytes. To address this problem, a combination of whole kidney isolation (poor recovery of leukocytes), CD45+ enriched isolation (excellent recovery of leukocytes) and Blood isolation (excellent recovery of circulating leukocytes) were tested and used.

The overarching hypothesis is that in AKI the populations of neutrophils present in the injured kidney dictate the recovery of kidney function. To capture cellular diversity with scRNASeq two complimentary approaches for isolation of single cells were tested: 1) an approach for isolating all cells of renal parenchyma and 2) an approach to enrich leukocytes associated with kidney. These complimentary approaches demonstrated

diversity in the kidney parenchyma and in immune cells, specifically tubular epithelium or macrophages and neutrophils. The data presented here demonstrates that there are novel populations of macrophage/monocytes and neutrophil diversity in the *uninjured* mouse kidney.

Results

Quality of single cell RNAseq and basic processing of datasets

Single cell RNA sequencing (scRNASeq) has been used to build single cell RNA transcript-based models of development, organs and disease(54-60). To develop a cellular map of kidney in the mouse strain 129Sv/Ev, whole kidneys from wild-type (WT) mice were processed with a MACs isolation kit to liberate single cells suitable for droplet-based scRNASeq. To facilitate comparison with experiments that involve surgeries, the body cavity was opened and closed to mimic a surgery such as bilateral clamping of the kidney pedicle (see Chapter 4). cDNA libraries were generated, sequenced, and aligned as described in methods. The resulting expression matrix was analyzed in R using Seurat(61).

To generate a dataset appropriate for downstream analysis the quality of the per cell libraries was assessed. In droplet-based scRNASeq there is a possibility of multiple cells being incorporated into one droplet resulting in a library that contains cDNA from more than one cell. The increase in cDNA can lead to a library with aberrantly high read counts following sequencing. Conversely, cells with a low read count suggest a dearth of cDNA and possibly a damaged or dying cell. Furthermore, cells with a compromised plasma membrane will have fewer cytoplasmic mRNA and their libraries will be over-represented by mitochondrial RNA. To quality control the cDNA libraries, libraries from whole kidney with high or low read counts or if the fraction of total mitochondria transcript reads was greater than 50% of the total reads were excluded from the analysis ((59)**Figure**

1.1). For libraries from cells enriched for immune cells, a more stringent 5% mitochondria fraction of total transcript reads was used(61, 62). The number of times a cDNA is sequenced is used as the measure of transcript abundance. However, it is not uncommon for all cDNAs to be low across a single cell-due to variations in library generation. To correct for this variation, read counts were normalized with Seurat's Log normalizing approach(61).

To identify cell types, there needs to be enough genes with high enough variance to elaborate an expected number of cell types. With a dataset from a sham surgery in WT mice and whole kidney isolation of cells, the top 10 highly variable genes include markers for neutrophils and epithelial cells suggest adequate complexity in the read counts and hence cells (**Figure 1.2**). To cluster and identify the cells represented by the read counts 30-40 principal components were determined from the normalized read-counts. To assess how many principal components to use for clustering an elbow plot or JackStraw process were performed (**Figure 1.3**). These principal components were used for 1) clustering the cells into populations and 2) visualization directly or with dimensionality reduction (**Figure 1.4**).

The cellular composition of 129Sv/Ev mouse kidneys

To establish a map of the mouse kidney, cells from wildtype mice after a sham surgery were analyzed from a combined dataset (see methods, **Figure 1.4A**). Using a combination of SingleR, and published markers the major cell types were identified ((63) **Figure 1.5**). The major epithelial cells of the nephron were identified. Furthermore, the specialized smooth-muscle cells, granular cells, of the juxtaglomerular apparatus were identified. The recovery of immune cells was poor, making it difficult to described immune cell subtypes and diversity (e.g. <30 putative macrophages, T-cells or neutrophils were recovered-outlined below).

Epithelial cells of the proximal tubule subsegments

The proximal tubule has been previously described into the three major segments, S1, S2 and S3 where S1 and S2 are a part of the proximal convoluted tubule and S3 is a linear tubule often found in medullary rays. These three segments have been classified by scRNASeq previously(59). Surprisingly, the epithelial cells of all three subsegments of the proximal tubule could be further subdivided with the S1 being composed of three distinct cluster (clusters 1,6 and 13, **Figure 1.4**), S2 comprised of two distinct clusters (clusters 4 and 7, **Figure 1.4**) and the S3 could be divided into three sub clusters (clusters 3, 8, 19, **Figure 1.4**). One of the S3 sub clusters (cluster 3) is reminiscent of the type 2 S3 proximal tubule cells (53).

Epithelial cells of the distal nephron

The distal nephron was also well represented in the disaggregated cells of the mouse kidney. There were clusters of cells identified as being from the loop of Henle (LOH), distal convoluted tubule (DCT), collecting network tubules (CNT) and collecting ducts (CD). Distal to the DCT is the cortical connecting tubule network. In these data it is found bridging the subsegments of distal tubules (**Figure 1.5**). Previously described markers were used to identify epithelial cells of the CD including principal cells (CD-PC) and two population of intercalating cells (CD-ICa and -ICb) were identified in the data ((59)**Figure 1.4B and 1.5**).

Endothelium and associated cells

An Endothelium cluster was identified that was comprised of multiple clusters- however a clear identification of subtypes could not be made. Furthermore, podocytes, by *Nphs* expression(52), are missing from the dataset. Although critical to acute glomerular nephritis and linked to septic-AKI, the role for podocytes in ischemic AKI is not

clear(64). Using *Ren1* the mouse gene for renin, a single cluster in UMAP space was highlighted, suggesting these were the specialized secretory smooth-muscle cells of the juxtaglomerular apparatus (**Figure 1.6**).

Leukocytes

The protocol used for isolation of cells from the disaggregated kidneys did not include specific steps for enrichment of immune cells. It was thus unlikely that significant number of immune cells would be captured. This was the case as small numbers of presumptive circulating neutrophils, B-cells, T-cells and NK cells were identified as well as few macrophages (**Figure 1.4B and 1.5**).

Isolation and CD45+ enrichment of immune cells

To address the poor recovery of immune cells from whole kidney isolation, a CD45+ enrichment approach was used. The enrichment protocol used density centrifugation and sorting with fluorescence activated cell-sorting of CD45 labeled cells. The density centrifugation was originally designed to enrich for neutrophils and was adapted here to enrich multiple types of immune cells (65)(**Figure 1.7A**). This approach was first proven by flow cytometry and used to generate single cells for sequencing (**Figure 1.7B**).

To establish a distribution of immune cell types in the mouse kidney, single cells for scRNASeq were isolated and enriched from whole kidneys. In the unchallenged kidney, a sham surgery, six kidneys from three mice were pooled to ensure an adequate yield of leukocytes. Data used here was from cells that had been integrated into a combined dataset (see methods). 20 clusters were identified spread across three groups in a UMAP plot (**Figure 1.8A**). Cell-types were classified by cluster with identification by SingleR, manually based on published markers and/or following differential expression

analysis (**Figure 1.8B** and **1.9**). In contrast to the whole kidney isolation, the use of a centrifugation and CD45⁺-cell sorting step increased the recovery of lymphocytes-including subclasses of T-cells and myeloid cells-including eosinophils, dendritic cells, macrophages and a monolithic cluster of neutrophils (**Figures 9** and **1.8B**).

Relative to immune cell recovery from the whole kidney isolation protocol, macrophages and lymphocytes saw some of the greatest increase in number and breadth of cell-types. Initially there was a small cluster T and NK cells and a small cluster of B cells in the whole kidney preparation (**Figure 1.4B** and **1.5**). After isolation and enrichment, T-cells were readily subclustered into CD8⁺ (cytotoxic T-cell), CD4⁺ (T-helper cell) and regulatory T-cells. Both NK and B cells were also isolated by the enrichment protocol (**Figures 1.4B** and **1.5B**). Like T-cells, the number and breadth of macrophage types was striking with multiple clusters including putative monocyte macrophages.

To explore sub-populations of the subtypes of macrophages and neutrophils, these cells were isolated from the CD45⁺ enriched dataset for further analysis. As kidneys were not perfused prior to isolation of single cells, cells are expected to include immune cells that have margined, those that have extravasated into the interstitium and cells in the blood. Thus, in a sham surgery we expect to detect a significant number and depth of most leukocytes originating from cells in the blood and kidney.

Monocytes and macrophages of the mouse kidney

Recent work has described three populations of macrophages in the mouse kidney- two infiltrating monocyte/macrophages and a third resident macrophage(60). These three types of macrophages were identified using the markers *Plac8* for infiltrating monocyte/macrophages, *Ear2* and *Chil3* for either Ly6chi and Ly6clo monocyte/macrophages respectively and *Cd81* for resident macrophages. These three populations were readily identified in the CD45⁺ enrichment isolation (**Figure 1.10A**).

There were also an additional three populations of monocyte/macrophages identified. These included a population similar to the Ly6chi macrophages but also expressing *Stmn1*, a marker of inactivation (Macrophage-Ly6chi-inactivated), and a two additional monocyte/macrophage populations that expressed *Plac8*, but not *Ear2* or *Chil3*, suggesting two additional infiltrating population of monocyte/macrophage (Monocyte-1 and Monocyte-2, **Figure 1.10B and C**).

Populations of neutrophils

To explore neutrophils subpopulations, neutrophils were first isolated from the CD45+ enriched dataset (sham surgery in WT mice). Because the neutrophil cluster was monolithic (**Figure 1.8B**), new principal components and clusters were determined. Following clustering, four distinct populations were identified (**Figure 1.11**). Differential expression (DE) analysis was performed to determine markers ($p < 0.05$, Bonferroni corrected) and possible functional characteristics for these populations (**Figure 1.12**). A highly and uniquely expressed marker could not be identified for Cluster 0-as if it were a parent cluster. Cells in this cluster were highly expressing the neutrophil markers S100a8 and S100a9. There were two differentially expressed transcripts identified in cluster 2, the proinflammatory cytokine *Il1b* and the secretory granule associated protein *Sgrn*. Although more robustly expressed in cluster 0, both transcripts are found, expectedly, in multiple neutrophil populations (**Figure 1.12**). Fortunately, the remaining clusters had unique markers identified by DE analysis. Cluster 1 was uniquely identified by two poorly characterized, yet proteins common to neutrophils, cystatins (*Gm5483* and *BC100530*). This suggests cluster 1 may be a motile neutrophil population(66). Cluster 3 markers included *Lgals3* and *Retnlg*. *Retnlg* may be a regulator of neutrophil activity, suggesting either a regulated and/or regulating neutrophil(67).

It is possible that myeloid derived suppressor cells (MDSC) may have been clustered erroneously in the neutrophil population. To test for this possibility, transcriptomics markers of granulocyte myeloid derived suppressor cell (G-MDSC) were investigated (*Cd84* and *Arg1*, **Figure 1.12**). The 4 putative neutrophil clusters were positive for typical neutrophil markers (*S100a8* and *S100a9*) but negative for markers of G-MDSCs (*Cd84* and *Arg1*)(60).

Discussion

The two single cell isolation protocols complement each other with cell-type specific sensitivity and specificity. Having both approaches will be critical to uncovering a better and deeper model of what is transpiring during AKI-especially the role of diverse types of leukocytes such as neutrophils.

The ability of scRNASeq to uncover transcriptional diversity was illustrated in both cell isolation protocols. The whole kidney approach without enrichment (whole kidney isolation) was able to uncover the proximal tubule subsegments. In the CD45+enriched preparation (CD45+ enrichment isolation) the T-cell, macrophage and neutrophil clusters had improved depth. T-cells separated into putative CD4+ and CD8+ clusters and macrophages were easily divided into infiltrating and resident clusters. Additionally, T-regs were resolved and several additional novel subtypes of infiltrating macrophages were uncovered. In total, the CD45+ enrichment protocol is a better approach for uncovering breadth and depth of immune cells.

After separating the neutrophils from the remainder of CD45+ cells, four putative subpopulations of neutrophils were identified. These included specific neutrophil subtypes that may be uniquely motile, antigen presenting or classically activated. Furthermore, these behaviors are highlighted by specific markers that may be used moving forward for cluster identification. It is reassuring that some of these behaviors have been described

previously(68, 69). Importantly, this is the first report of an unbiased census of neutrophil subtypes in or associated with an organ-in this case the kidney.

Neutrophil diversity has been studied in the context of infection, injury and cancer. In AKI it is expected that neutrophil diversity will expand and change. For instance, the tubular epithelium may drive neutrophil recruitment in unexpected ways or specific neutrophil subpopulations may be the sole source for signaling. There may be subpopulations of those presented here or completely novel populations all responding to tissue damage and changes in cell signaling within the kidney milieu.

Methods

Animals and surgeries

All mice were treated and cared for based on approved animal handling and surgery protocols as outlined in Chapter 4. Only sham surgeries are used in this chapter.

Kidney dissociation and isolation of single cells

The protocol used for kidney dissociation was provided by Janosevic et al.(70). Briefly, both kidneys from one male 129Sv/Ev mouse were removed after a sham surgery and minced together on a glass petri dish into ~8 pieces total and placed in Miltenyi Biotec tubes (C-tubes) with tissue digestion mix from the Multi Tissue Dissociation Kit 2 (Miltenyi Biotec) and agitated by a gentleMACs Dissociator (Miltenyi Biotec) followed by rotation on the MACSMix Tube Rotator (Miltenyi Biotec) for 30 minutes at 37°C and a final agitation cycle on the gentleMACs Dissociator. RPMI+5% BSA was added to quench the enzymatic reactions and the suspension was passed through a 40 µm strainer that was washed with 5 mL RPMI with 0.04% BSA. The eluent was passed through a second 30 µm strainer and wash with 5 mL of RPMI with 0.04% BSA. The total eluent was centrifuged at 300 x g for 5 minutes at 4°C and the pellet resuspended in 1 mL chilled RBC Lysis Buffer (Sigma)

and incubated for 5 minutes at 4°C. 10 mL cold RPMI with 0.04% BSA was added to dilute the lysis buffer and the sample was spun at 1000 rpm in a tabletop centrifuge at 4°C (Eppendorf 5430). The cells were washed three times with 5-minute spins to pellet the cells. After the final wash the pellet was resuspended in 1 mL of cold RPMI with 0.04% BSA. Dead cells were removed from the suspension using the EasySep Dead Cell Removal by Annexin V Kit (Stemcell Technologies). The magnetic beads were isolated using a multi-tube magnet for 1.5 mL tubes (Invitrogen). After removal of the dead cells the cell suspensions were transferred to 15 mL conical tubes and centrifuged at 1200 rpm in the Eppendorf 5430 tabletop centrifuge at 4°C. The cell pellet was resuspended in 1-3 mL of RPMI with 0.04%. This suspension was handed off to the genomics core for 10x processing.

Kidney dissociation and enrichment of CD45+ leukocytes

Both kidneys from four male 129Sv/Ev mice (eight kidneys total) were removed following a sham surgery and both pairs of kidneys placed in two separate Falcon 12 x 75 mm tubes with 1 mL iced Hank's balanced salt solution. Kidneys were homogenized with a TissueMiser on ice by making 10 passes three times. The tissue slurry was incubated with collagenase type IA for 30 min at 37°C in a water bath. To clarify the slurry the suspension was passed through a 70 µm strainer into a 50 mL centrifuge tube. The strainer was washed with a total of 14 mL PBS+1% fetal bovine serum (FBS). The eluent was centrifuged at 2000 rpm for 10 min (~1,600 x g) and the supernatant removed. To remove red blood cells and cellular debris the suspension was clarified on a Percoll gradient(65). Room temperature and sterile Percoll was prepared at 100% and either diluted to 40% or 70% in 1x PBS+1%FBS. At room temperature, the cell pellet was resuspended in 8 mL of the 40% Percoll in 1xPBS+1%FBS and layered on top of 3 mL of 70% Percoll in 1x PBS+1%FBS at room temperature. The gradient was spun for 30

minutes at 900 x g at room temperature. The centrifuge brake was turned-off to not disturb the formed gradient and separated cells. Following the spin there was a fatty cellular debris layer at the top of the gradient, a fuzzy “buffy coat” at the interface between the 40% and 70% Percoll, a thin band of red blood cells just below that and a pellet of red blood cells. The buffy coat was removed and diluted to 15 mL with PBS+1%FBS and spun at 800 x g for 10 min at 4°C. After removing the supernatant, the pellet was resuspended in 1 mL PBS+0.1%FBS. In preparation for labeling with CD for sorting by the flow cytometry facility, the suspension was centrifuged and resuspended in 100 µL to which CD16/32 antibody (BDBioscience) was added and incubated for 5 minutes at room temperature to block Fc gamma receptors. To label the cells with CD45 antibody, 10 µL (1.5 µg) APC conjugated CD45 antibody (clone 30F11, Miltenyi) was added to the 100 µL suspension and incubated for 30 minutes at 4°C. Centrifuge for 1 minute at ~6000 x g and remove supernatant. Resuspend both pellets (from each mouse) in 300 µL PBS+FBS and add 300 µL of 2x working concentration of propidium iodide (PI). The suspensions from both mice were combined prior to sorting. The sorting was carried out in the flow core. Briefly, the PI was used to gate on live cells and APC on our cells of interest (leukocytes). The sorted cells were collected on ice and taken to the genomics core for processing on the 10x platform v1.

Flow cytometry of immune cells isolated by differential centrifugation

Cell isolated by differential centrifugation were blocked with CD16/32 antibody (BDBioscience) and stained for FITC-CD11b, APC-Cy7-Ly6G and PE-CD45 for 30 minutes. After washing the cell suspension was stained with a 2X working concentration of PI. Single stained mouse bone marrow cells were used for controls to calibrate the flow cytometer and adjust compensation matrices. Bone marrow was extracted from the femur of adult mice, washed and split into four stains for CD11b, Ly6G, CD45, and PI. A fifth

sample was used as an unlabeled control. Samples were run on a Guava benchtop flow cytometer (Millipore). Results were saved and processed with FlowJo (FlowJo LLC).

Staining of tissue sections

Mouse kidney fresh-fixed in 4% paraformaldehyde for 24 hours were cut into 50 μm sections and stored at 4°C. For staining sections were washed in 1XPBS 3-5x and blocked in blocking buffer, 1XPBS, 0.1% Triton X-100 and 5-10% normal goat serum (Jackson Immunology), for 5-30 minutes. Primary antibody was prepared in block and stained overnight in a sealed container. Primary antibodies used included anti-Ly6G (clone 1A8, Biolegend) and anti-KIM-1 (cat#AF1817, R&D Systems). Following labeling with primary the sections were rinsed in 1x PBS 3-4x and washed in blocking buffer for ~30 minutes 2-3 times. Secondary antibodies with DAPI and OregonGreen488-phalloidin were prepared and sections were stained overnight in a sealed container. Sections were rinsed and wash as above and mounted in ProLong Glass under a #1.5 coverglass. The mount was cured for 48-72 hours prior to sealing with nail-polish.

Confocal large-scale imaging of tissue

Imaging was performed on a Leica SP8 upright confocal microscope with a motorized stage, 2 HyD and 2 PMT detectors with 4 lasers at 405 nm, 488 nm, 552 nm and 635 nm controlled by LASX software. Automated tile scanning and mosaic imaging was performed in four channels to cover the whole tissue in x, y, and z. The captured volumes were stitched in LASX and visualized in Fiji (71, 72).

Single cell 3' RNA-seq

Single cell 3' RNA-seq experiments were conducted using the Chromium single cell system (10x Genomics, Inc) and Illumina sequencers at the Center for Medical

Genetics of Indiana University School of Medicine. Each cell suspension was first inspected under microscope for cell number, cell viability, and cell size. Depending on the quality of the initial cell suspension, the single cell preparation included centrifugation, re-suspension, and filtration to remove cell debris, dead cells and cell aggregates. Single cell capture and library preparation were carried out according to the Chromium Single cell 3' Reagent kits V2 or V3 User Guide. Appropriate number of cells were loaded on a multiple-channel micro-fluidics chip of the Chromium Single Cell Instrument (10x Genomics) with a targeted cell recovery of ~10,000. Single cell gel beads in emulsion containing barcoded oligonucleotides and reverse transcriptase reagents were generated with the v2 or v3 single cell reagent kit (10X Genomics). Following cell capture and cell lysis, cDNA was synthesized and amplified. Illumina sequencing libraries were then prepared with the amplified cDNA. The resulting libraries were assessed with an Agilent TapeStation or Bioanalyzer 2100. The final libraries were sequenced using a custom program on Illumina NovaSeq 6000. 26 or 28 bp of cell barcode and UMI (unique molecular indices) sequences, and 91 bp RNA reads were generated.

Analysis of scRNA-seq sequence data

CellRanger 2.1.0, 3.0.2 or 3.1.0 (<http://support.10xgenomics.com/>) was used to process the raw sequence data generated. Briefly, CellRanger used bcl2fastq (<https://support.illumina.com/>) to demultiplex raw base sequence calls generated from the sequencer into sample-specific FASTQ files. The FASTQ files were then aligned to the human reference genome mm10 with RNA-seq aligner STAR. The aligned reads were traced back to individual cells and the gene expression level of individual genes were quantified based on the number of UMIs detected in each cell.

Analysis of expression matrices

The R package Seurat(61), was used extensively in the analysis of the expression data. In general, the processing included loading, quality control (outlined in results), normalization, alignment of multiple datasets to enable comparisons between conditions (batch correction), clustering and visualization. QC parameters were set based on the sample being isolated. In the whole kidney isolation, immune cells were first subject to the less stringent %-mitochondrial QC parameter as all other cells (50%). Immune cells were reprocessed with a more stringent cut-off appropriate for immune cells (5%, (61)). Cell types were identified by SingleR(63) or based on literature review. In the cases of neutrophils and macrophages a recursive clustering analysis was performed to resolve subpopulations.

Combined dataset of cells from single cell isolation protocols

To facilitate future comparisons between treatments and conditions for scRNASeq datasets from all AKI interventions (Chapter 2) and THP genetic models (Chapter 3) were combined into one dataset by single cell isolation protocol-CD45+ enrichment isolation or whole kidney isolation. With this approach batch effects are managed by alignment of normalized expression levels by cell across all the conditions. These integrated values provide the basis for principal components used in both the generation of clusters and dimensionality reduction. Thus, cluster definitions are assigned across datasets and can be used for comparisons. Expression levels are determined by the normalized RNA levels.

Data availability

Raw and processed data will be made available online at GEO hosted by the National Center for Biotechnology Information.

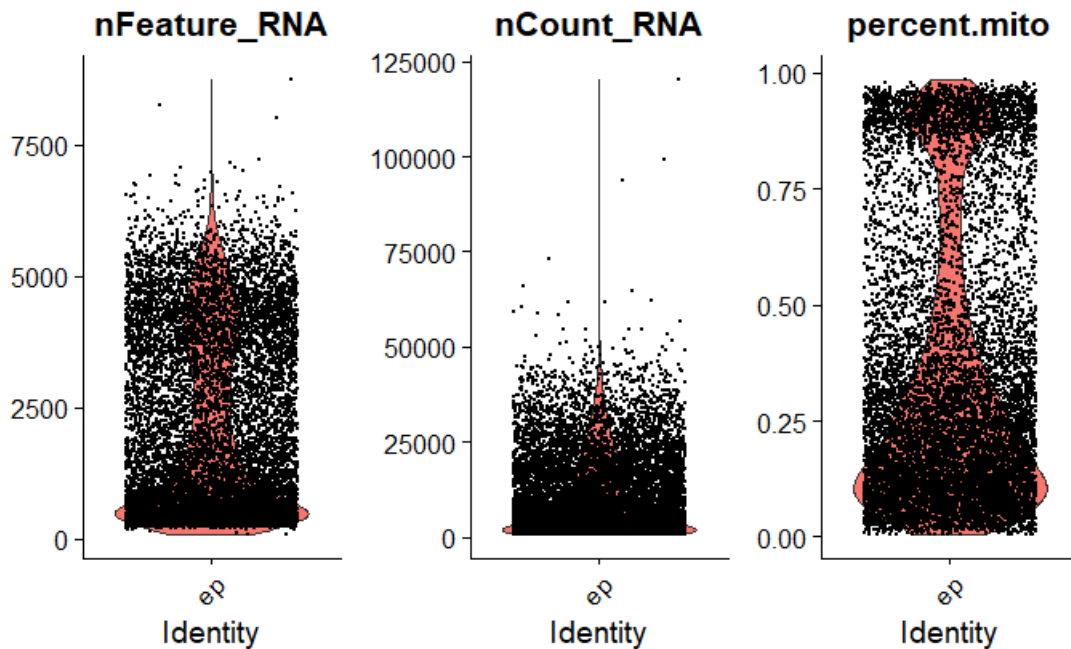


Figure 1.1. Initial quality control metrics. Total cells were isolated from sham surgery kidneys, processed on the 10X Chromium platform, libraries sequenced using next generation sequencing, reads mapped to genes and expression tables by cell created. The expression tables were imported into the R package Seurat v 3.1 and the percentage of mitochondrial reads calculated. The number of RNAs detected (`nFeatures_RNA`), the number reads per RNA (`nCount_RNA`) and the percentage of mitochondrial reads (`percent.mito`) are plotted.

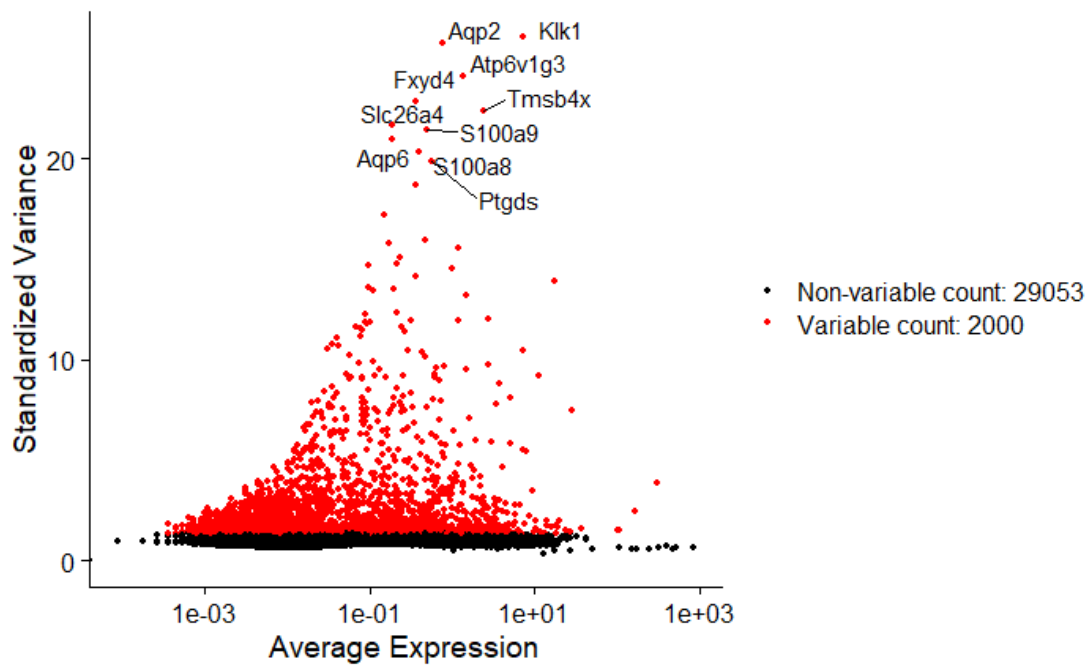


Figure 1.2. Detecting the variable genes for use in calculating principal components. After applying QC parameters, the average expression of a gene was plotted versus its variance across all cells. The top ten genes most highly variable genes are annotated. The annotated genes can be broken into renal epithelial cells (e.g. Aqp6, Aqp2, Slc26a4) and myeloidal cells (e.g. S100a8 and S100a9)

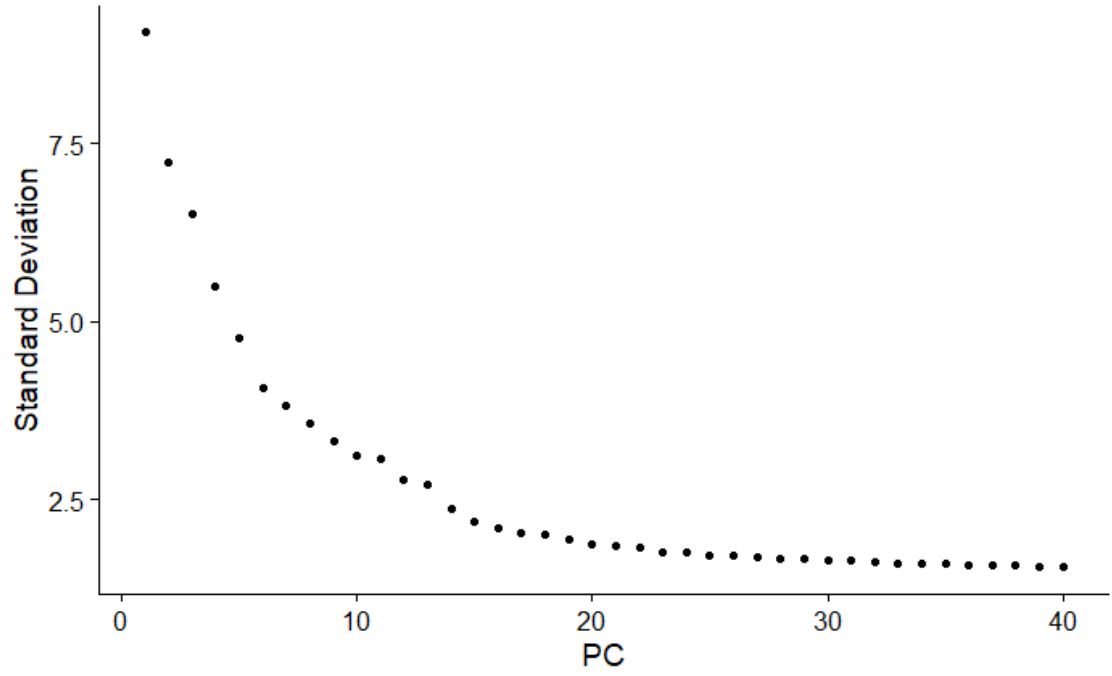


Figure 1.3. Elbow plot of principal components. An Elbow plot of the standard deviation of the whole population that is covered by each principal component (PC). In this example using 20-30 principal components for downstream clustering and dimensionality reduction is appropriate.

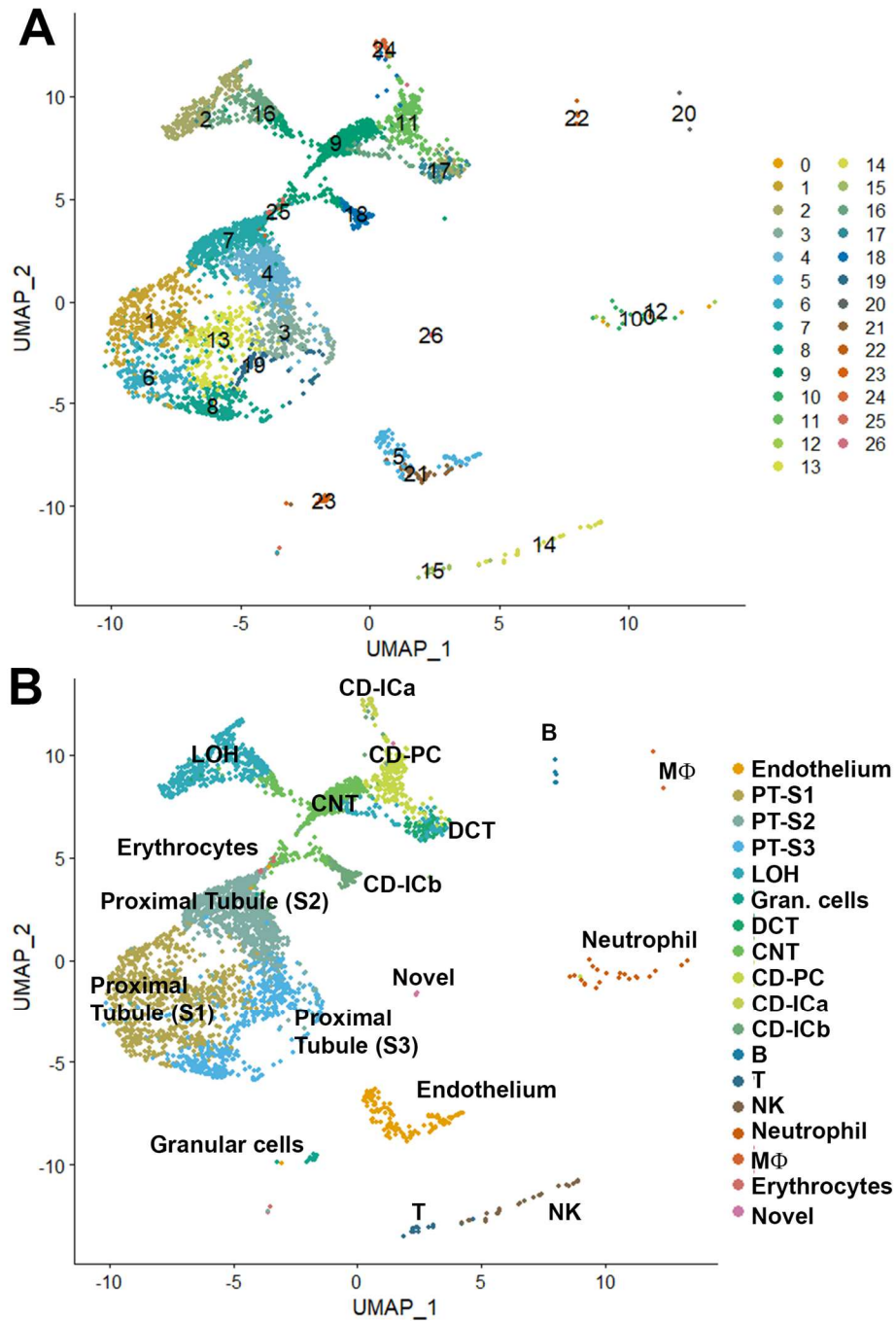


Figure 1.4. Clustering and dimensionality reduction of kidney scRNASeq data. Cells from whole kidney were isolated and processed for 10X chromium library generation, sequenced, and processed as indicated in the methods. Individual cells have been quality controlled, removing high count libraries/cells and those with excessive mitochondrial

transcripts. **A.** Clustering identified 27 populations of cells. **B.** Markers for cell-types found in the mouse kidney were collated and used to identify all clusters. A putative cluster of secretory granular cells of the juxtaglomerular apparatus was identified (cluster 23, Gran. Cells). One novel cell-type was not identified. The expression of Aqp1 suggests this may be descending vasa recta endothelium.

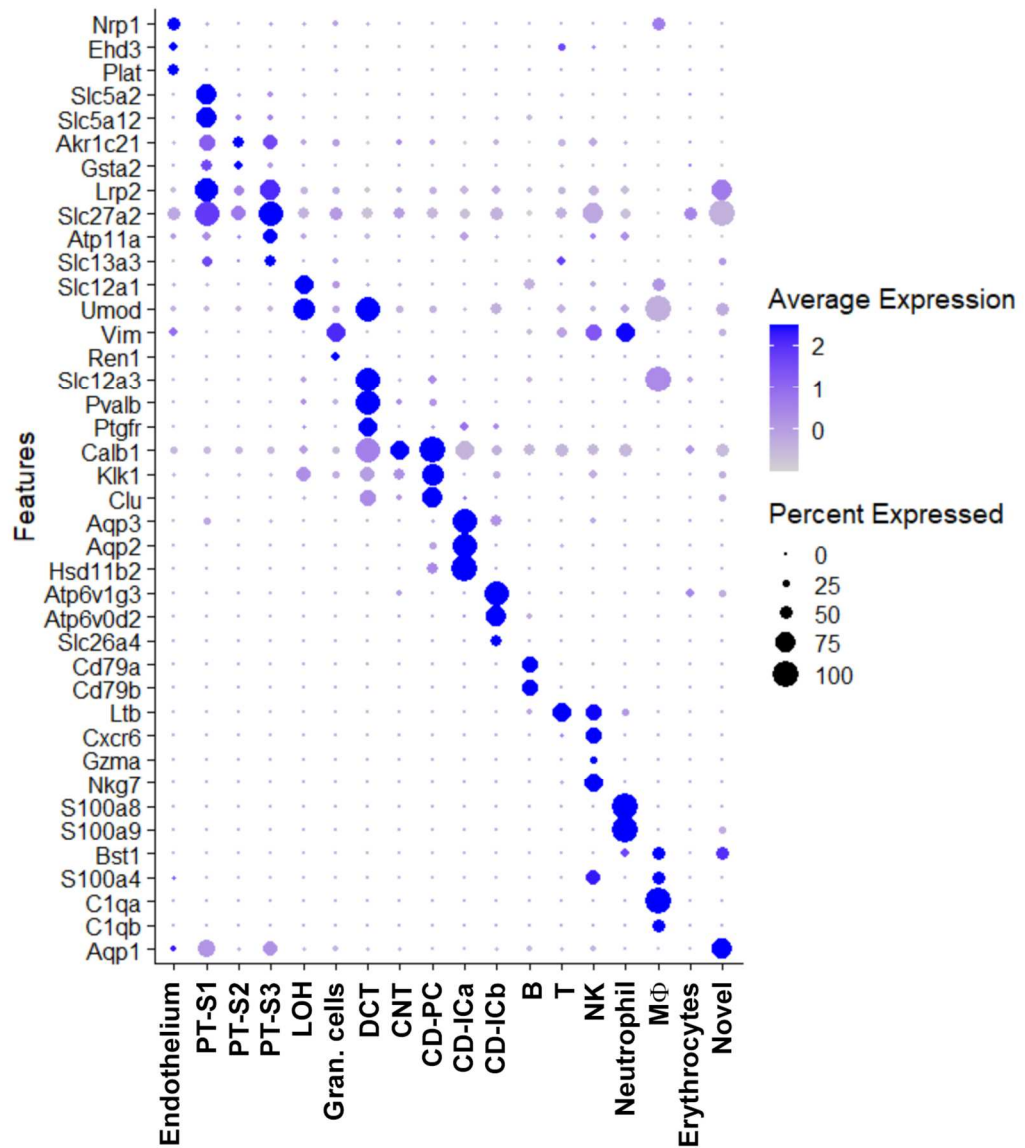


Figure 1.5. Identifying cell types in whole kidney using published markers. Markers for cell-types found in the mouse kidney were collated and used to identify all clusters. Expression level is by color and the fraction of cells expressing the gene is indicated by the size of the dot (scales included).

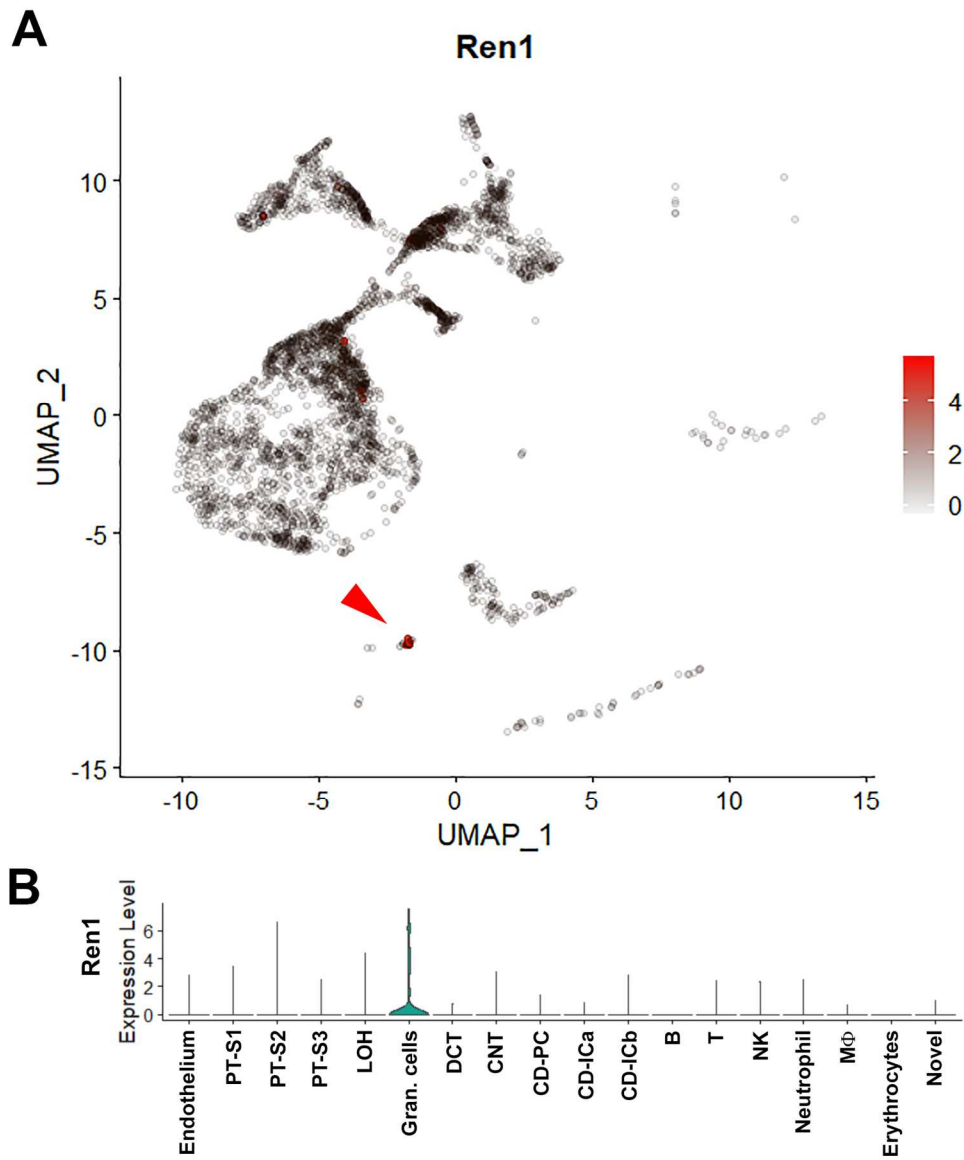


Figure 1.6. Identification of granular cells of the juxtaglomerular apparatus. Using Ren1 expression, a small cluster of cells was identified as the specialized secretory smooth-muscle cells of the juxtaglomerular apparatus (Gran. cells). The cells expressing Ren1 are highlighted by expression level, in red, and indicated with the red arrowhead.

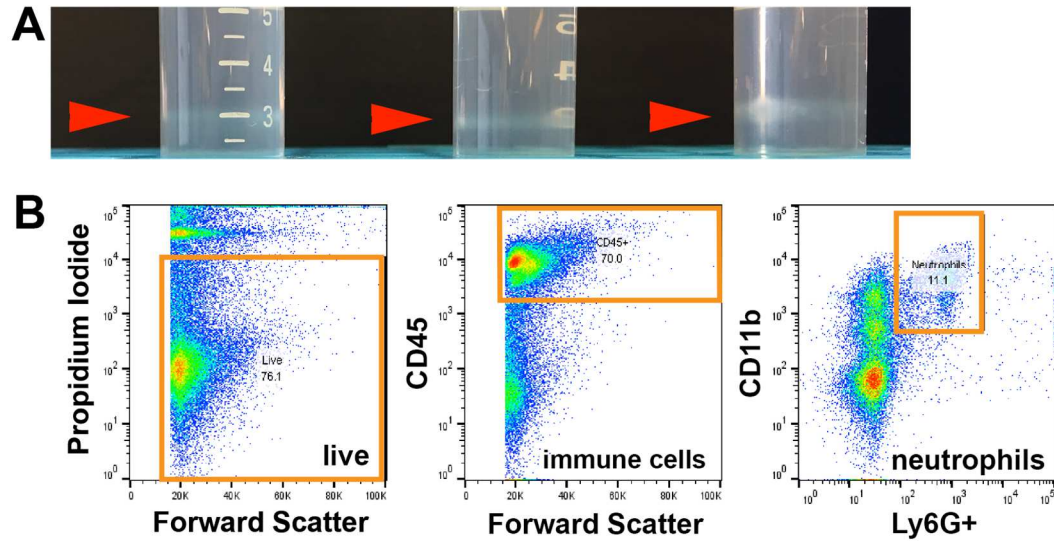


Figure 1.7. Differential centrifugation for isolation of immune cells from whole kidneys. Cells were enzymatically disaggregated and separated on a Percoll gradient. The cells were isolated from the buffy coat, stained with antibody against CD45 and purified by fluorescence activated cell sorting. **A.** Example of buffy coat cells were isolated from (red arrow heads). **B.** Flow cytometry of the isolated cells. Cells from buffy coat were stained for CD45, CD11b and Ly6G and run on a benchtop Guava flow-cytometer. Results were analyzed and plotted in FlowJo. Gates and percentages are indicated.

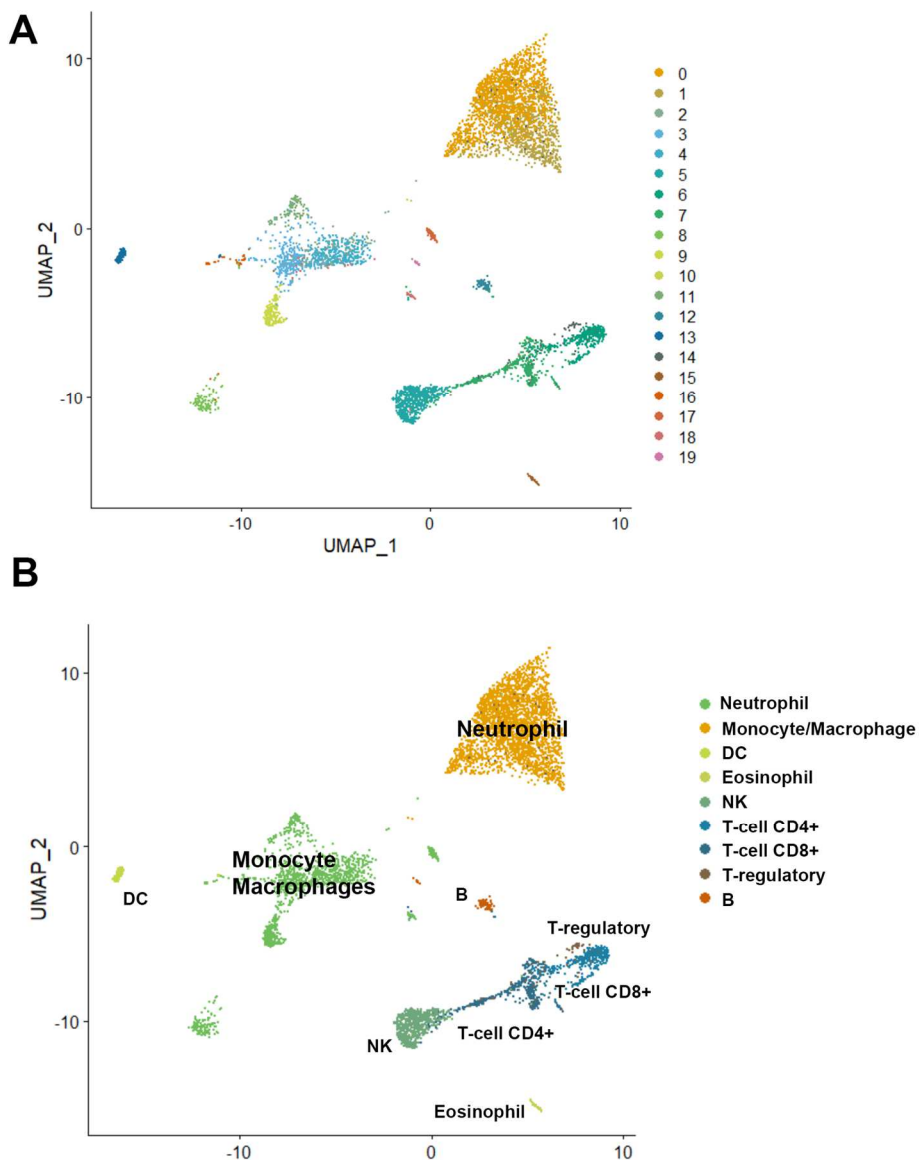


Figure 1.8. Clustering and dimensionality reduction of CD45+ enriched scRNASeq data. Cell from whole kidney were disaggregated and separated by differential centrifugation and CD45+ FACS for processing with 10X Chromium to generate libraries, sequenced and processed as indicated in the methods. Individual cells have been quality controlled, removing high count libraries/cells and those with excessive mitochondrial transcripts. **A.** Clustering identified 19 cell populations. **B.** Markers for cell-types found in the mouse immunes were collated and used to identify all clusters.

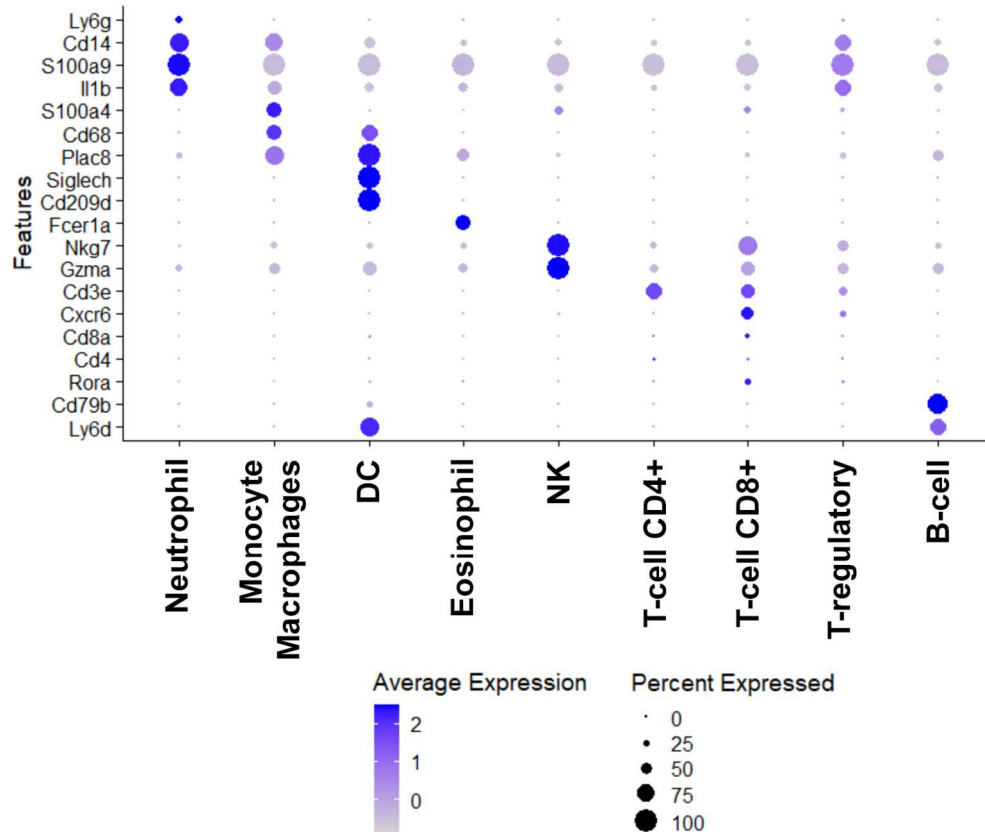


Figure 1.9. Identifying cell types in the CD45+ enrichment isolation using published markers. Markers for mouse immune cells were collated and used to identify the clusters identified by Seurat. The major immune cell classes were identified including neutrophils, subpopulations of mononuclear phagocytic cells (monocytes, macrophages and dendritic cell) and lymphoid cells. Expression level is by color and the fraction of cells expressing the gene is indicated by the size of the dot (scales included).

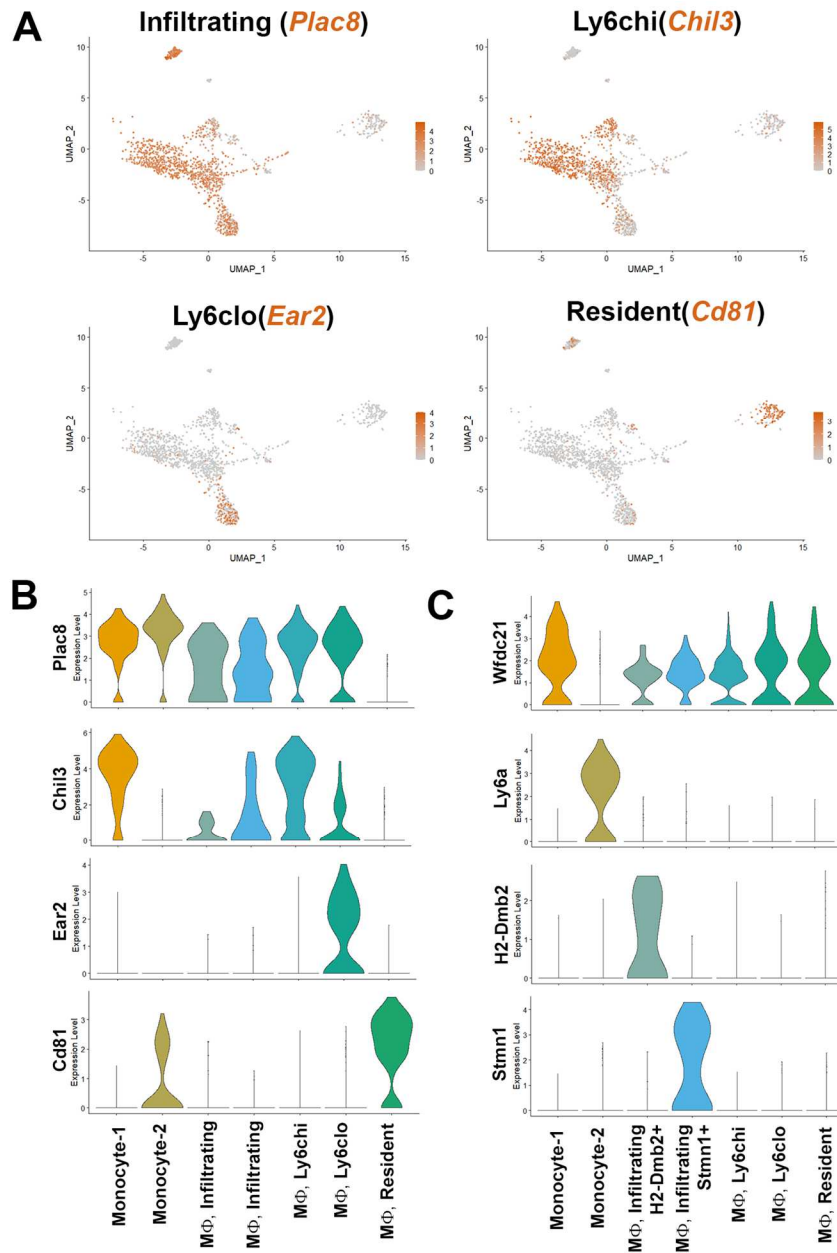


Figure 1.10. Subdividing monocytes/macrophages into resident and infiltrating populations. The putative macrophage clusters were isolated from the combined dataset and markers for the sub-population defined with Seurat. A. Feature plots of gene expression as indicated to subdivide the cells into infiltrating Ly6chi and Ly6clo monocyte/macrophages and tissue resident macrophages. B. Expression level per

markers for infiltrating versus resident macrophages. C. Markers for novel populations identified in the monocyte/macrophage super-cluster.

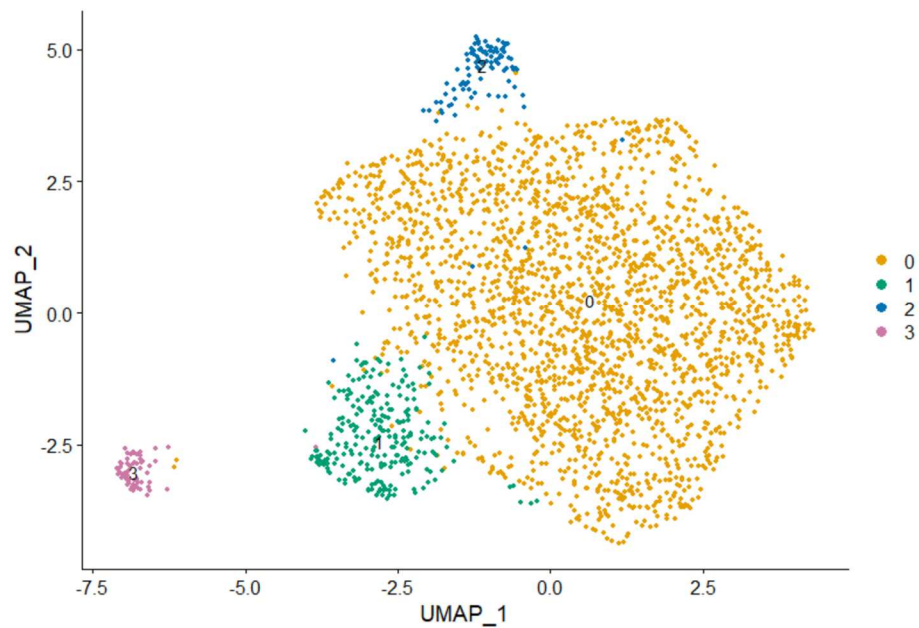


Figure 1.11. Four neutrophil subtypes identified in wild-type mice after sham surgery. Cell from whole kidney were disaggregated and separated by differential centrifugation and CD45+ FACS for processing with 10X Chromium to generate libraries, sequenced and processed as indicated in the methods. Neutrophils were classified by *S100a8*, *S100a9* and *Ly6g* and copied to a new dataset and in which principal components were calculated, clustered, and projected into UMAP space. There were four clusters of neutrophils identified.

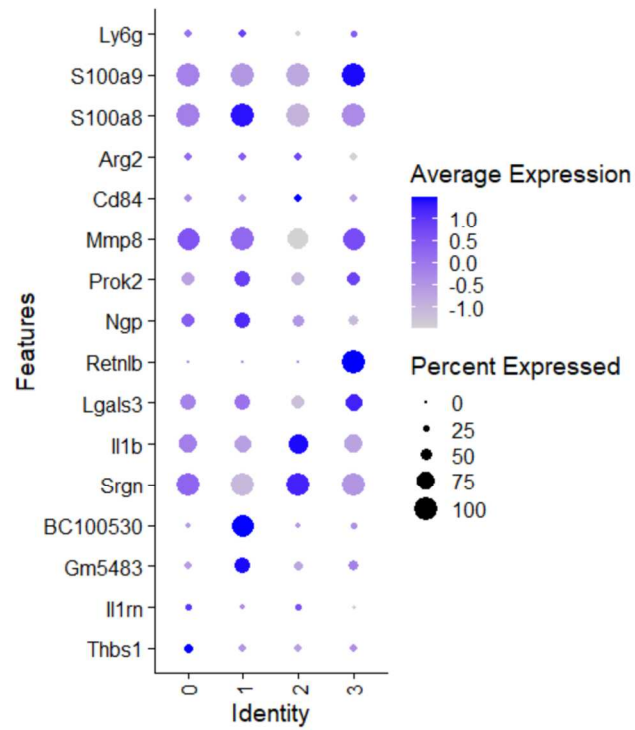


Figure 1.12. Markers of neutrophil subpopulations identified in wild-type mice after a Sham surgery. scRNASeq was performed as described in the methods on cells isolated from uninjured kidneys and enriched by CD45+ FACS. Marker genes were identified using differential expression analysis in Seurat and curated here with expected neutrophil markers (*S100a8*, *S100a9* and *Ly6g*), neutrophil activity markers (*Ngp*, *Mmp8* and *Prok2*), and control markers for myeloid-derived suppressor cells (*Arg2* and *Cd84*).

Chapter 2. Neutrophil diversity and cellular census of kidneys after ischemic injury

Introduction

AKI and early immunological responses.

Neutrophils and NKT cells are the earliest immune cells recruited to the kidney following IRI(3, 17, 19). Neutrophil recruitment is CXCL2(MIP-2) dependent(48). Once in the kidney, neutrophils can undergo NETosis (neutrophilextracellulartrap-osis) contributing to tubular necrosis(18, 32, 33, 73). NETosis is a regulated expelling of uncondensed DNA from neutrophils to trap damage and pathogens associated molecular patterns (DAMPs and PAMPs) at sites of infection and injury(31, 74). Consistent with this finding, depletion of neutrophils or inhibiting NETosis reduces tubular necrosis and plasma creatinine levels 24 hours after injury(32, 48). Importantly, the work on NETosis in AKI has used severe injury models (28-35 min IRI) predominantly in C57BL/6 mice. After severe injury in C57BL/6 mice, there is poor recovery of kidney function and acute mortality suggesting extreme kidney injury and kidney failure in these models(32, 33). Thus, the immunological processes in these models reflect an extreme. The role of the severity of injury in modulation of neutrophil biology during AKI is poorly understood. In our work we have shown that in *our model of moderate injury (22 minutes ischemia)* in 129Sv/Ev (wt, taconic) mice, we can model moderate AKI(46, 75). This is indicated by an elevated serum creatinine (~2x baseline at 24 hours), the presence of infiltrating neutrophils in the kidney, cast formation in renal tubules and tubular necrosis. Furthermore, in *our model of severe injury (30 minutes ischemia)*, we observe further elevated serum creatinine (~10x baseline at 24 hours), an increase in neutrophil infiltrates and increased numbers of casts and tubular necrosis(21, 75). Importantly, in this severe model, serum creatinine levels return to baseline after 1 week indicating recovery of renal function. Thus, these two models can be used to understand the impact of the severity of

injury. I hypothesized that the severity of injury dictates the types of neutrophils recruited to the kidney to shape recovery of kidney function.

Neutrophil migration into injured tissue is driven by surface proteins on endothelial cells and neutrophils. Generally, selectins (e.g. E-selection) on endothelial cells (ECs) interact with the P-selectin, PSGL1, on neutrophils as they roll along ECs. This interaction stimulates adherence through neutrophil integrins. These integrins bind to endothelial ICAM-1 and ICAM-2 upregulated by proinflammatory cytokines such as IL-1 β . Neutrophils may then crawl along the endothelial cells until identifying an EC junction. Once at an EC junction, vascular permeability is increased through an ICAM-1/2 dependent signaling cascade that leads to the turnover of the tight junction protein VE-Cadherin. Extravasation is somewhat of a misnomer in that migration of neutrophils through the EC layer can be tightly sealed with Rho dependent actin rings forming at the site of neutrophil diapedesis. Migration into the tissue further requires transiting the basement membrane and spaces between pericytes to the site of injury. In some cases, this could be hundreds of microns away(28).

In the kidney there are at least two major flavors of capillary beds-glomerular and peritubular. Neutrophils associate with EC in both beds and only extravasate in peritubular capillary beds. Neutrophil adherence/tethering in glomeruli is driven by PSGL1-selectin and integrin-ICAM-1 complex formation and is reinforced by patrolling monocytes. Neutrophils and monocytes together lead to glomerular inflammation and injury. In the peritubular capillary beds, the same molecular players are present, with additional stimulus from cytokines (tissue and neutrophil derived) and the injury dependent upregulation of CD44 on neutrophils that facilitates extravasation via VAP-1 on pericytes(76).

In sterile injury, such as acute kidney injury (AKI) it is thought that neutrophils are recruited to the damaged tissue directly by damage associated molecular patterns

(DAMPs) and by chemokines released by injured cells and resident immune cells. Neutrophils recognize DAMPs, including histones, DNA, n-formyl peptides, etc. in a toll like receptor dependent manner(74). Neutrophils are also recruited to sites of injury and inflammation by chemokines and lipid signaling molecules released by tissue resident immune cells and damaged tissue cells (e.g. keratinocytes, and endothelial and epithelial cells). For instance, in humans the neutrophilic chemokines CXCL8, CXCL1, CXCL2 and leukotriene B₄ (LTB₄) are made and released in the kidney following AKI. In mice CXCL1, CXCL2 and CXCL3 are functional homologs of CXCL8. Blocking CXCL1, CXCL2 or LTB₄ in mice, reduces neutrophil infiltrate, kidney injury and improves kidney function. Neutrophils also make a repertoire of cytokines and chemokines that can further drive an inflammatory response including, but not limited to, the recruitment of additional neutrophils, monocytes and macrophages(18, 22, 77).

In this work neutrophil diversity in AKI is uncovered and the cytokine mechanisms that may be involved in driving this diversity of neutrophils and their transcriptional programs is elucidated. It is hypothesized that the severity of ischemic injury and reperfusion specifically affects a cellular response that correlates with recovery of kidney function. Specifically, the severity of injury affects the behaviors and census of neutrophils to affect recovery of kidney function. The following work will demonstrate 1) the full diversity of neutrophils and their transcriptional programs associated with AKI, 2) the proportions of these subpopulations in AKI, 3) the impact of the severity of injury on these proportions and 4) a possible role for an underappreciated CXCR2 ligand.

Results

Quality of RNA libraries during ischemic injury

Ischemia reperfusion injury of the kidney causes significant damages to the tubules, especially the S3 segment of the proximal tubule highlighted by a loss of

brushborders and necrosis (**Figure 2.1**). To ensure that high-quality libraries could be generated from damaged tissue, the number of reads, reads per cells and the percentage mitochondria were compared between severe injury and a sham surgery. The injury did not appear to alter the quality of the libraries (**Figure 2.2 versus 1.1**).

Tubular epithelium expression of injury markers increases following ischemia

To test if there is detectable injury in the kidney, vibratome sections were stained with the injury marker KIM-1(*Havcr1*) and the brush border(F-actin) marker phalloidin, and imaged by confocal microscopy. KIM-1 staining was detected in a subset of proximal tubule S3 segments following 6 hours of reperfusion after severe or moderate ischemia (**Figure 2.1**). Furthermore, the two injuries can be discerned by microscopy. This would suggest that transcriptionally there should be an indication of injury in the tubular epithelium. The normalized and scaled expression matrices from whole-kidney single-cell isolations after severe and moderate injury and ~6 hours of reperfusion were aligned with the Sham dataset described in chapter 1. Cluster labels from chapter 1 were also transferred. With ischemia there was an expected increase in immune cells, most significantly neutrophils (**Figure 2.3**). These will be discussed in detail below.

The expression level of tubular injury markers in the epithelium of injured versus sham surgery was used to assess tubule damage with moderate and severe injury (**Figure 2.4**). As expected, there was *Kim-1/Havcr1* expression, albeit very low, in the S3 of the proximal tubules. There was also expression of *Lcn2* (NGAL) in the LOH and intercalating cell-a of the collecting duct. This is similar to a previous report with a mouse *Lcn*-reporter strain that identified *Lcn2* expression in the LOH and intercalating cells of the CD(78). Although with ischemia there was an increase in injury marker expression, it was harder to differentiate between the two ischemia times. Lastly, the expression levels of the pro- and anti-apoptotic genes, *Bax* and *Bcl-2*, respectively, were tested. As with the injury

markers, there was little difference between moderate and severe injury and in some cell-types there was little difference between sham and injury (**Figure 2.4**).

Functional changes in the epithelium induced by injury.

Different lengths of ischemia are expected to change the transcriptional programs of the tubular epithelium as blood flow drops, nutrients fall, and metabolic by-products rise. To characterize the cellular response of the kidney epithelium to ischemic injury, pathway analysis comparing the injured epithelial cells to the uninjured epithelial cells was performed on the whole kidney isolation. *Positive* differentially expressed genes of clusters from individual tubule types, were analyzed by pathway analysis in ReactomePA or by using clusterProfiler (79).

Endothelium.

The endothelium, after a sham surgery, is expressing genes for pathways associated with metabolism including glycolysis, oxidative phosphorylation and gluconeogenesis. With moderate injury this shifts to a population of cells that has upregulated pathways associated with toll-like receptor (TLR) regulation and Rho GTPase driven NADPH Oxidase activity (**Figure 2.5**). After severe injury, the endothelium does not change significantly except for a hint of TLR regulation (**Figure 2.5**).

Sub-segments of the nephron.

The proximal tubule is damaged in ischemic AKI. With severe injury, brush borders are lost, and necrosis is visible in the outer stripe of the medulla-where the S3 segment is found (**Figure 2.1**). The S1 subsegment was, at baseline, expressing a suite of transporters and maintaining cell-cell contacts and communication. Following moderate injury there was little change. After severe injury there were still few changes-only an

indication of TLR pathway upregulation (**Figure 2.6A**). The S2 segment was metabolic at baseline but responded to the ischemia with stress pathways and readying cell division through dissolution of the centrosome and regulation of the cell cycle (**Figure 2.6B**). The S3 segment was like the S1 segment at baseline and had an abundance of transporters upregulated. After moderate, the S3 segment transitioned to pathways associated with ECM organization including the assembly of collagen fibrils. For both moderate and severe injury the S3 segment had upregulation of TLR pathways (**Figure 2.6C**). Like the S1, the S3 segment also upregulates a suite of transporters after injury. Cells of the LOH and DCT respond to the increasing time of ischemia by upregulating pathways associated with the extracellular matrix (**Figure 2.7**). Of note was an upregulation of apoptotic pathways in the DCT and CD-PC after ischemic injury (**Figure 2.8B, and 2.9**). Intercalating cells did not significantly upregulate pathways in either moderate or severe injury.

Injury induced expansion of immune cells

To determine how ischemic injury affects recruited immune cells, the relative percentage of immune cells from injured CD45+ enrichment isolations was calculated (**Figure 2.10 and 2.11**). As expected, the CD45+ enrichment yielded more neutrophils, NK cells and macrophages (**Figure 2.10 and 2.11**). The monocyte populations increased dramatically following the moderate 22-minute IRI. Compared to the 30-minute IRI, there was also more NK cells in the 22-minute IRI. In contrast to the 22-minute IRI, there was a dramatic increase in infiltrating pro-inflammatory Ly6chi monocyte/macrophages after 30-minutes of ischemia (**Figure 2.11**).

Injury expands neutrophil subtypes in a severity of injury dependent manner

To determine if ischemic injury alters the sub-populations of neutrophils recruited to the kidney, neutrophils were taken from the whole kidney and CD45+ enriched datasets from the different ischemic injuries and sham condition and aligned with Seurat. To facilitate downstream analyses, this was combined with cells classified as neutrophils from whole blood single cell isolation for both ischemic times (**Figure 2.12**). The whole blood isolation contained clusters of neutrophils with Hbb-bt expression. This suggests they may be cells that have phagocytosed red blood cells. To avoid hemoglobin contributing to the identification of neutrophil subtypes associated with the kidney, these cluster were excluded. After combining these datasets and processing in Seurat, the number of neutrophil clusters expanded from the four described in chapter 1 to fourteen transcriptionally defined neutrophil populations (**Figure 2.12**).

A new marker panel was generated from conserved genes to address the new clusters of neutrophils (**Figure 2.13**). Some of the neutrophil populations described in chapter 1 were uncovered in the combined dataset. For instance, the cystatin homolog *BC100530* is a marker for cluster 7 and was a marker for cluster 1 in chapter 1(**Figure 2.13**). Overall, several novel populations were added with the inclusion of both the blood and injury scRNASeq datasets. New group of cells expressing markers of MHC I antigen presenting or MHC II antigen presenting markers were detected and clustered in cluster 11 or 8 respectively. Even with the removal clusters with high hemoglobin transcript as described above, cells that may have phagocytosed RBCs, based on the preponderance of hemoglobin transcripts, were detected in cluster 12-a cluster found predominantly in the blood preparations (**Figure 2.13**). Based on both their position in UMAP space (**Figure 2.14**) and their expression of common markers (**Figure 2.15**), it is possible that clusters 1,6,4,2,5 and 13 are a continuum of the same or similar neutrophils from less-activated (low *Ltf* and *Camp*) to active and transmigration competent (high *Ltf*, *Camp*, *Prok2*,

Cd177 and *Mmp8*). CXCR2 ligands, *Ccr11* and *Il1b* were highly expressed in cluster 9 and 3-cytokine rich populations. To control for MDSC contamination, the new clusters were checked for *Cd84* and *Agr2* expression. Of the 14 clusters, cluster 6 had higher levels of these markers and may represent MDSC cells. Based on these analyses, working classifications were defined for the 14 clusters and a sort order was established to align putative connectedness between the clusters (**Figure 2.13** and **Table 2.1**).

To test if neutrophil subpopulations are sensitive to the severity of injury, the fraction of each cluster in the sham surgeries and the ischemic injuries were compared (**Figure 2.14**). Cluster 8 (antigen presenting), a cluster of cells enriched for transcripts involved in antigen presentation was found in its greatest proportion with 22-minute IRI. In contrast cluster 13 (activated), is a cluster expressing *Ltf* (a marker of activated neutrophils) mostly associated with 30-minute IRI (**Figure 2.13**).

The kidney affects neutrophil subtype proportions and transcriptional programs

The microenvironments of the kidney are expected to induce specific population of neutrophils, as seen in cancer and cardiac ischemia. Following ischemia, the fraction of Cluster 8, 9 and 10 is high in the kidney and negligible in the blood (**Figure 2.14**). This suggests these populations may be induced by the kidney milieu and are not readily found in the blood.

The transcriptional program of the neutrophil subpopulations may also be sensitive to the kidney milieu. To test for this, pathway analysis with ReactomePA was performed on the combined neutrophil dataset in two ways. The first approach determined the markers of a given cluster relative to the other clusters within a condition and compared those *upregulated pathways* for clusters between conditions (e.g. in the blood versus in the kidney, **Tables 2.2 and 2.3**). The second was to ask how a given cluster was different between two conditions (e.g. in the blood versus in the kidney **Tables 2.5 and 2.6**). As

the two ischemia times may also alter the transcriptional state of neutrophils in the blood, a differential expression and ReactomePA analysis was performed to assess changes in circulating neutrophils between the different lengths of ischemia as well. As expected, the upregulated pathways of the 14 clusters from neutrophils in the blood were different than those isolated from the kidney (**Tables 2.2 and 2.3**). More striking though, was the change in pathways in neutrophils associated with the kidney when comparing the two ischemia times. Neutrophils from across multiple clusters with 22-minute IRI were expressing genes associated with antigen presentation, pattern recognition and IL-1 signaling (**Table 2.2**). This contrasts with neutrophils from 30-minute IRI, who were expressing genes associated with reactive oxygen detoxification and/or E-selectin and vascular wall interaction, with minimal antigen presentation and IL-1 signaling (**Table 2.3**). Directly comparing the two ischemia times further demonstrates the unique effect moderate and severe injury have on upregulated pathways in neutrophil clusters. In 22-minute IRI multiple clusters are upregulating antigen processing pathways, in contrast to 30-minute IRI in which platelet activation was upregulated in many clusters (**Table 2.4**).

To assess how a specific population changes once in the kidney each cluster was also directly compared to itself between the blood and the kidney. These analyses demonstrate a further shift in the transcriptional program of each neutrophil cluster and shows that these changes are sensitive to the severity of the ischemic injury (**Tables 2.5 and 2.6**). Comparing between neutrophil clusters localized to the blood or after 22-minute or 30-minute IRI, neutrophils in the blood were broadly upregulating Rho GTPase pathways suggesting motile neutrophils (**Table 2.5 and 2.6**). Neutrophils prepared from the kidney following 22-minute IRI, consistently upregulated TLR pathways and to a lesser degree vascular wall interaction pathway (**Table 2.5**). With 30-minute IRI, the neutrophils, across clusters, either upregulated metabolism or detoxification of reactive oxygen pathways and increased pathways involving interactions with the vascular wall by E-

selectins (**Table 2.6**). As with the previous analysis the kidney milieu dramatically impacts the transcriptional program. Furthermore, the transcriptional program was uniquely impacted by the degree of injury.

Recruitment of neutrophils to the injured kidney via the CXCR2 axis

The recruitment of neutrophils to injured tissue is dependent upon a combination of cytokine signaling and pattern-recognition. In ischemic AKI there is a clear requirement for ligands of the CXCR2 cytokine axis(44, 46, 80-82). To test for an association of CXCR2 signaling with the recruitment of neutrophils and determine probable source(s) of this signaling, the expression of CXCR2 ligands was assessed in cells isolated from the kidney. This included transcripts for the CXCR2 ligands *Cxcl1*, *Cxcl2* and *Cxcl3* (*Cxcl5* was not detected in these data, **Figure 2.15**). As expected *Cxcl1* and *Cxcl2* are expressed in several cellular compartments with 22-minute IRI. The highest *Cxcl2* expressing cells were neutrophils followed by macrophages, neither of which expressed *Cxcl1* (**Figure 15A**). There was low expression of *Cxcl1* in epithelial cells of S1 and S3 subsegments of the proximal tubule and in the intercalating cells of the collecting duct (**Figure 2.15B**). With 30 minutes of ischemia injury the neutrophils continued to be the highest expressing cells. Additionally, in contrast to 22-minute IRI, S1, S2 and S3 subsegments of the PT and the LOH expressed *Cxcl2*. Surprisingly, there was an increase in *Cxcl1* and *Cxcl2* transcript in ~20% of the secretory granular cells of the juxtaglomerular apparatus-both were expressed above the levels in other subsegments of the nephron including the S3 segment of proximal tubule (**Figure 2.15B**).

After 30 minutes of ischemic injury there was an unexpected expression of *Cxcl3* in ~30% of neutrophils (**Figure 2.15A**). Expression of *Cxcl3* by specific neutrophil clusters, was investigated in neutrophils from the kidney. *Cxcl3* was most highly expressed in neutrophil clusters 3, 9 and 11 with intermediate levels in clusters 6, 0, 10, 7 and 12

(**Figure 2.16B**). There was robust expression of *Cxcl2* and *Cxcl3* in cluster 9, irrespective of severity of injury, suggesting a cytokine active population of neutrophils. The expression of *Cxcl3* in response to severe injury and in specific neutrophil subtypes suggests a unique role for *Cxcl3* in signaling with CXCR2 in severe AKI.

Neutrophils in AKI share markers with neutrophils in cancer

If the neutrophil clusters defined here are robust and significant, they should be detectable in other mouse datasets, especially pathologies expected to include neutrophils. To test this, a publicly available scRNASeq dataset from a mouse model of breast cancer metastasis was processed in Seurat and clusters identified(58). These clusters were screened with the neutrophil panel described in **Figure 2.13** to identify similar neutrophils populations in AKI and cancer (**Figure 2.17**). The neutrophil clusters identified in cancer were 0,1,2,4,6 and 8 (**Figure 2.17**), most closely resemble the AKI super-cluster defined by 1,2,4,5 and 13 (**Figure 2.12 and 2.13**). Furthermore, the remaining cluster in the cancer dataset, had analogous populations in AKI (**Figure 16B and A**). The putative motile (cluster 7 in AKI) and antigen presenting (cluster 8 in AKI) had similar population in cancer (clusters 5 and 7 respectively). Cluster 3 in AKI and cancer also appear similar yet expression of *Cd84* and *Arg2* in the cancer cluster suggest these are the G-MDSC described previously(58).

Discussion

There was little difference in expression of injury makers between the two ischemia times. For instance, less than 20% of the S3 segment of the proximal tubule upregulated *Havcr1* (KIM-1) although it was detectable by confocal microscopy as well as obvious differences in tubular necrosis between the two ischemia times. *Lcn* was upregulated in tubule subsegments-similar to previous reports-but did not discriminate between the two ischemia times. This would suggest either 1) the epithelium has not reacted differently to

the increased tissue damage, which is unlikely given the tubular necrosis seen by microscopy, or 2) that these markers are not sufficient for discriminating between the damage caused by the two different ischemia times. To explore the later possibility, pathway analysis was used to uncover differences in the transcriptional program between a sham surgery and injury. From these analyses, it was clear that the epithelium has responded by changing the complement of solute transporters, increasing pattern recognition pathways via TLR and NADPH oxidases and altering interactions with the extracellular cellular matrix. Thus, although the injury markers did not discriminate between the injury times, a *combination* of genes changing points to transcriptional shifts in the tubular epithelium that correlate with ischemia time. At least at this early time point, 6 hours after reperfusion, this illustrates the difficulty of developing biomarkers especially those that can give an indication of how much injury has occurred.

Neutrophil diversity was detected in the blood of injured mice and the kidneys of both injured and uninjured mice. There were neutrophil subpopulations specific to either the blood, kidney, or both. Furthermore, the kidney milieu drives additional transcriptional differentiation of neutrophils resulting in clear phenotypic differences between the neutrophils isolated from the blood versus the kidney. These differences are further exacerbated by the severity of ischemic injury. In severe injury, 30 minutes of ischemia, neutrophils are primed for transmigration, detoxifying a damaged tissue and are activating platelets. Additionally, cluster 9, a source of CXCR2 ligands and cluster 13, putative activated neutrophils, are proportionally increased in severe injury vs sham or moderate injury. Thus, in severe injury there is both increased signaling for infiltration via CXCR2 and an increase in activated neutrophils. With moderate injury, the neutrophils are expressing pattern recognition genes and pathways associated with antigen presentation. Furthermore, cluster 8, a cluster of cells enriched with transcripts for antigen presentation are found in the greatest numbers after the moderate injury. This suggests that these

neutrophils may be important in moderate injury. For instance, these neutrophils may limit damage through sensing with pattern receptors and modulating further immune response, such as NK infiltration, with antigen presentation pathways. Thus, a further 8 minutes of ischemia is sufficient to cause tissue damage that dramatically shifts the neutrophil response in terms of diversity and transcriptional programs.

The striking difference in the transcriptional states of neutrophils found in the kidney between the two ischemic times suggested there may be significant differences in cytokine and chemokine signaling. When comparing CXCR2 signaling between the two ischemic times *Cxcl2* is found in both IRIs and in Sham surgery, while a second ligand, *Cxcl3* is uniquely detected with the longer ischemia times. This suggests that *Cxcl2* and *Cxcl3* are acting together in severe injury. Perhaps, when both are present, neutrophils are more likely to infiltrate the kidney and lead to further tissue damage. Interestingly, this ligand is expressed almost exclusively in a subset of neutrophils. This suggests a role for a previously underappreciated CXCR2 ligand that is produced by a subset of neutrophils. However, these findings have two important limitations: we do not know 1) how much of this transcript is translated into active cytokines and 2) what the effect of 20% of proximal tubules expressing CXCR2 ligands versus most of the infiltrating neutrophils? For instance, by a multiplexed bead assay, CXCL2 was *upregulated* after severe injury and 6 hours of reperfusion versus a sham surgery-suggesting the complexity is not fully address by these data(83). Confirming the importance of *Cxcl3* in CXCR2 signaling and neutrophil recruitment during AKI will require further exploration of these cytokines in the kidney using microscopy and/or a multiplexed bead assay and neutralization experiments.

The origin of CXCR2 ligands changed between ischemia times. In both injuries, the highest expression is in neutrophils and secondly, macrophages. Importantly, CXCR2 ligands are also coming from the epithelium. What was unexpected was a shift in sources of CXCR2 ligands in the epithelium. With 22-minute IRI the ligands were expressed in the

proximal tubule. With 30-minute IRI, the expression dramatically shifted to the secretory granular cells of the juxtaglomerular apparatus. This suggests an unappreciated role for specialized granular cells and the juxtaglomerular apparatus in responding to ischemic injury via expression of neutrophilic chemokines. Furthermore, although the expression of the cytokines was low in the granular cells (relative to neutrophils), the juxtaglomerular apparatus is poised to modulate immune cell recruitment (neutrophils) and modulate filtration and hemodynamics of the nephron. Understanding how the juxtaglomerular apparatus might function in this role could be important to uncovering new therapeutics at the junction of immunomodulation and hemodynamics of the kidney.

Ly6chi-monocyte/macrophage and the novel Monocyte-1 population are the most dramatic shifts in populations in severe and moderate injury, respectively. Although not elaborated here, their preponderance suggests an important role in the recovery of kidney function. Ly6chi-monocyte/macrophages are traditionally thought of as pro-inflammatory- in contrast to Ly6clo-monocyte/macrophages which are patrolling and involved in tissue repair(84). The correlation of a pro-inflammatory monocyte/macrophage with 30-minute IRI is not unexpected. The behavior and nature of this novel monocyte/macrophage population, monocyte-1, is unclear. With this dataset, it is possible to test for monocyte chemokines such as Ccr2 ligands, and co-conspirators to unravel this mechanism as was done here with putative role of *Cxc/3* in neutrophil recruitment in AKI.

The neutrophil diversity associated with AKI and the kidney is striking. This work is the first unbiased holistic description of neutrophil transcriptional and functional diversity in the kidney. Based on similarities in cluster markers and pathway analysis across the neutrophils there appears to be two major “super-clusters” comprised of sub clusters and a number of additional neutrophil clusters with specialized functions. The first “super-cluster” is composed of clusters 0,3,9 and 10 and the second is composed of clusters 1,4,5 and 13. From these data, the first “super-cluster” is a source of CXCR2 signaling

while the later “super-cluster” is reminiscent of a classically active neutrophil. These two “super-clusters” are joined by 6 ancillary clusters that have specific activity (e.g. cluster 8 and 11 are antigen presenting via MHCII or MHCI respectively and cluster 7 is motile). It is especially exciting that two of the neutrophil populations identified in AKI are also present in a mouse model of cancer. This suggests 1) the neutrophil diversity detected here is reproducible, and 2) these data have enough breadth and depth to capture neutrophil types seen in an orthogonal disease. The correlation of the clusters described here with outcomes in AKI suggests the complex etiologies of AKI may be founded in our poor understanding of the complexity of neutrophil biology. The neutrophil as the early hunter-killer belies their phenotypic complexity and their mechanistic impact in disease.

Methods

Animal handling and surgeries.

All surgeries were performed in compliance with institutional review and under approved protocols. Ischemic injury of mouse kidneys was performed as indicated in Chapter 4.

Isolation of single cells from injured kidneys

Isolation of total kidney and CD45+ enriched cells in injured kidneys was performed as given in chapter 1. For total kidney isolations two kidneys from one male were used as starting material. For CD45+ enriched cells, 3 kidneys were isolated from two male mice with 22 min ischemic time and reperfusion for 6 hours and 4 kidneys were isolated from two male mice following 30 min ischemia and reperfusion for 6 hours.

Isolation of immune cells from blood for scRNASeq

Immune cells for scRNASeq were isolated from blood from mice following ischemic injury for either 22 or 30 minutes after six hours of reperfusion. ~1.5 mL per condition, or ~700 uL per animal whole blood was sampled by a jugular bleed. The blood was immediately mixed with 5 mL 1x Red blood cell (RBC) lysis buffer and incubated for 10 min at room temperature and diluted with 8mL 1XPBS+1%FBS. Cells were pelleted by centrifugation at 0.4 x g for 7 minutes and resuspended in 5 mL of RBC lysis buffer. The pellet was lysed three more times for a total of 4 rounds of lysis. After the final pelleting the cells were washed in 8 mL 1XPBS+1%FBS before resuspension in 300 μ L 1XPBS+1%FBS and processed for 10x in the genomics core.

Bioinformatics

Seurat analysis was performed as outlined in Chapter 1 with Seurat v 3.1. Scripts and code are available via github. Pathway analysis was performed in ReactomePA. Gene lists were generated in Seurat using either *FindConservedMarkers* for assessing a common phenotype across genetic and injury conditions or with *FindMarkers* with different subset selections to achieve comparisons as indicated. To facilitate multiple comparison clusterProfiler was used with gene lists as well. Gene lists for differential expression analysis and used in pathway analyses were filtered for 1) a threshold of significance of $p < 0.05$ with and without corrections for multiple comparisons (as indicated in the text) and 2) ribosomal proteins were removed by gene name prior to pathway analysis. Tables of ReactomePA pathways were manually curated based on 1) the ~top 50% of gene ratios (fraction of genes in ReactomePA pathway represented in genelist) or gene hits 2) an adjusted p-value > 0.05 (in most cases it was > 0.01) and 3) dismissal of highly ranked metabolic or transcriptional pathways if criteria 1 and 2 could be met.

Generation of figures.

Plots and graphs were generated in R with Seurat, ReactomePA or custom scripts (stacked bar plots) unless otherwise noted.

Data availability.

Raw and processed data will be made available online at GEO hosted by the National Center for Biotechnology Information.

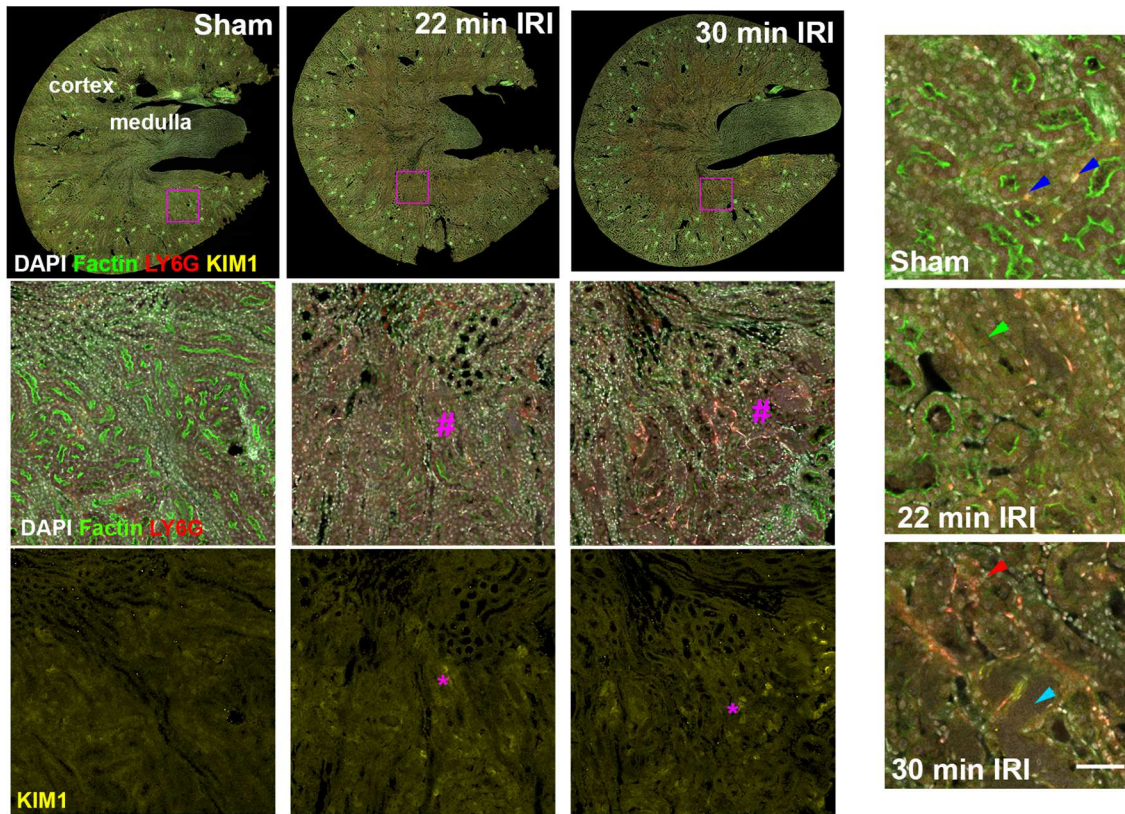


Figure 2.1. Morphological indications of kidney injury. A. Examples of IRI experiment with either 22- or 30-minutes of ischemia and 6 hours of reperfusion in wild-type mice. Sections were stained for Ly6G and KIM-1 and with phalloidin and DAPI and imaged by confocal microscopy. Insets at bottom show the injury marker KIM1 (asterisk) and loss of brushborder (pound). In small fields at right arrows indicate neutrophils in capillaries (blue) and clustering in the interstitium (red), loss of brushborders (green) and casts (cyan). Scale bar = 100 μ m.

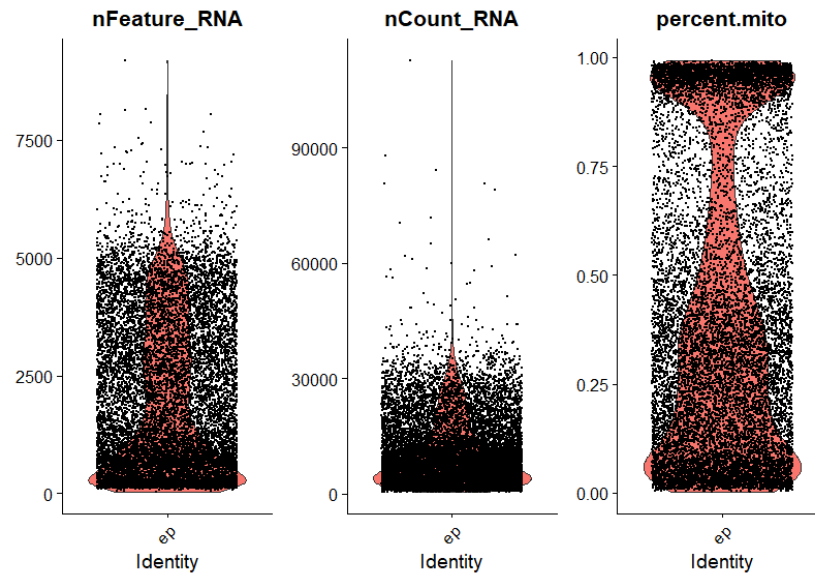


Figure 2.2. Quality control metrics in injured tissue. Total cells were isolated from mouse kidneys after 30-minute ischemia and 6 hours of reperfusion, processed on the 10X Chromium platform, and expression tables created. The expression tables were analyzed in the R package Seurat v 3.1. The number of RNAs detected (`nFeatures_RNA`), the number reads per RNA (`nCount_RNA`) and the percentage of mitochondrial reads (`percent.mito`) are plotted.

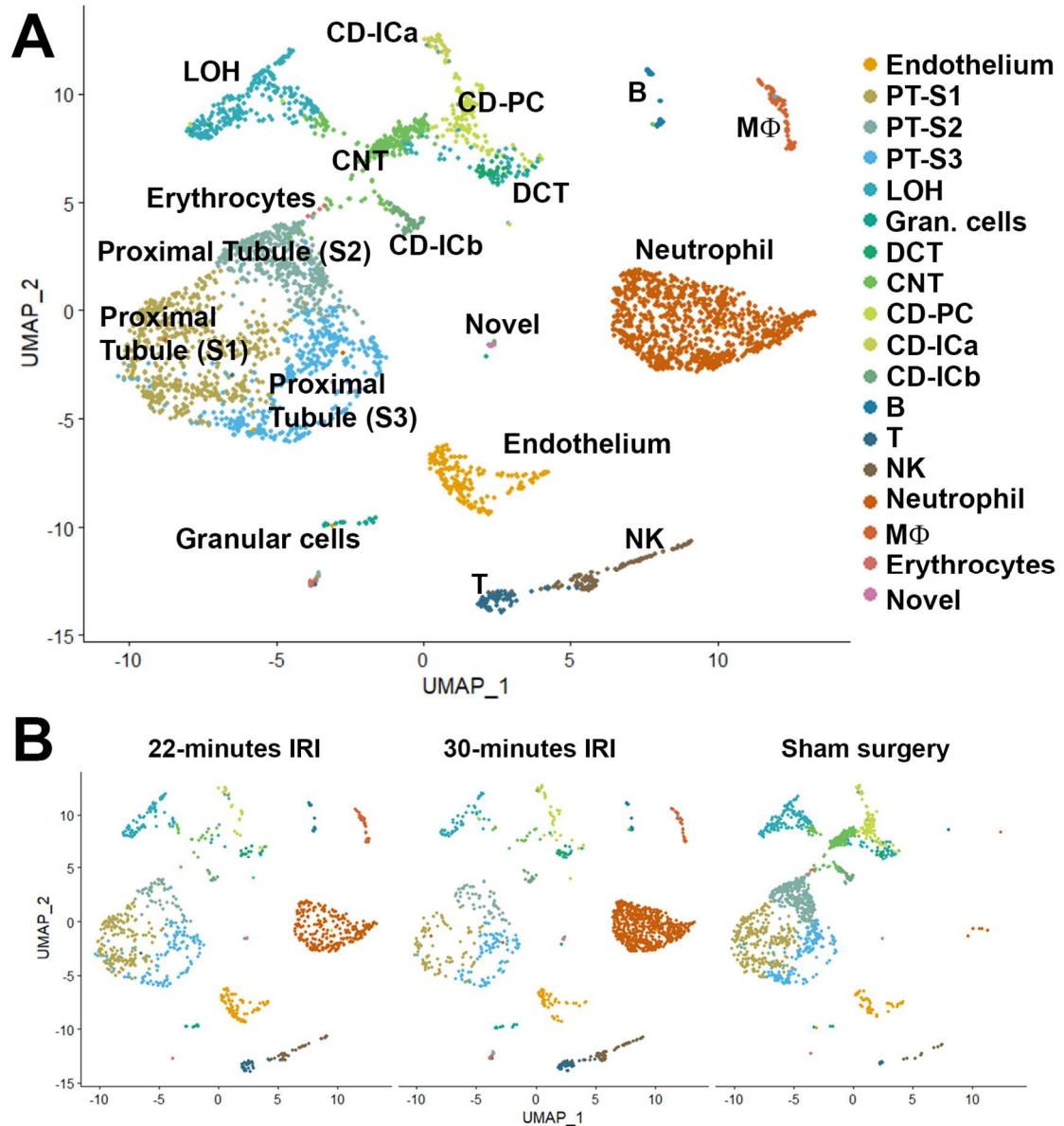


Figure 2.3. UMAP plot of all cells from whole kidney. Cells from were isolated from kidneys after sham surgery, 22- or 30-minutes of ischemia and 6 hours of reperfusion, processed for 10X chromium library generation, sequenced, and processed as indicated in the methods. Individual cells have been quality controlled, removing high count libraries/cells and those with excessive mitochondrial transcripts. Clustering identified 26 populations of cells. These cells were classified by cluster based on collated markers (Figure 1.5). Cells from the two ischemia surgeries and the sham surgery were plottd separately to show the cells recovered in each of the conditions by cell-type.

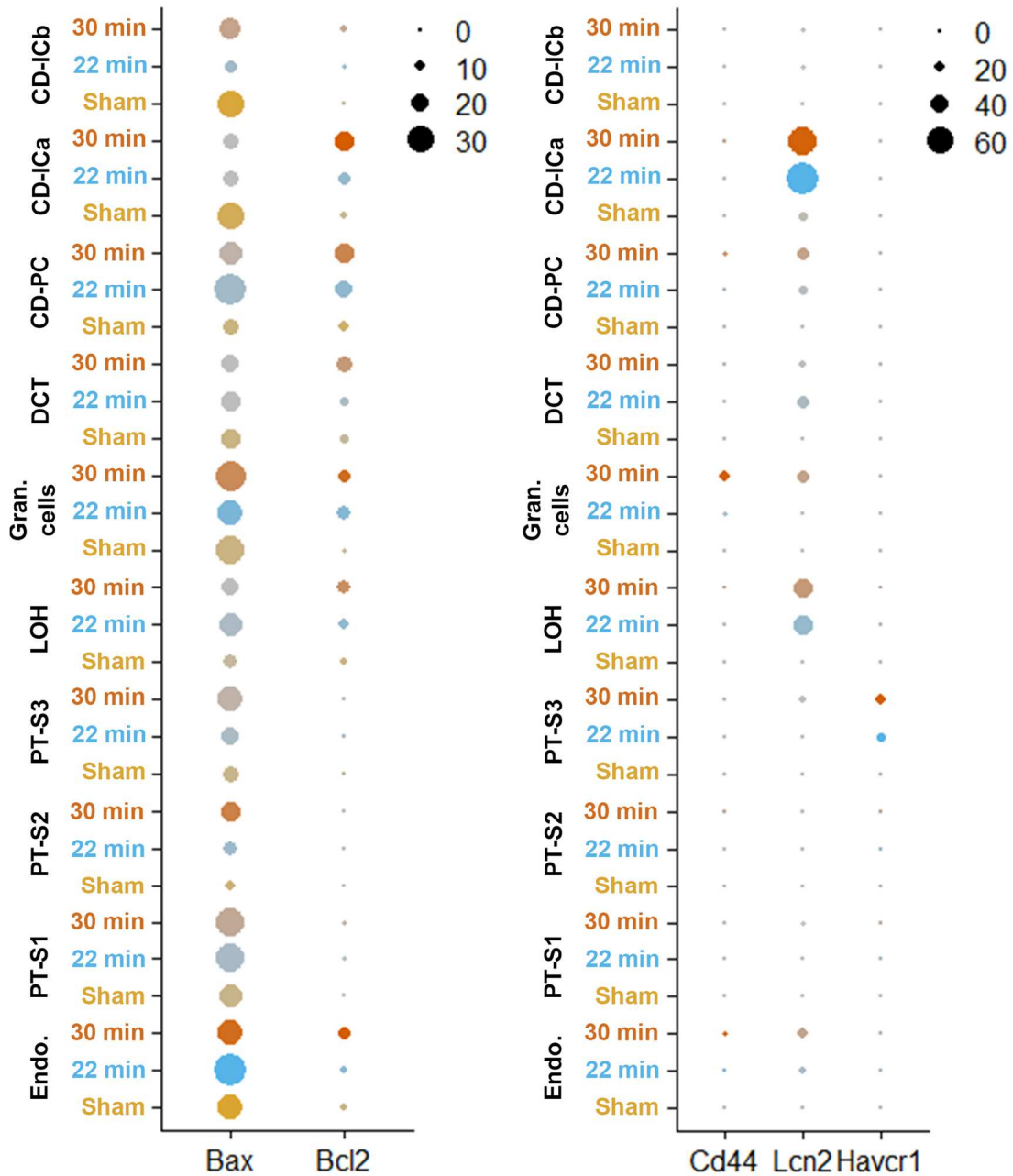


Figure 2.4. Injury and apoptosis marker expression in the kidney following ischemic injury. Injury and apoptotic marker indicate changes in kidney cells following ischemia. The proapoptotic marker *Bax* and anti-apoptotic marker *Bcl2* expression levels are given at left. The injury markers *Cd44*, *Lcn* (N-GAL) and *Havcr1* (KIM-1) are given at right. Expression level is by color and the fraction of cells expressing the gene is indicated by the size of the dot (scales as indicated).

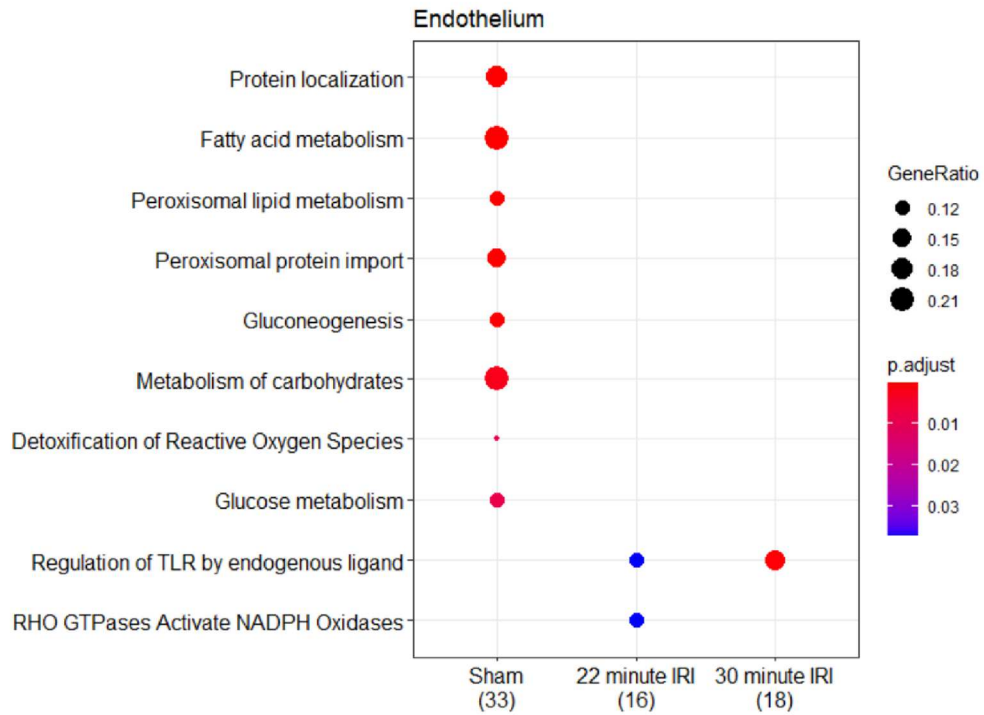


Figure 2.5. ReactomePA analysis of endothelium. Differential expression analysis was performed between endothelium in the sham surgery versus both injury condition and for either injury condition versus the sham surgery. The differentially expressed genes were limited to increased expression and corrected (Bonferroni) p-values <0.05.

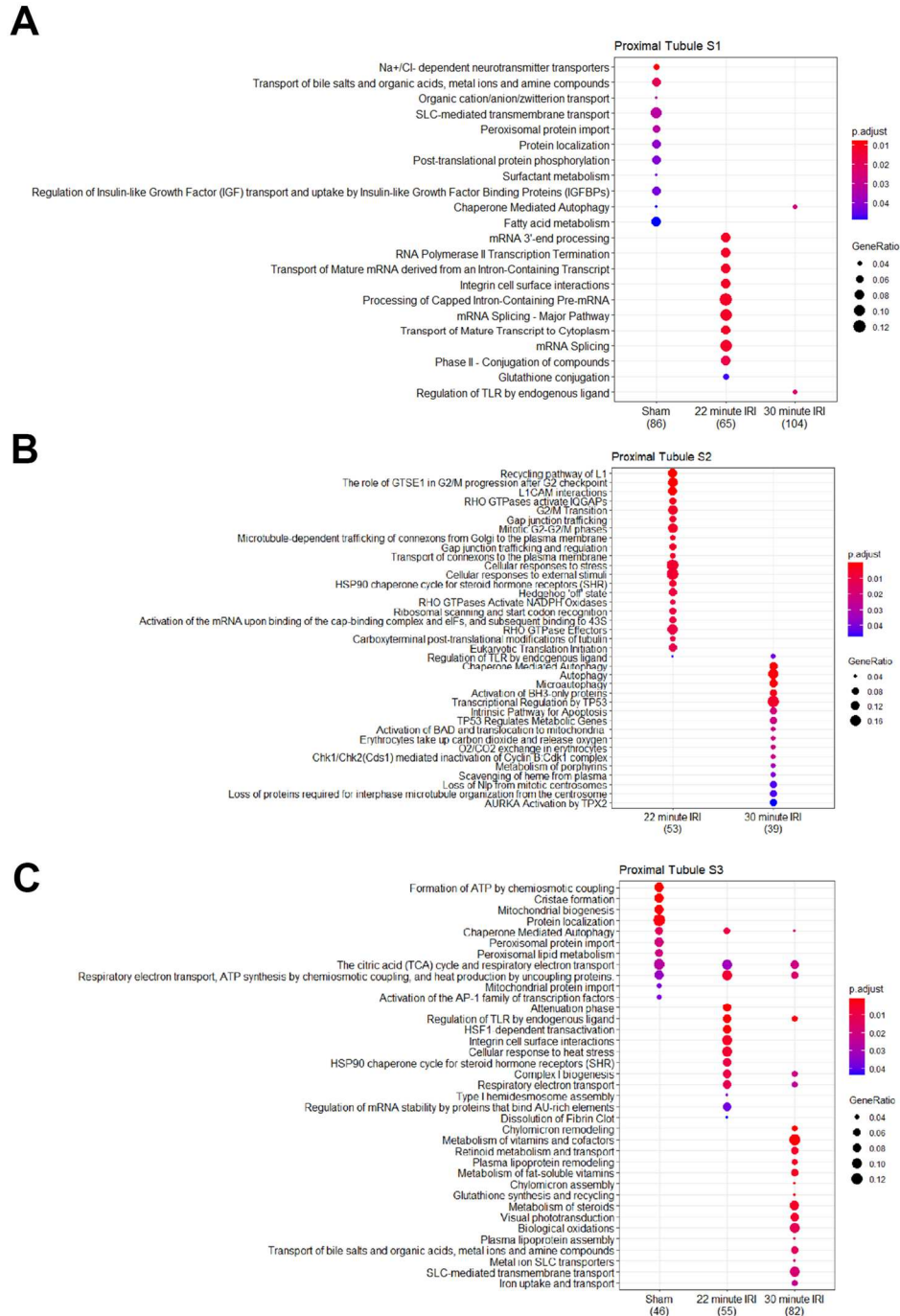


Figure 2.6. ReactomePA analysis of proximal tubule subsegments. Differential expression analysis was performed between tubular epithelium in the sham surgery versus both injury condition and for either injury condition versus the sham surgery. The differentially expressed genes were limited to increased expression and corrected (Bonferroni) p-values <0.05.

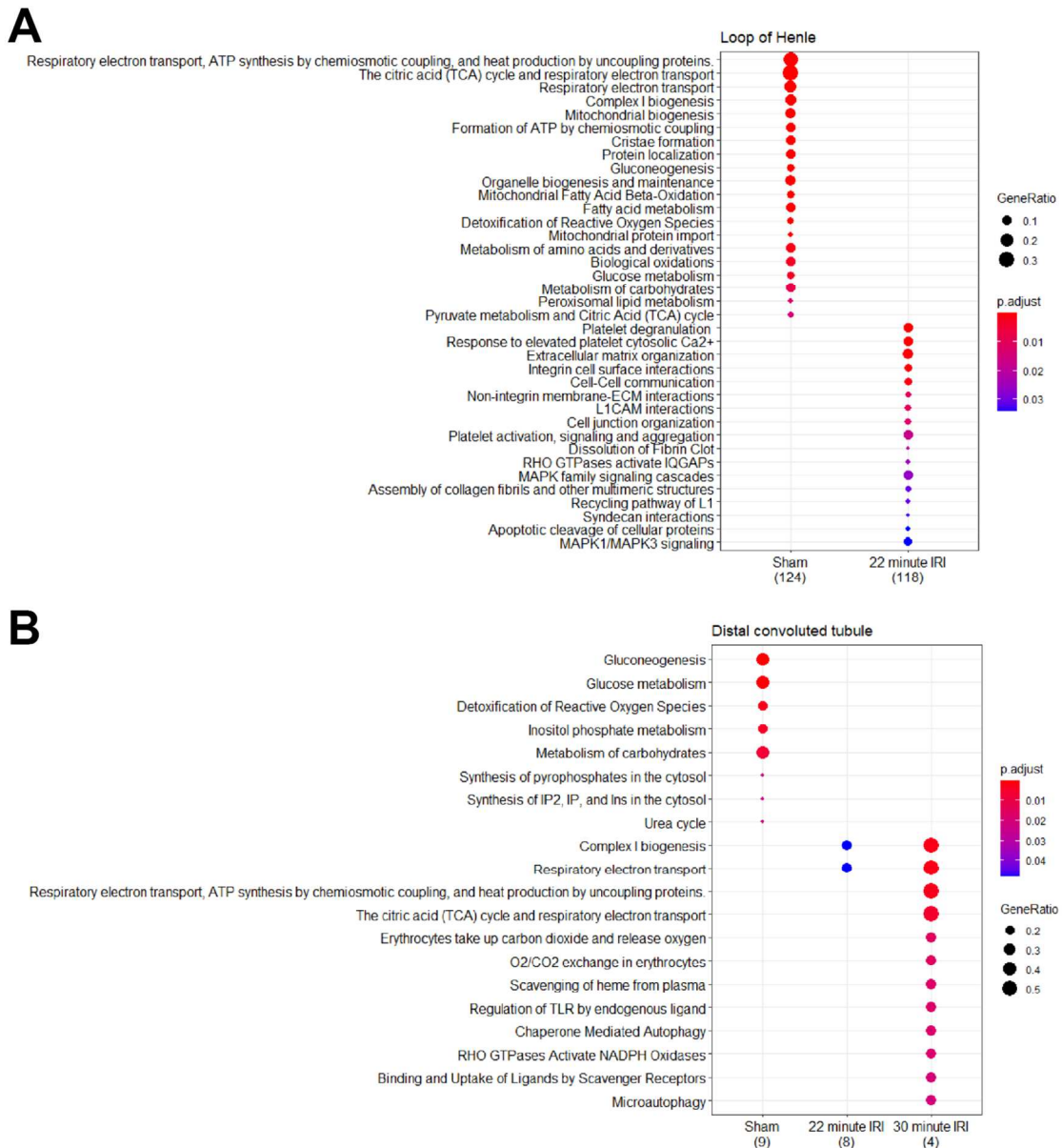
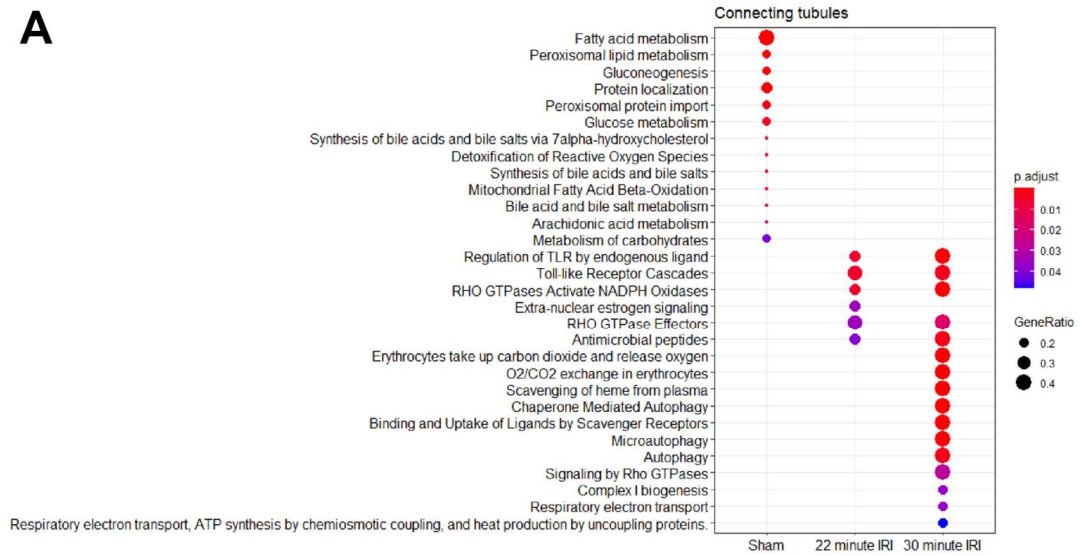


Figure 2.7. ReactomePA analysis of loop of Henle and distal convoluted tubule.

Differential expression analysis was performed between tubular epithelium in the sham surgery versus both injury condition and for either injury condition versus the sham surgery. The differentially expressed genes were limited to increased expression and corrected (Bonferroni) p-values <0.05.

A



B

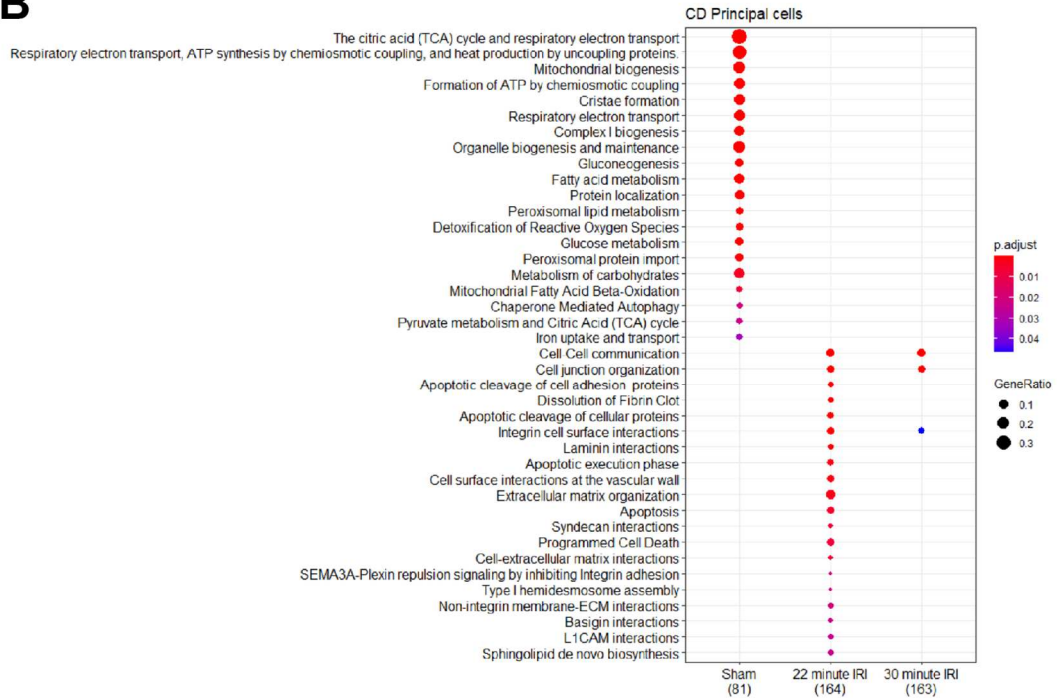


Figure 2.8. ReactomePA analysis of connecting tubules and collecting duct principal cells. Differential expression analysis was performed between tubular epithelium in the sham surgery versus both injury condition and for either injury condition versus the sham surgery. The differentially expressed genes were limited to increased expression and corrected (Bonferroni) p-values <0.05.

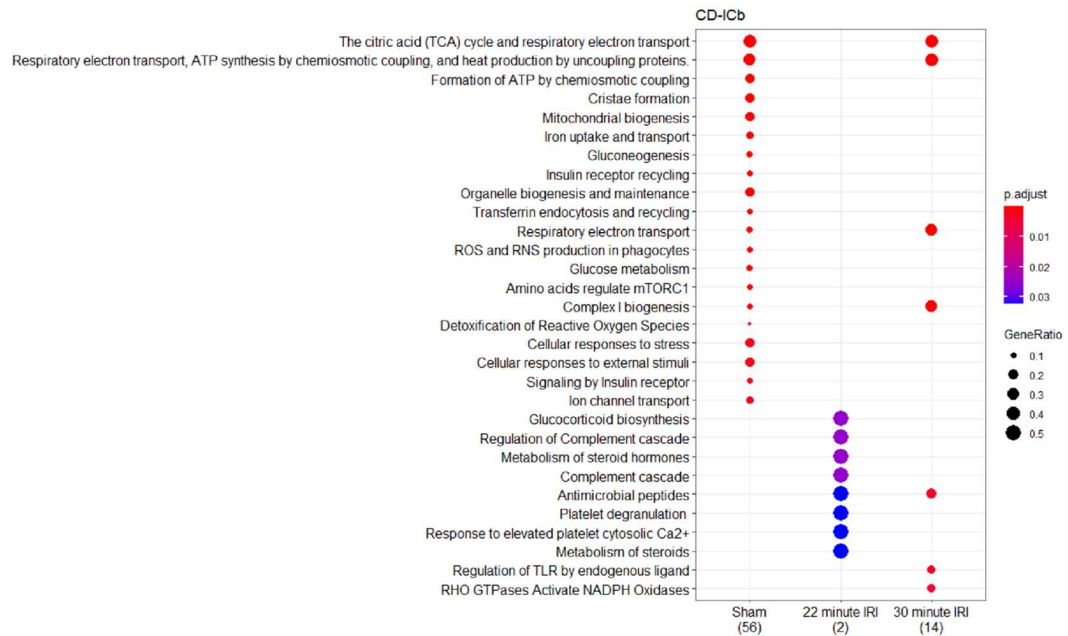


Figure 2.9. ReactomePA analysis of collecting intercalating cells A. Differential expression analysis was performed between tubular epithelium in the sham surgery versus both injury condition and for either injury condition versus the sham surgery. The differentially expressed genes were limited to increased expression and corrected (Bonferroni) p-values <0.05.

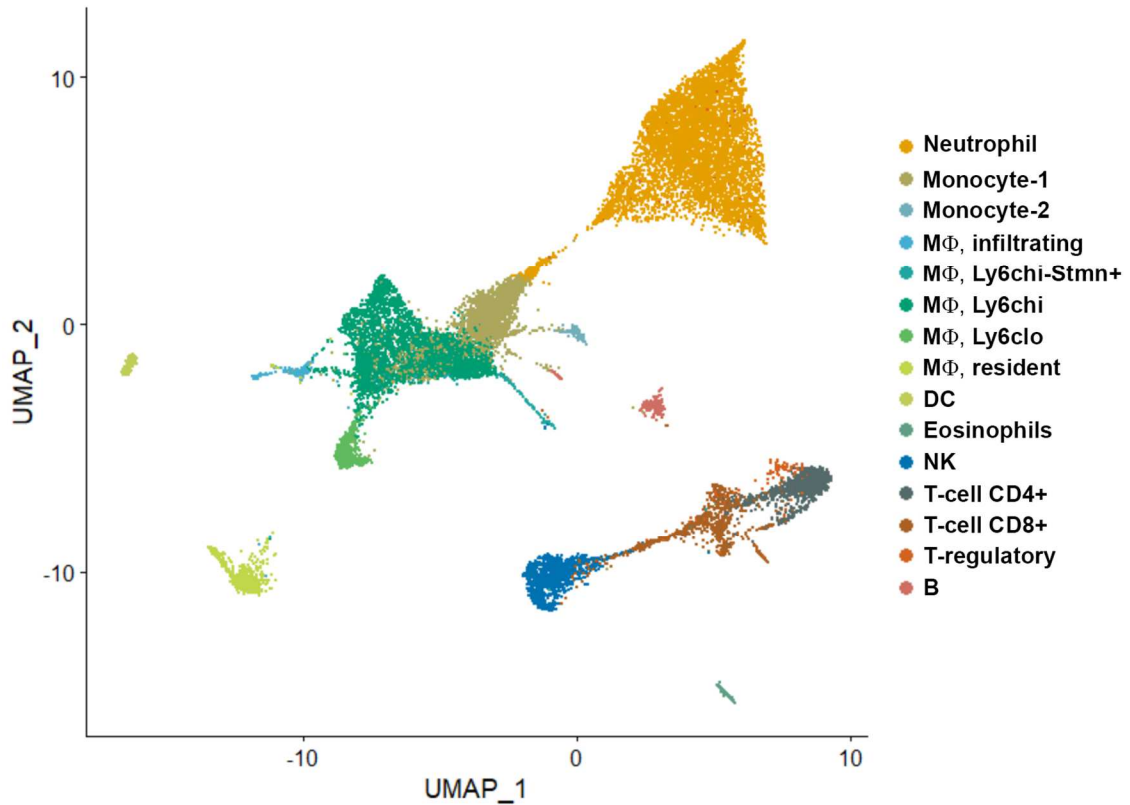


Figure 2.10. UMAP projection of classified immune cells from sham and injury surgeries. Cells from CD45+ enrichment of sham and injured kidneys were processed for scRNASeq to generate expression. The individual matrices were normalized, scaled, aligned, cluster identified and plotted in the same UMAP plot. The 22-minute ischemia added a significant number of monocytes to the combined dataset (Monocyte-1).

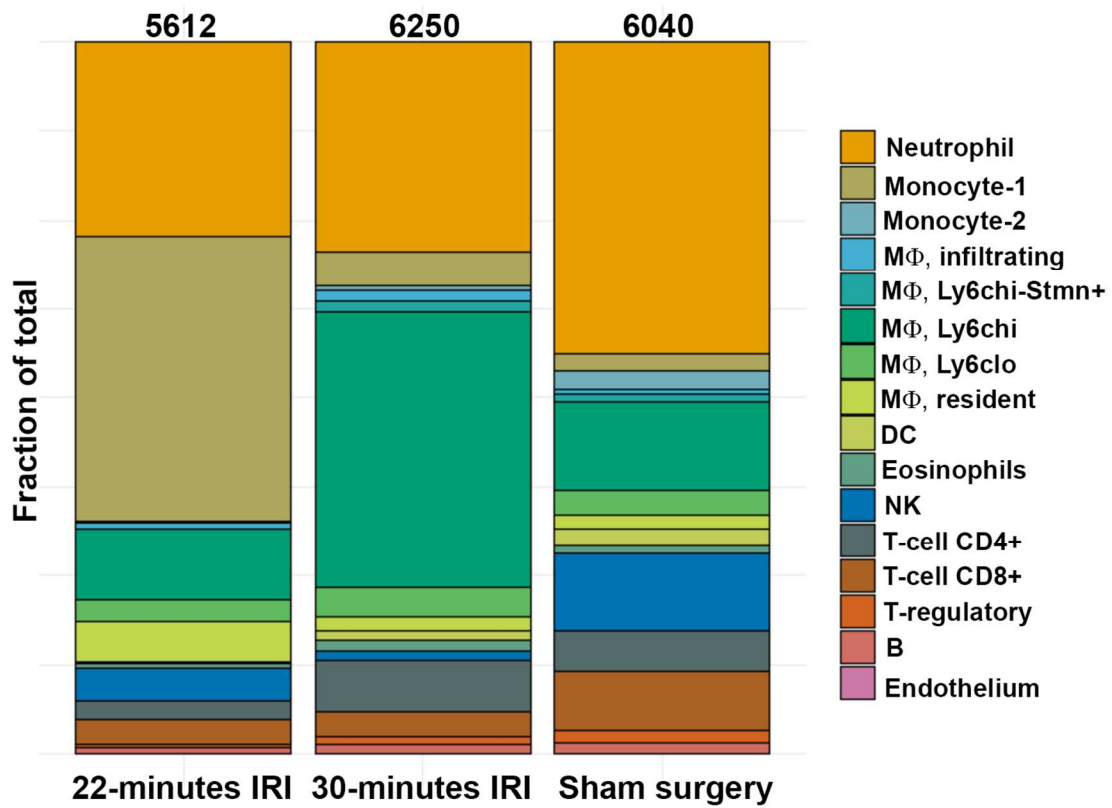


Figure 2.11. Distribution of immune cells in response to ischemia reperfusion injury. Immune cells from CD45+ enrichment isolation from 22- and 300minute IRI and sham surgery were tabulated, and fractions of total cells calculated. Total immune cells per condition is given at the top of each bar.

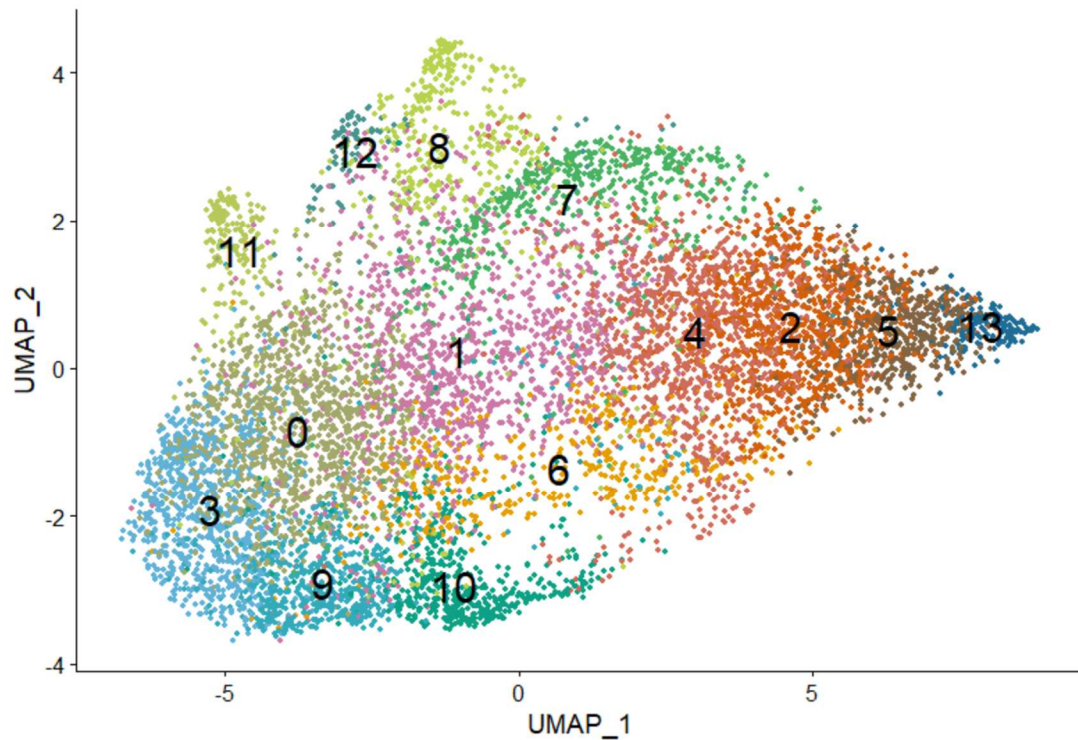


Figure 2.12. UMAP of neutrophils isolated from kidneys after sham and injury.

Neutrophils from whole kidney, CD45+enrichment, and blood isolation were combined into one dataset. Each dataset was individually normalized prior to alignment and recalculation of principal components. Neutrophils from whole kidney were preprocessed with more stringent QC parameters to facilitate combining with neutrophils from the blood and the CD45+ enrichment isolation. New clustering identified 14 clusters of neutrophils. Neutrophils from the whole kidney isolation and the CD45+ enrichment isolation are given as a UMAP plot.

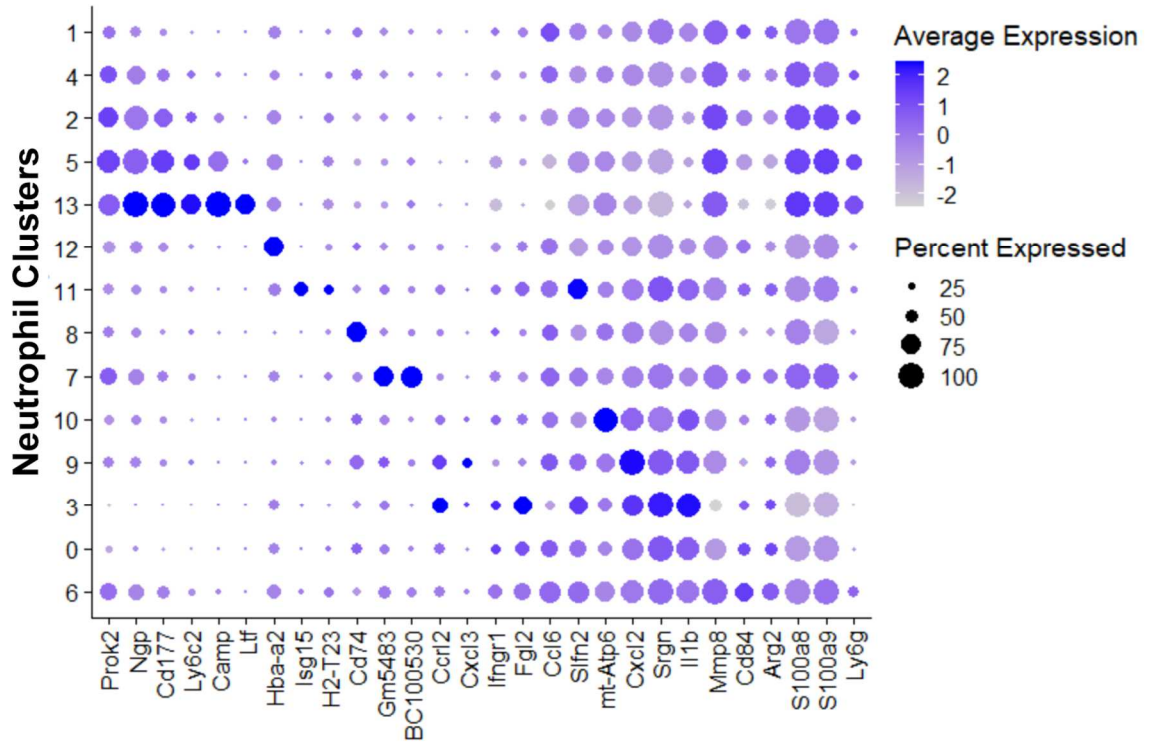


Figure 2.13. Markers of neutrophil subpopulations. Differential expression analysis on the 14 clusters was performed and markers for populations were curated. The neutrophil cluster were separated into two “super-clusters” and five additional clusters based on this marker analysis. The first super-cluster was composed of clusters 1,4,2,5 and 13 and the second included 0,3,9 and 10. Of the five remaining, 4 resembled clusters previously identified (this work) and the fifth, cluster 6, may represent an MDSC population (see *Cd84* and *Arg2*).

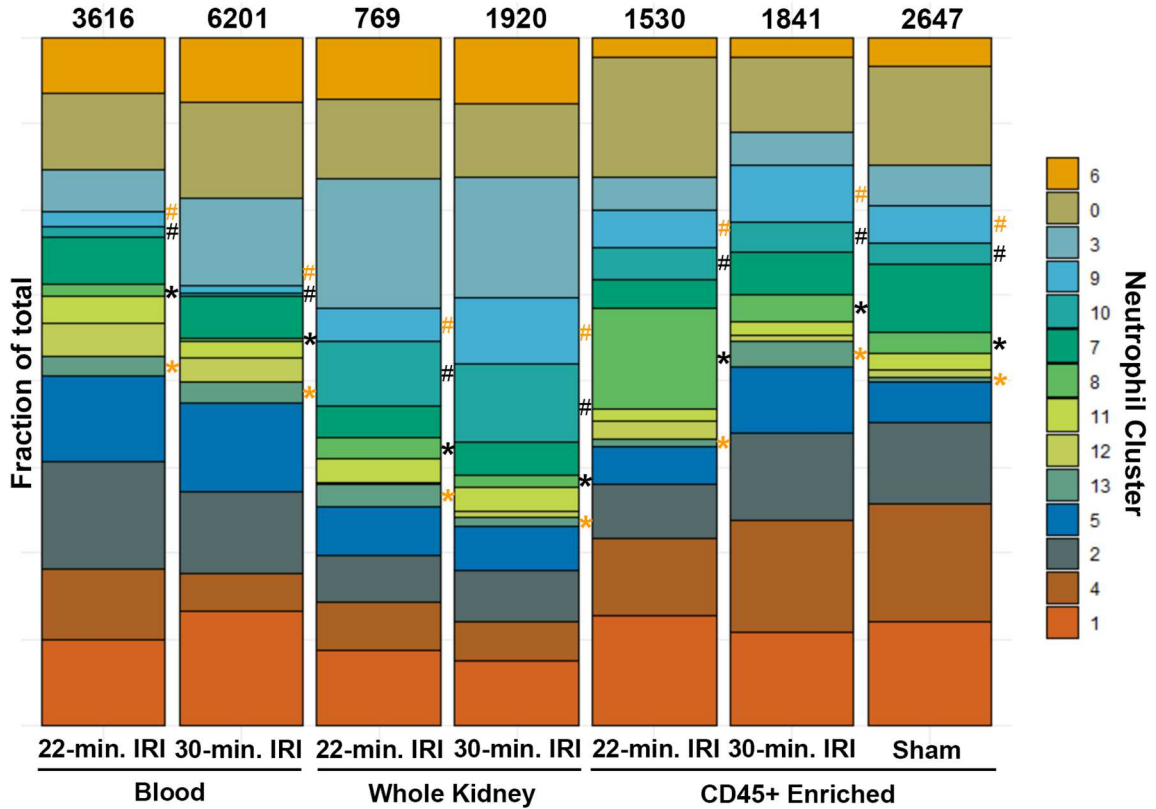


Figure 2.14. Distribution of neutrophil subpopulations is sensitive to compartment and severity of injury. Neutrophil populations from all datasets (Sham conditions from whole kidney were excluded due to low yield of neutrophils) were ordered by neutrophil super cluster comprised of 1,4,2,5 and 13, separated by clusters 7,8,11,12 and the second super cluster comprised of 0,3,9 and 10. The number of cells per cluster were tabulated and the fraction of totals calculated. The total number of cells per condition is given above each column. Specific populations are poorly represented in the blood isolations (black and orange pounds and black asterisks). Specific populations are upregulated by 22- and 30-minute IRI (black and orange asterisks).

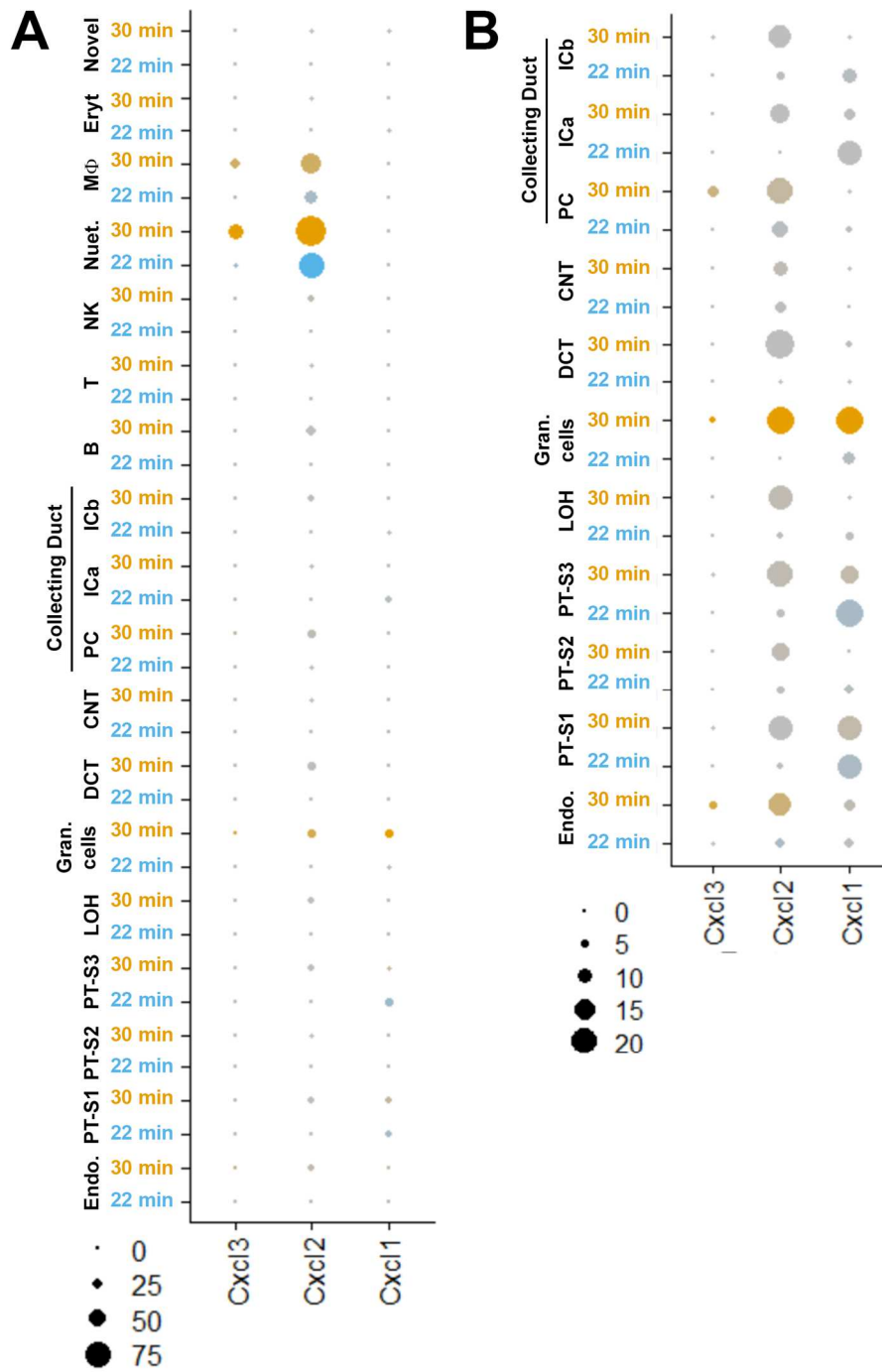


Figure 2.15. Expression analysis of CXCR2 ligands. Neutrophils and macrophages express CXCR2 ligands with sensitivity to the severity of injury. Using the combined whole kidney dataset and selecting the 22- or 30-minutes of IRI *Cxcl1*, *Cxcl2* and *Cxcl3* expression level was plotted on a dot plot where intensity represents level of expression

and size of dot indicates the fraction of the cell-type expressing the transcript. A. Plotting all cell types. B. Selecting only cell-types from the nephron demonstrates lower levels of expression in the proximal tubule and secretory granular cells (Gran. cells) of the juxtaglomerular apparatus depending upon the severity of injury. Note dot scale.

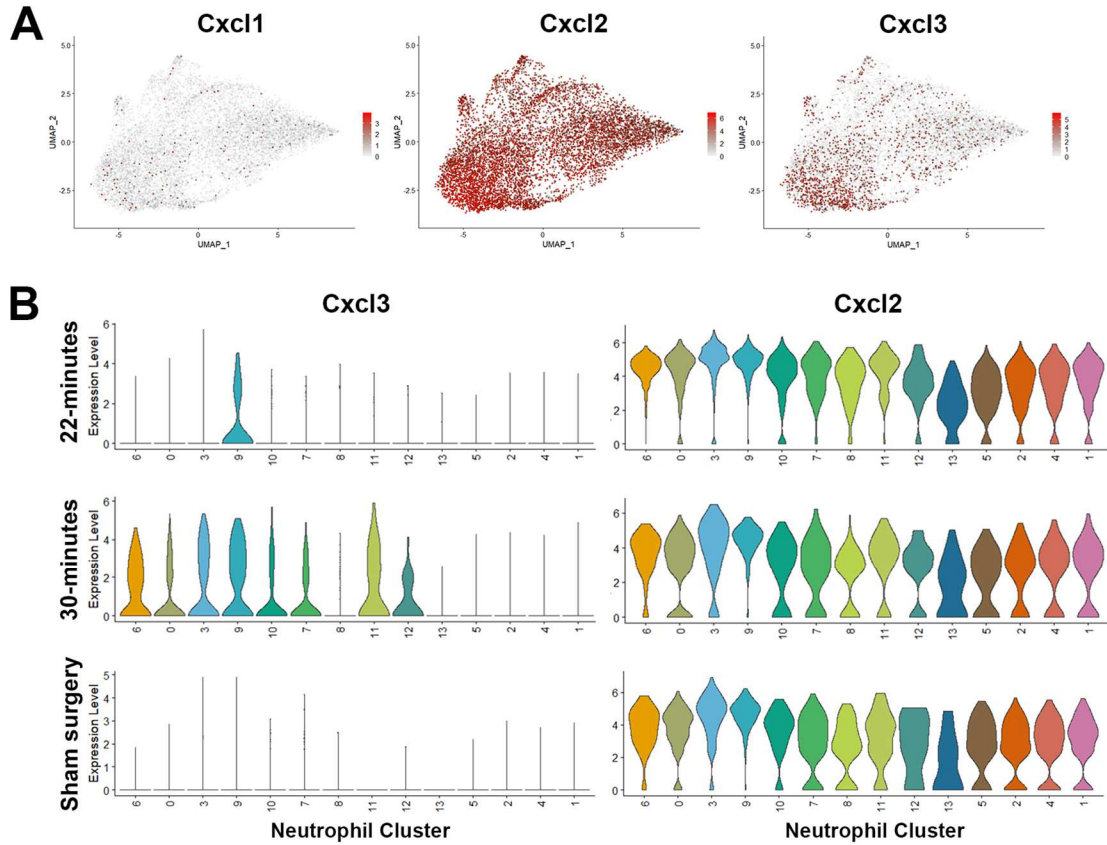


Figure 2.16. Injury affects *Cxcl3* and *Cxcl2* expression by neutrophil clusters. *Cxcl2* is consistently expressed across ischemia conditions and the sham while *Cxcl3* is uniquely expressed after ischemia. A. Expression level of cytokines was plot as the color of each cell plotted in a UMAP plot. Cells are from both ischemic injuries and the sham. B. *Cxcl3* transcription is uniquely sensitive to ischemic injury. Chemokine expression for all cells in each subpopulation (cluster) was plotted by cluster number per ischemia condition or the sham surgery.

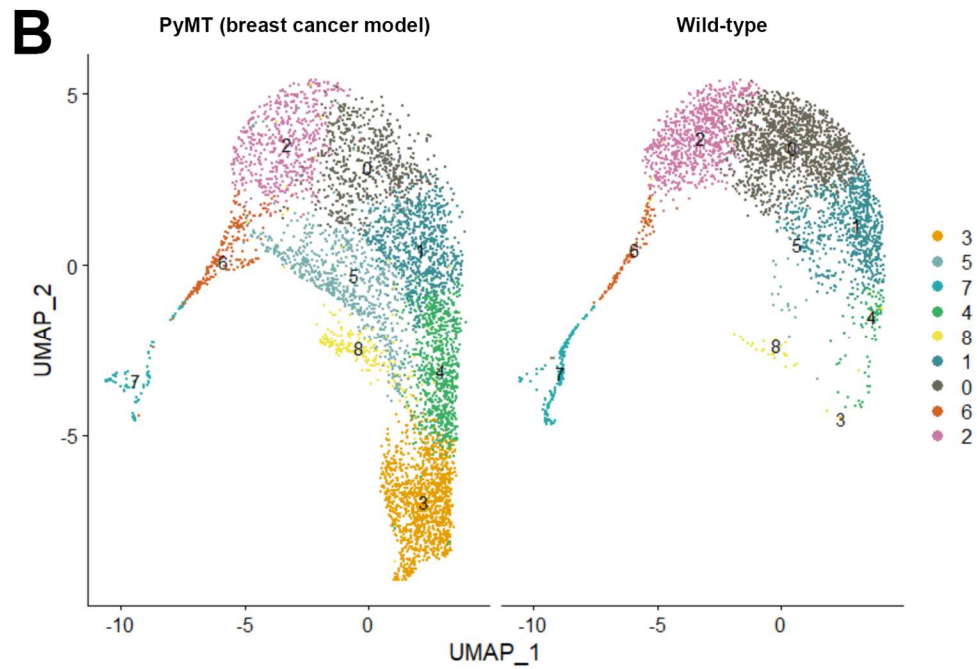
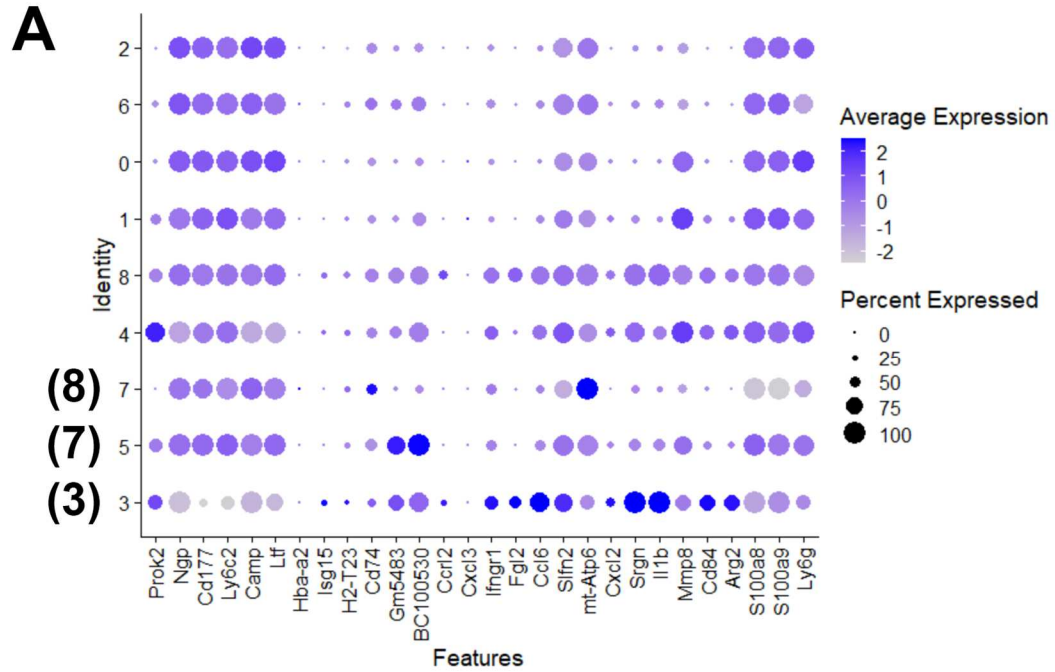


Figure 2.17. Neutrophils from a breast cancer metastasis model mirror population identified in AKI. A publicly available dataset was downloaded from GEO (GSM4131336 and GSM4131337) and processed in Seurat. A. The clusters identified in the cancer dataset were screened with the markers identified for neutrophils in AKI. Clusters

2,6,0,1,8 and 4 are like the activated super-cluster seen in AKI while clusters 7, 5, and 3 are like clusters 8,7 and 3 in AKI (green annotation at left). B. UMAP plot of cells in the cancer model and a wild-type control. Cancer clusters 3,5,7 and 4 are associated with cancer.

Table 2.1. Working Neutrophil Definitions

transcriptionally related clusters are color coded

Cluster	Description	Markers
0	Primed	<i>Srgn</i>
1	Primed-Infiltrating	<i>Prok2</i>
		<i>Srgn</i>
2	Infiltrating	<i>Prok2</i>
		<i>Cd177</i>
3	Signaling-Infiltrating	<i>Srgn</i>
		<i>Il1b</i>
4	Infiltrating	<i>Prok2</i>
5	Infiltrating	<i>Prok2</i>
		<i>Mmp8</i>
6	Infiltrating	<i>Prok2</i>
		<i>Srgn</i>
7	Motile	<i>Gm5483</i>
		<i>BC100530</i>
8	Antigen Presenting (MHC II)	<i>Cd74</i>
9	Cytokine Active	<i>Cxcl2</i>
		<i>Cxcl3</i>
10	Metabolic	<i>mt-Atp6</i>
11	Antigen Presenting (MHC I)	<i>H2-T23</i>
		<i>Isg15</i>
12	Phagocytic	<i>Hbb-ba</i>
13	Activated	<i>Ltf</i>
		<i>Ly6c2</i>

Table 2.2. Pathways upregulated by neutrophil clusters within the blood or kidney with 22-minute IRI			
Cluster	Blood 22min IRI (versus other IRI clusters)	kidney 22min IRI (versus other kidney 22min IRI clusters)	Markers
0	IL-4, IL-13 signaling	IL-1 signaling	<i>Srgn</i>
	IL-1 signaling	Class II MHC antigen presentation	
1	Siliac acid metabolism	Dectin-1 pattern recognition	<i>Prok2</i>
		RUNX2 myeloid differentiation	<i>Srgn</i>
2	Anti-microbial peptides	RUNX2 myeloid differentiation	<i>Prok2</i>
		GTSE1 G2/M progression	<i>Cd177</i>
3	IL-1 signaling	E-Selectin interactions	<i>Srgn</i>
	Secretory granule packing	Cell surface interaction vascular wall	<i>Il1b</i>
4	Motility	TLR trafficking	<i>Prok2</i>
	Infiltration	Dectin-1 pattern recognition	
5	Rho GTPase signaling	IL-1 signaling	<i>Prok2</i>
	Detoxification of Reactive Oxygen	TLR signaling	<i>Mmp8</i>
6	Golgi trafficking	Interleukin signaling	<i>Prok2</i>
	Formyl peptide signaling	Response to hypoxia	<i>Srgn</i>
7	Golgi trafficking	IL-1 signaling	<i>Gm5483</i>
		Antigen processing presentation	<i>BC100530</i>
8	PF4 minimize NET size	IL-1 signaling	<i>Cd74</i>
	Platelet pathways	Antigen processing presentation	
9	IL-1 signaling	IL-1 signaling	<i>Cxcl2</i>
	TLR7,8,9	Antigen processing presentation	<i>Cxcl3</i>
10	Mitochondrial	Dectin-1 pattern recognition	<i>mt-Atp6</i>
		IL-1 signaling	
11	Class I MHC antigen presentation	Antigen processing presentation	<i>H2-T23</i>
	IL-1 signaling	C-Lectin receptors	<i>Isg15</i>
12	RBC Phagocytic	Interleukin signaling	<i>Hbb-ba</i>
		C-Lectin receptors	
13	Antigen presentation	C-Lectin receptors	<i>Ltf</i>
	Regulation of Metabolism	Dectin-1 pattern recognition	<i>Ly6c2</i>

Table 2.3. Pathways upregulated by neutrophil clusters within the blood or kidney with 30-minute IRI			
Cluster	Blood 30 min IRI (versus other Blood 30 min IRI clusters)	kidney 30 min IRI (versus other kidney 30 min IRI clusters)	Markers
0	Ccl3,4,6	Detoxification of reactive oxygen	<i>Srgn</i>
	IL-1 signaling	E-Selectin interactions	
1	Formyl peptide signaling	Antigen processing presentation	<i>Prok2</i>
	Ccl6 signaling	RUNX2 myeloid differentiation	<i>Srgn</i>
2	Anti-microbial peptides	TLR signaling	<i>Prok2</i>
		Cell response to stress	<i>Cd177</i>
3	Interleukin signaling	Detoxification of Reactive Oxygen	<i>Srgn</i>
	TLR47,8,9	E-Selectin interactions	<i>Il1b</i>
4	Ccl6 signaling	Detoxification of Reactive Oxygen	<i>Prok2</i>
		E-Selectin interactions	
5	Rho GTPase signaling	Detoxification of Reactive Oxygen	<i>Prok2</i>
	Detoxification of Reactive Oxygen	TLR signaling	<i>Mmp8</i>
6	Apoptosis	Detoxification of Reactive Oxygen	<i>Prok2</i>
		Cell response to stress	<i>Srgn</i>
7	Cystatins	GTSE1 G2/M progression	<i>Gm5483</i>
		Cell response to stress	<i>BC100530</i>
8	PECAM-1 and intergin interaction	Detoxification of Reactive Oxygen	<i>Cd74</i>
	Cell surface interaction vascular wall	TLR signaling	
9	CXCR2 signaling	Cell response to stress	<i>Cxcl2</i>
		Cell surface interaction vascular wall	<i>Cxcl3</i>
10	PIP3 and AKT signaling	E-Selectin interactions	<i>mt-Atp6</i>
	PTEN regulation	Cell surface interaction vascular wall	
11	Class I MHC antigen presentation	Cell response to stress	<i>H2-T23</i>
		IL-1 signaling	<i>Isg15</i>
12	RBC Phagocytic	Detoxification of Reactive Oxygen	<i>Hbb-ba</i>
		E-Selectin interactions	
13	Rho GTPase signaling	Detoxification of Reactive Oxygen	<i>Ltf</i>
		Cell response to stress	<i>Ly6c2</i>

Table 2.4. Pathways differentially upregulated by cluster in the kidney between ischemic injuries			
Cluster	Kidney 22 min IRI (versus kidney 30 min IRI)	Kidney 30 min IRI (versus kidney 22 min IRI)	Markers
0	RUNX3 expression	TLR signaling	<i>Srgn</i>
	Antigen cross presentation	Rho GTPase Signaling	
1	RUNX2 transcriptional reg.	Rho GTPase Signaling	<i>Prok2</i>
	Metabolism	Platelet activation	<i>Srgn</i>
2	Metabolism	NS	<i>Prok2</i>
	Antigen cross presentation		<i>Cd177</i>
3	Metabolism	Metabolism	<i>Srgn</i>
			<i>Il1b</i>
4	RUNX3 expression	Platelet activation	<i>Prok2</i>
	Metabolism	Interleukin signaling	
5	Dectin signaling	Platelet activation	<i>Prok2</i>
	Endosomal TLR response	Interleukin signaling	<i>Mmp8</i>
6	Translation	Platelet activation	<i>Prok2</i>
	Antigen cross presentation	Interleukin signaling	<i>Srgn</i>
7	NS	MAPK signaling	<i>Gm5483</i>
		Interleukin signaling	<i>BC100530</i>
8	Dectin signaling	Metabolism	<i>Cd74</i>
	C-type lectin receptors	Cellular response to stress	
9	Interleukin signaling	Rho GTPase Signaling	<i>Cxcl2</i>
	Class I MHC antigen processing		<i>Cxcl3</i>
10	Antigen processing-cross presentation	Rho GTPase Signaling	<i>mt-Atp6</i>
	Class I MHC antigen processing		
11	Antigen processing-cross presentation	Rho GTPase NADH Oxidase	<i>H2-T23</i>
	RUNX2 transcriptional reg.		<i>Isg15</i>
12	Antigen processing-cross presentation	NS	<i>Hbb-ba</i>
	C-type lectin receptors		
13	RUNX2 transcriptional reg.	ROS and RNS production	<i>Ltf</i>
	FBXL7 mitosis entry	Metabolism	<i>Ly6c2</i>

Table 2.5. Pathways differentially upregulated by cluster when in the blood versus the kidney with 22-minute IRI			
Cluster	Blood 22 min IRI (versus kidney)	kidney 22 min IRI (versus blood)	Markers
0	Integrin signaling	Metabolism	<i>Srgn</i>
1	Integrin signaling	TLR signaling	<i>Prok2</i>
		MHCII antigen presentation	<i>Srgn</i>
2	Rho GTPase signaling	Detoxification of reactive oxygen	<i>Prok2</i>
	Programmed cell death		<i>Cd177</i>
3	Metabolism	Metabolism	<i>Srgn</i>
		Inflammasome	<i>Il1b</i>
4	Rho GTPase signaling	TLR signaling	<i>Prok2</i>
	Integrin signaling		
5	Rho GTPase signaling	Chemokine receptor binding	<i>Prok2</i>
			<i>Mmp8</i>
6	TLR signaling	Cell surface interactions vascular wall	<i>Prok2</i>
		E-Selectin interactions	<i>Srgn</i>
7	Cell-cell communication	TLR signaling	<i>Gm5483</i>
	Rho GTPases activate oxidases		<i>BC100530</i>
8	Integrin signaling	Cellular response to heat stress	<i>Cd74</i>
	Rho GTPase signaling	TLR signaling	
9	Rho GTPases activate oxidases	TLR signaling (4/7/8/9)	<i>Cxcl2</i>
			<i>Cxcl3</i>
10	Autophagy	Metabolism	<i>mt-Atp6</i>
11	Pattern recognition	Metabolism	<i>H2-T23</i>
			<i>Isg15</i>
12	Scavenge receptors	TLR signaling (3/2/5/6/7/8/9)	<i>Hbb-ba</i>
	Heme uptake		
13	Pattern recognition	Metabolism	<i>Ltf</i>
	Scavenge receptors		<i>Ly6c2</i>

Table 2.6. Pathways differentially upregulated by cluster when in the blood versus the kidney with 30-minute IRI

Cluster	Blood 30 min IRI (versus kidney)	kidney 30 min IRI (versus blood)	Markers
0	TLR signaling	Cell surface interactions vascular wall	<i>Srgn</i>
	TNF-alpha and beta production		
1	MHC I antigen presentation	Detoxification of reactive oxygen	<i>Prok2</i>
	TLR signaling (7/8/9)	Cell surface interactions vascular wall	<i>Srgn</i>
2	Integrin signaling	TLR signaling	<i>Prok2</i>
		Detoxification of reactive oxygen	<i>Cd177</i>
3	Immunoregulatory (lymphoid)	TLR signaling	<i>Srgn</i>
		E-Selectin interactions	<i>Il1b</i>
4	TLR signaling	Detoxification of reactive oxygen	<i>Prok2</i>
	Death Receptor signaling	Metabolism	
5	Rho GTPase signaling/effectors	Detoxification of reactive oxygen	<i>Prok2</i>
		TLR signaling	<i>Mmp8</i>
6	Autophagy	Detoxification of reactive oxygen	<i>Prok2</i>
		TLR signaling	<i>Srgn</i>
7	TLR signaling (7/8/9)	E-Selectin interactions	<i>Gm5483</i>
		Detoxification of reactive oxygen	<i>BC100530</i>
8	NS	NS	<i>Cd74</i>
9	Metabolism	Metabolism	<i>Cxcl2</i>
			<i>Cxcl3</i>
10	Rho GTPase signaling and effectors	Metabolism	<i>mt-Atp6</i>
	MAPK signaling		
11	pro-survival NFkB signaling	Detoxification of reactive oxygen	<i>H2-T23</i>
	MAPK signaling		<i>Isg15</i>
12	Rho GTPase signaling	Metabolism	<i>Hbb-ba</i>
	MAPK signaling		
13	Rho GTPase signaling	Metabolism	<i>Ltf</i>
			<i>Ly6c2</i>

Chapter 3. Uromodulin dependent change in neutrophil transcriptomes

Introduction

Uromodulin (Tamm-Horsfall protein, THP) is made solely in the kidney(85). Specifically, it is made in the thick-ascending limb of the Loop of Henle (LOH). A large fraction is secreted into the urine where it forms oligomers and fibers. These oligomers have been shown to play a role in controlling urinary tract infection and act as a sink for cytokines in the lumen of kidney tubules(86). Soluble THP monomer is secreted basolaterally where it has immunomodulatory activity(46). Within the kidney, basolateral secreted THP modulates myeloid cells through regulation of the IL17/IL23 axis(83, 87). Systemically, THP has further effects on myeloid cells and neutrophils by regulating granulopoiesis. In a THP knock-out (THP^{-/-}) mouse there is systemic neutrophilia-a state of increased circulating neutrophils (87). Compared to wild-type mice, the THP^{-/-} mouse is sensitive to kidney injury and shows poor recovery of kidney function after ischemic injury(75).

A THP knock-out (THP^{-/-}) mouse strain is susceptible to severe ischemic injury. With wild-type mice 30 minutes of ischemia results in significant injury to the kidney(75). In a THP^{-/-} mouse this damage is exacerbated with increased tubular destruction in the outer stripe and loss of S3 proximal tubules, a shift to necrotic vs apoptotic cell death and a decrease in kidney function (serum creatinine levels). This damage is accompanied by an increase in neutrophil infiltrates in THP^{-/-} mice. Functionally, by serum creatinine levels, a shorter ischemic time, 22 minutes, better mimics the 30 minutes of injury in wild-type mice. Importantly, with the shorter ischemic time there is still a significant increase in neutrophils infiltrating the kidney compared to a sham surgery or wild-type mice. I am poised with an intervention (22 minutes of ischemia) and the knock-out mice to better understand the role of THP in modulating neutrophil polarization in the injured kidney.

Compared to a wild-type mouse, the milieu of the injured kidney in the THP^{-/-} mouse is severely dysregulated. After 22-minutes of ischemia the cytokine profile shows distinct dysregulation at 6, 24, and 48 hours after injury. This includes transient pro-inflammatory cytokines at 24 hours and the absence of anti-inflammatory cytokines at 48 hours seen in wild-type mice(83). It is hypothesized that this altered chemokine and cytokine profile will correlate with the polarization of neutrophils early (6h) in injury. This work will demonstrate that dysregulation of the tubular epithelium, immune cells and cytokine signaling in the absence of THP correlates with a change in neutrophils including the upregulation of pathways associated with complement cascade, cellular senescence and death pathways leaving the kidney more susceptible to AKI.

Results

Validation of THP^{-/-} and effects of gene knockout

The THP knock-out mouse used in these studies is a knock-out for exons 1-4 and a small fragment of the THP promoter. As such, THP transcript should not be detectable by scRNASeq. The THP transcript was not detected in the whole kidney isolation datasets from THP^{-/-} mice (**Figures 3.1 and 3.2**). This contrasts with detectable signal of THP in the putative LOH clusters in the wild-type mice after sham surgery (**Figures 3.1 and 3.2**).

Neighboring gene regulation in the THP^{-/-} mouse

scRNASeq provides a unique opportunity to test for polar effects, the effect of the knockout on expression of neighboring genes, in the THP^{-/-} mouse. To assess the transcriptional change in neighboring genes, scRNASeq data for genes neighboring THP was compared between sham surgeries in knock-out versus wild-type mice (**Figure 3.1**). As expected, there is no THP transcript detected in the THP^{-/-} mouse and it was detected

robustly in the LOH and DCT in the wildtype mouse. Of the four neighboring genes, only *Acsm2* was detected in both the wild-type and knockout mouse. *Acsm2* is acyl-coenzyme A synthetase involved in fatty acid metabolism not known to have an immunomodulatory role or affect granulopoiesis. The expression of *Acsm2* is similar between the wild-type and mutant mice. Of note is the decrease in *Acsm2* expression the proximal tubules sub-segments, LOH and DCT (**Figure 3.2**). This suggests a mild polar effect on *Acsm2* may exist in the THP^{-/-} mouse.

Functional differences of kidney epithelium in THP^{-/-} mice

The loss of THP and its role in tubular crosstalk with the S3 segment suggests that there may be functional changes in the tubular epithelium of the kidney. To test this, first, epithelial and endothelial cells from the whole kidney THP^{-/-} mice were mapped to the subsegment clusters identified in chapter 1. With these cells, pathway analysis was performed on genes differentially expressed between THP^{-/-} and wild-type mice to assess changes in the transcriptional programs of these subsegments. Strikingly, the endothelium has a pro-inflammatory profile with upregulation of interferon alpha and beta pathways while also expressing genes involved in MHC I antigen presentation. The proximal tubule, LOH and collecting duct expressed new sets of solute transporters as compared to tubule subsegments from wild-type mice. Lastly, the connecting network tubular epithelium activated a suite of mitotic entry pathways suggesting a subsegment undergoing active mitosis (**Table 3.1**).

Changes in kidney epithelium during injury in THP^{-/-} mice

Like wild-type mice after 30-minutes IRI, THP^{-/-} mice recover poorly from AKI. Thus, it is expected that the THP^{-/-} mice would have a kidney epithelium like the wild-type

mice after 30-minutes IRI (Chapter 2). Instead, after 22-minutes of IRI in THP^{-/-} mice the kidney epithelium shifted to pathways driving and responding to extracellular matrix and TGF β signaling (**Table 3.1**).

Monocyte/macrophages distribution in THP^{-/-} mice is altered

Myeloid cells are dysregulated in the THP^{-/-} mouse(83, 87). The myeloid cells are similarly dysregulated in these data. In the CD45⁺ enrichment isolation from THP^{-/-} mice after a sham surgery, the resident monocyte/macrophages have expanded with an apparent loss of Ly6chi monocytes versus the sham surgery in wild-type mice. With injury the expansion is reminiscent of severe injury in wild-type mice, but not to the same extent as over half of the immune cells isolated in THP^{-/-} mice were neutrophils (**Figure 3.3**).

Neutrophil distribution in THP^{-/-} mice is like wild-type mice with moderate injury

To test if THP plays a role in regulating the diversity of neutrophils, neutrophils from THP^{-/-} mice the combined CD45⁺ enriched and kidney isolation dataset were aligned to the wild-type data (**Figure 3.4**). All the neutrophil clusters were detected in the THP^{-/-} mouse and 2 clusters were over-represented (3 and 8). An expansion in cluster 8 was similar to the expansion seen with a 22-minute IRI in wild-type mice, suggesting the neutrophil populations may be already responding to a kidney milieu unlike what is found in the wild-type mouse and possibly similar to 22-minute IRI (**Figure 3.5**). In contrast to wild-type mice, Cluster 5 is lost in THP^{-/-} mice without injury suggesting, that Cluster 5 is dependent upon THP expression in the kidney.

Neutrophils in THP -/- mice are uniquely primed for tissue damage

The transcriptional programs of the neutrophils may change even if the diversity of neutrophils was not affected by the absence of THP. To test for this possibility, pathway analysis with ReactomePA was performed on the combined CD45+ enriched and kidney isolation datasets comparing neutrophil populations between THP-/- and wild-type mice. The transcriptional programs of the neutrophils in the THP-/- mice upregulated pattern recognition pathways via TLR and complement cascade pathways (**Table 3.2**). The preponderance of complement cascade pathways was not seen in any wild-type IRI.

Injury in THP-/- mice expands specific neutrophil subtypes

The THP-/- mouse is sensitive to AKI. THPs role in granulopoiesis argues that in AKI, THP may modulate neutrophil subpopulations either by altering the distribution of neutrophils or by altering the transcriptional program of neutrophils. To test for the possibility that the distribution of neutrophil populations is altered in the absence of THP during injury, neutrophils from a 22-minute IRI in THP-/- mice were tabulated by subpopulation. This relative distribution was compared to both wild-type ischemia for 22- or 30-minute IRI in the CD45+ enriched samples and between blood and kidney isolations (**Figure 3.5 and 3.6**). Following 22-minute IRI, there was further expansion of cluster 8- the antigen presenting population (versus THP-/- sham, **Figure 3.4**). There was also an expansion of population 3 a putative member of the cytokine signaling super cluster in the CD45+ enrichment isolation but not in the whole kidney isolation (**Figure 3.5**). Like injury in wild-type mice, the neutrophils isolated from the kidney versus the blood were enriched for cluster 8 and 9. The putative cluster 10 did not appear to be enriched in the kidney as seen in wild-type mice after injury (**Figure 3.6 and Figure 2.14**).

Toll-like receptor signaling and complement cascade pathways after injury in THP-/- mice

The kidney epithelium of THP-/- mice is oxidative relative to wild-type mice(88). This environment is expected to specifically alter upregulated pathways in neutrophils. When comparing the upregulated pathways for a given cluster between the blood and kidney after injury, neutrophils in THP-/- mice upregulated pattern-recognition pathways, and most dramatically, toll-like receptor (TLR) pathways (both TLR4 and TLR7/8/9) and complement cascade. The upregulation in TLR signaling and complement cascades in multiple neutrophils subpopulations suggests, irrespective of a neutrophil's presumptive phenotype (antigen presentation, motile, etc. **Table 2.1**), the kidney milieu is causing a dramatic shift in the transcriptional program across neutrophil subpopulations (**Table 3.3 and 3.4**).

CXCR2 axis is dysregulated in THP-/- mice versus wild-type mice

In wild-type mice after 30-minute IRI the combination of *Cxcl2* and *Cxcl3* correlates with a change in the distribution of neutrophil subpopulations, neutrophil transcriptional pathways, and poor recovery of kidney function. To test if there is a similar correlation of CXCR2 activation, neutrophil transcription and recovery of kidney function, in THP-/- mice, the expression level of CXCR2 ligands was assessed in neutrophils following 22-minute IRI from THP-/- mice. In the THP-/- mouse following 22-minute IRI, neutrophils expressed CXCR2 ligands-including *Cxcl2* and *Cxcl3*. There was also *Cxcl1* expression in the S1 and S3 subsegments of the proximal tubule. In THP-/- mice there is CXCR2 ligand expression similar to 30-minute IRI (*Cxcl3* expression) and 22-minute IRI (*Cxcl1* expression in the proximal tubule) in wild-type mice (**Figure 3.7A**). Approximately 20% of the neutrophils after IRI THP-/- mice are expressing *Cxcl3*. The neutrophil clusters primarily expressing *Cxcl3* included 6, 3,9,10 and 11(**Figure 3.7B**). These are some of the same clusters expressing *Cxcl3* after 30 minutes of ischemia in wild-type mice (**Figure**

2.16B). The clusters not expressing *Cxcl3* include 0, 7 and 12. Of these, cluster 12 was not detected after injury (it is more abundant in blood specimens, **Figure 2.14**).

Discussion

The kidney environment was altered in the absence of THP. For instance, the subsegments in the THP^{-/-} mouse express solute carriers and transporter pathways distinct from the wild-type mouse. The pathways upregulated in neutrophils were also dramatically affected by the absence of THP.

TLRs are a first line of defense when the immune system is faced with either pathogens or tissue damage. TLR pathways may act as gate keepers of further immune system activation and thus play a role in immunomodulatory processes. After ischemic AKI in THP^{-/-} mice TLR4 is expressed on proximal tubule cells(75). In the case of ischemia in THP^{-/-} mice, the large swing towards TLR signaling in neutrophils suggests that TLR signaling may be responding to significant tissue damage or possibly that THP normally, and beneficially, represses TLR expression (the absence of TLR4 is protective in AKI(89)).

The upregulation of complement cascade pathways, especially prior to injury, was unique to the neutrophils isolated from THP^{-/-} mice. It seems likely complement cascade pathways play a significant role in the sensitivity of the THP^{-/-} mouse to AKI. In chapter 2, in wild-type mice, there was a correlation between an increase in cluster 8 (putative MHCII antigen presenting cluster) and 22-minute IRI and thus better recovery of kidney function. Here, in THP^{-/-} mice, this cluster is likewise increased but the sensitivity to AKI remains. If cluster 8 is better for recovery of kidney function as the data in wild-type mice suggested, then perhaps it is no match for the upregulation of complement cascades seen in the THP^{-/-} mice. It should be noted that cluster 8 also upregulates complement cascade pathways in THP^{-/-} mice. Thus, by pathway analysis there was uniformity in the response

of neutrophils in the kidneys of THP *-/-* mice not seen in wild-type mice after 22-minute IRI.

CXCR2 signaling in the THP $-/-$ mouse had characteristics of both moderate and severe injury in wild-type mice. There was robust *Cxcl1* expression in the S1 and S3 segments of the proximal tubule after 22-minute IRI in the THP $-/-$ mouse, as seen in wild-type mice after 22-minute IRI. In contrast to 22-minute IRI in wild-type mice, *Cxcl3* was expressed by neutrophils in THP $-/-$ mice after 22 minutes of ischemic injury. Furthermore, cluster 3, which expands in injury is also expressing *Cxcl3* after injury. *Cxcl3* was only detected in wild-type mice with 30-minute IRI (Chapter 2). Lastly, a low level of *Cxcl1* expression was seen in granular cells. Thus, CXCR2 signaling was dysfunctional as compared to wild-type mice and had characteristics of both ischemia injury times tested here in wild-type mice. This suggests that THP may modulate CXCR2 signaling by repressing *Cxcl3* and *Cxcl1* in specific cell types possibly via repression of the IL17/IL23 axis(90).

In the absence of THP the mouse kidney is a stressed environment, as suggested by the high levels of oxidation in the cortex of the THP $-/-$ kidney and systemically(88). In these data, this environment correlated with upregulation of complement cascade pathways in neutrophils. In injury these neutrophils may cause or be primed to cause significant tissue damage. This is combined with dysregulated CXCR2 ligands that drive more neutrophils into the tissue(90). Thus, a two-hit mechanism of neutrophil behavior and cytokine dysregulation may lead to the increased sensitivity to AKI of the THP $-/-$ mouse.

THP was required for modulating the distribution of neutrophils without IRI. After IRI it was less important as the distribution of neutrophil following 22-minute IRI in the THP $-/-$ mice was like what was seen in wild-type mice following 22-minute IRI. However, the kidney milieu (e.g. chemokines) was altered as illustrated by *Cxcl1*, *Cxcl2* and *Cxcl3*

expression more like the expression pattern of CXCR2 ligands after severe injury in wild-type mice. Furthermore, the transcriptional programs and pathways of neutrophil subpopulations were shifted to TLR signaling and complement cascade pathways irrespective of the putative neutrophil subpopulation. This suggests that THP may have a global effect on neutrophil behavior, via the kidney milieu(88) and granulopoiesis(90), and/or direct effects on pathway regulation in neutrophil subpopulations including chemokine regulation.

Methods

Animal handling and surgeries

All surgeries were performed in compliance with institutional review and under approved protocols. Ischemic injury of mouse kidneys was performed as indicated in Chapter 4.

Isolation of single cells from injured kidneys

Isolation of total kidney and CD45+ enriched cells in injured kidneys was performed as given in chapter 1. For total kidney isolations two kidneys from one male were used as starting material. For CD45+ enriched cells, 4 kidneys were isolated from two male THP $-/-$ mice with 22 min ischemic time and reperfusion for 6 hours and 4 kidneys were isolated from two male THP $-/-$ mice following a sham surgery.

Isolation of immune cells from blood for scRNASeq

Immune cells for scRNASeq were isolated from blood from THP $-/-$ mice following ischemic injury for 22 after six hours of reperfusion. ~700 uL per animal and from two animals' total whole blood was sampled by a jugular bleed. The whole blood was processed as outlined in Chapter 2.

Data availability

Raw and processed data will be made available online at GEO hosted by the National Center for Biotechnology Information.

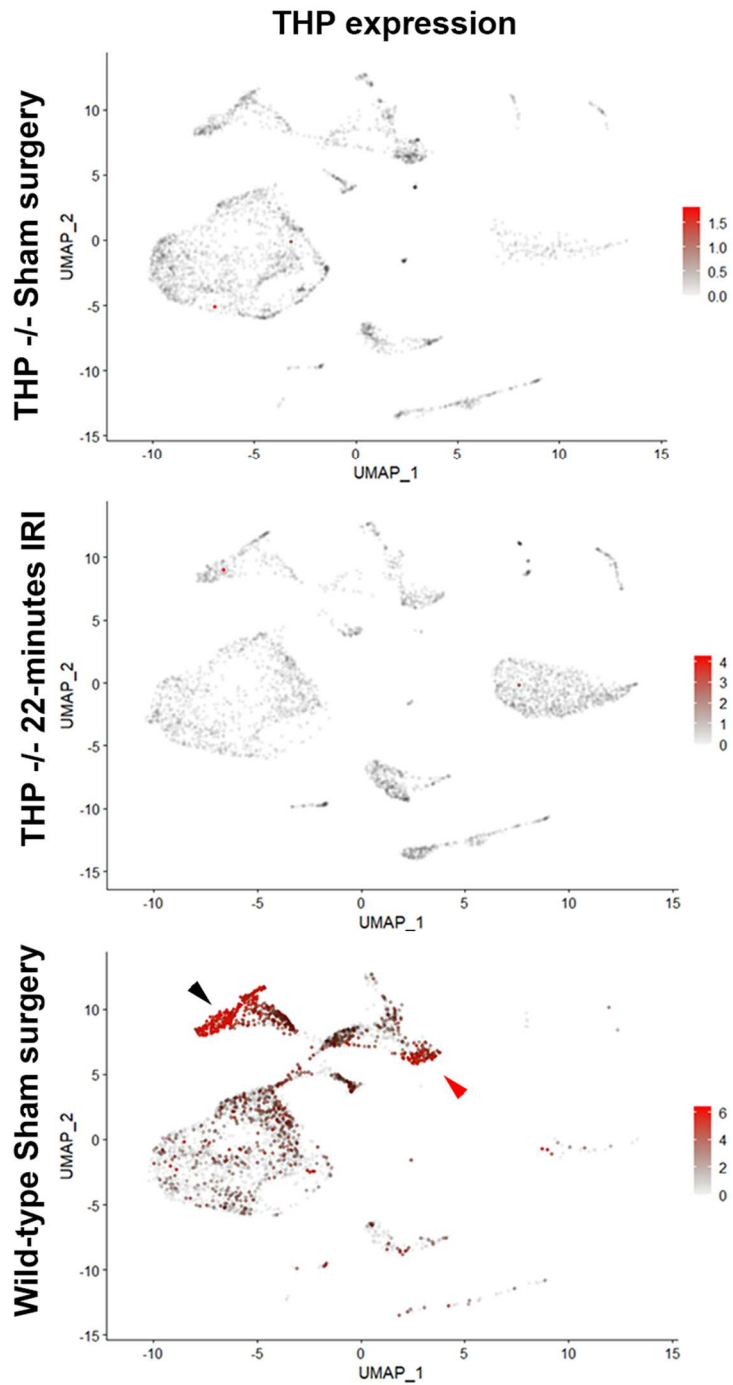


Figure 3.1. THP transcript is not detected in the THP-/- mouse. UMAP plots of single cells from sham and 22-minutes IRI in THP-/- mice and sham surgery from wild-type mice was color-coded by cell for expression level of THP. There wasn't any expression of THP in the knock-out mouse

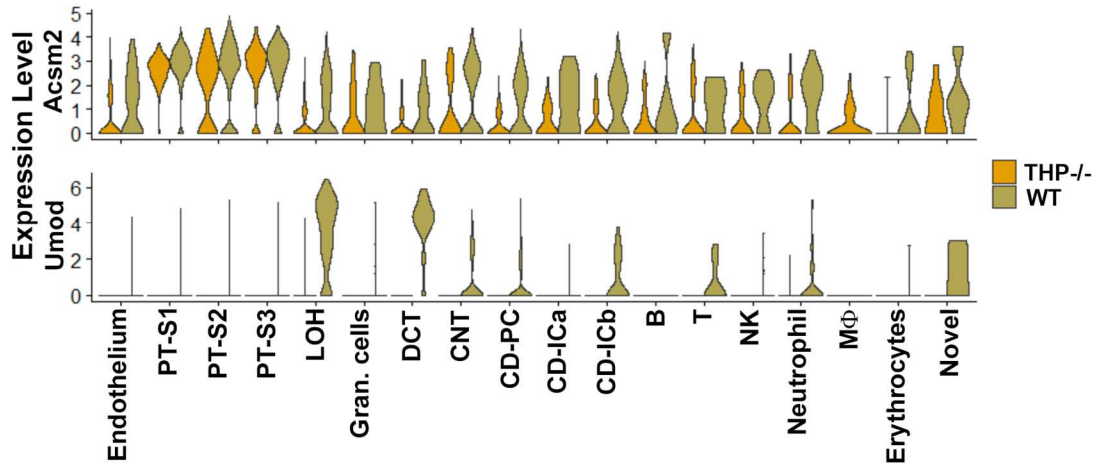


Figure 3.2. Exploring polar effects in the THP-/- mouse. Of the genes neighboring THP(Uromodulin) only one had detectable levels of transcript in the whole kidney isolations-*Acsm2*. *Acsm2* has a mild polar effect in the LOH and distal segments of the nephron by scRNASeq.

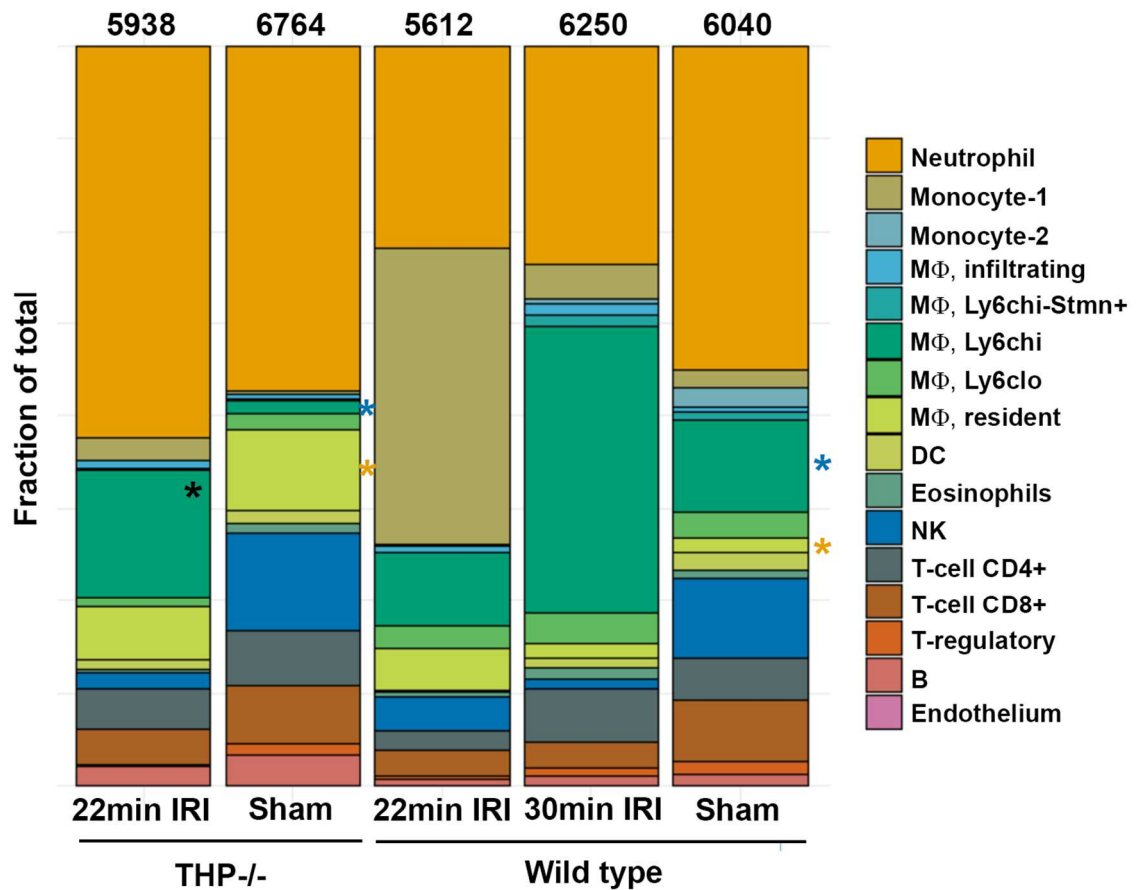


Figure 3.3. The distribution of immune cells is sensitive to the presence of THP. All immune cells from CD45+ enrichment isolation of wild-type and THP-/- mice were tabulated and plotted. THP is required for baseline infiltration of Ly6chi macrophages (blue asterisks) and regulating the number of resident macrophages (orange asterisks). Ly6chi-macrophages expand in injury in THP-/- mice (black asterisk). The total cells counted is given at the top of each column.

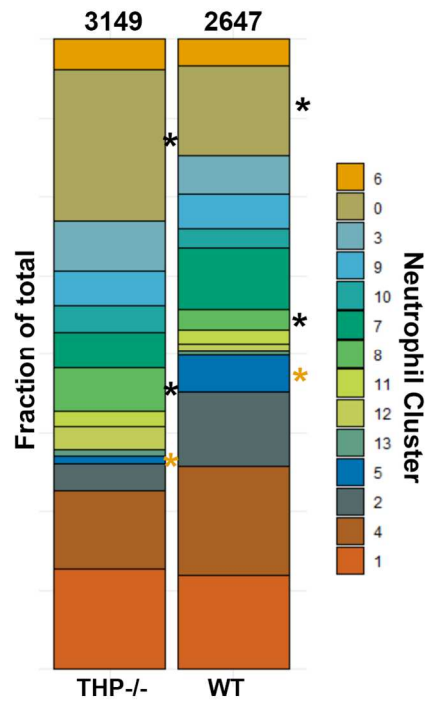


Figure 3.4. The distribution of neutrophils is modulated by THP. Neutrophils from either knock-out or wild-type sham surgeries were tabulated by neutrophil cluster. The relative proportion of cluster 0 and 8 goes up in the absence of THP (black asterisks) and the proportion of cluster 2 goes down (orange asterisks). The total number of cells per conditions is given at the top of each column.

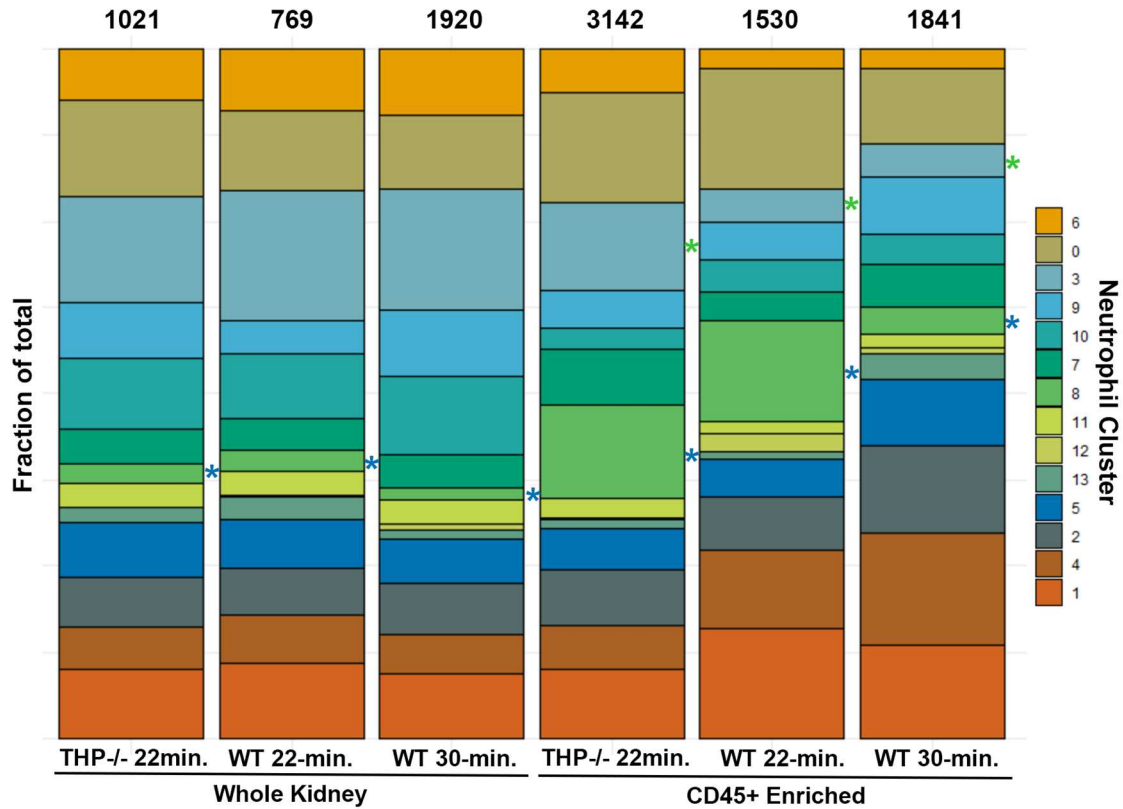


Figure 3.5. Injury in THP-/- mice affects the distribution of neutrophils. Neutrophils from either knock-out or wild-type sham surgeries were tabulated by neutrophil cluster from either whole kidney or CD45+ enrichment isolations separately. Cluster 8 is consistently upregulated after injury in THP-/- mice versus severe injury in wild-type mice (blue asterisks). Cluster 3 expands in the CD45+ enrichment isolation (green asterisks). The total number of cells per conditions and isolation is given at the top of each column.

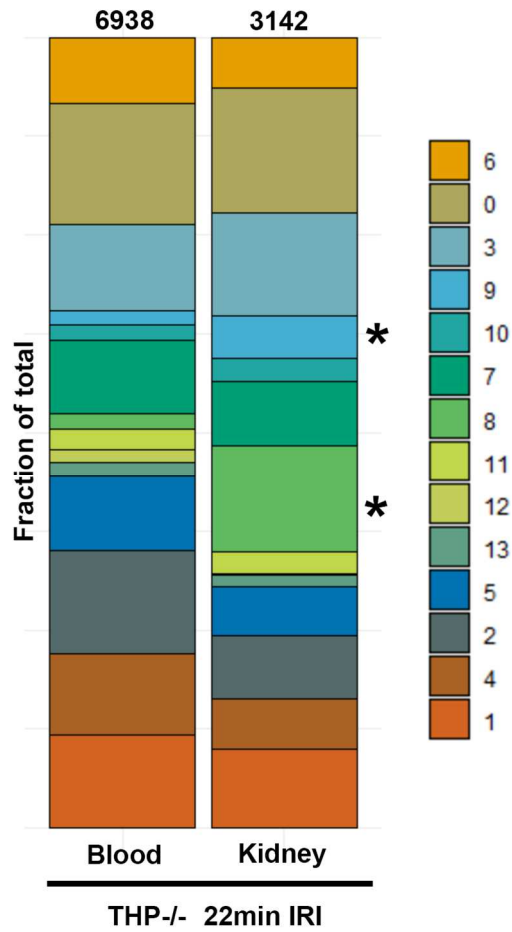


Figure 3.6. Distribution of neutrophil subpopulations is sensitive to the compartment in THP-/- mice. Neutrophils from knock-out sham or 22-minute IRI surgeries were tabulated by neutrophil cluster. The relative proportion of cluster 9 and 8 goes up in the in the kidney (asterisks).

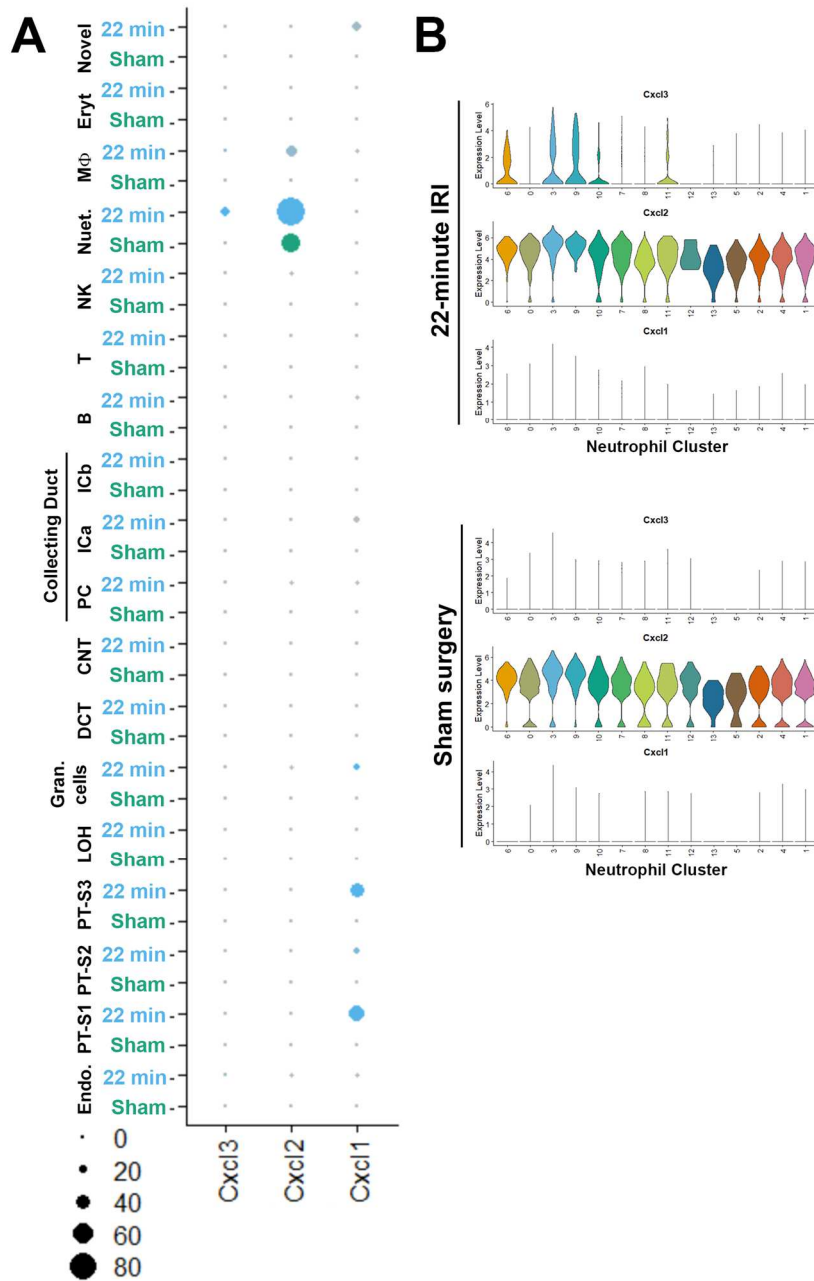


Figure 3.7. CXCR2 signaling in the THP^{-/-} mouse after ischemic kidney injury. Using whole kidney isolations from THP^{-/-} mice, CXCR2 ligands *Cxcl1*, *Cxcl2* and *Cxcl3* (*Cxcl5* was not detected) were tested for expression level in both sham surgery and after 22-minutes of ischemia and 6 hours or reperfusion. **A.** A dot plot of the expression levels-scale as indicated. Surgical interventions are labeled and colored for 22-minutes IRI (blue)

or a sham surgery (green). **B.** Expression level of CXCR2 ligands in neutrophil subpopulations in a 22-minute IRI or sham surgery. Specific neutrophil subpopulations express Cxcl3 following 22-minute IRI.

Table 3.1. Exemplar ReactomePA pathways in THP ^{-/-} mice		
Cluster	THP ^{-/-} Sham surgery (versus wt Sham surgery)	+22 minutes IRI (versus THP ^{-/-} Sham surgery)
Endo.	Class I MHC I antigen presentation	Signaling by receptor tyrosine kinases
	Interferon-alpha/beta	Platelet signaling
PT-S1	Amino acid transport	Integrin interactions
	Protein phosphorylation	
PT-S2	ND	RhoGTPase signaling
		GTSE1 in G2/M transition
PT-S3	Amino acid transport	Cellular response to heat stress
	Organics transport	TLR regulation
LOH	Ion channel transport	Platelet signaling
	Protein phosphorylation	ECM organization
Gran. Cells	Signaling by receptor tyrosine kinases	Platelet signaling
	ECM organization	ECM organization
DCT	ND	VEGFA-VEGFR2 pathway
		Signaling by receptor tyrosine kinases
CNT	APC/C degradation of cell cycle proteins	TGFbeta signaling, SMAD
	GTSE1 in G2/M transition	TGFbeta signaling
CD-PC	Ion channel transport	Cellular response to heat stress
	Stimuli-sensing channels	Translation
CD-ICa	ABC transporters	Signaling by receptor tyrosine kinases
	Hedgehog ligand biogenesis	VEGFA-VEGFR2 pathway
CD-ICb	mRNA splicing	ND

Abbreviations: Endo. = endothelium; PT = proximal tubule; LOH = loop of Henle, Gran. Cells = granular cells of the juxtaglomerular apparatus; DCT = distal convoluted tubules; CNT = connecting tubules; CD-PC = collecting duct principal cells, -ICa or -ICb = intercalating cells a or b.

Table 3.2. Pathways upregulated in neutrophils from THP-/- versus wild-type kidneys after a sham surgery	
Cluster	Kidney THP-/- Sham
0	Complement cascade
	TLR signaling
1	Complement cascade
	TLR signaling
2	Complement cascade
	TLR signaling
3	TLR signaling
	Oxidative Stress Induced Senescence
4	Complement cascade
	TLR signaling
5	WNT signaling
	MAPK signaling
6	Cellular Senescence
	Complement cascade
7	Complement cascade
8	Cellular Senescence
	Complement cascade
9	Complement cascade
	TLR signaling
10	IKK signaling
	TLR signaling
11	IKK signaling
	TLR signaling
12	Cellular Senescence
	negative regulation of MAPK
13	NS

Table 3.3. Pathways upregulated by neutrophil clusters in the blood or kidney with 22-minute IRI in THP-/- mice			
Cluster	Blood THP-/- 22 min IRI (versus other Blood THP-/- 22 min IRI clusters)	THP-/- kidney 22 min IRI (versus other THP-/- kidney 22 min IRI clusters)	Markers
0	<i>Ccl3,4,6</i>	C-Lectin receptors	<i>Srgn</i>
	IL-1 signaling	IL-1 signaling	
1	Formyl peptide signaling	TLR signaling	<i>Prok2</i>
	<i>Ccl6</i> signaling		<i>Srgn</i>
2	Anti-microbial peptides	Formyl peptide signaling	<i>Prok2</i>
		Clathrin-mediated endocytosis	<i>Cd177</i>
3	Interleukin signaling	Formyl peptide signaling	<i>Srgn</i>
	Cell surface interaction vascular wall		<i>Il1b</i>
4	Motility	Detoxification of Reactive Oxygen	<i>Prok2</i>
	Infiltration	C-Lectin receptors	
5	Rho GTPase signaling	E-Selectin interactions	<i>Prok2</i>
	Detoxification of Reactive Oxygen	IL-1 signaling	<i>Mmp8</i>
6	NF-kappaB signaling	Detoxification of Reactive Oxygen	<i>Prok2</i>
		TLR signaling	<i>Srgn</i>
7	Cystatins	TLR signaling	<i>Gm5483</i>
		TLR signaling	<i>BC100530</i>
8	Platelet pathways	TLR signaling	<i>Cd74</i>
	MAPK integrin signaling		
9	CXCR2 signaling	Clathrin-mediated endocytosis	<i>Cxcl2</i>
	TLR4,7,8,9	TLR signaling	<i>Cxcl3</i>
10	Mitochondrial	Clathrin-mediated endocytosis	<i>mt-Atp6</i>
		TLR signaling (7,8,9)	
11	Class I MHC antigen presentation	Cell response to stress	<i>H2-T23</i>
		TLR signaling	<i>Isg15</i>
12	RBC Phagocytic	IL-1 signaling	<i>Hbb-ba</i>
		TLR signaling (4,7,8,9)	
13	Rho GTPase signaling	TLR signaling	<i>Ltf</i>
	Detoxification of Reactive Oxygen	Clathrin-mediated endocytosis	<i>Ly6c2</i>

Table 3.4. Pathways differentially upregulated by cluster when in the blood versus the kidney with 22-minute IRI in THP -/- mice			
Cluster	Blood 22 min IRI -/- mice (versus kidney)	kidney 22 min IRI -/- mice (versus blood)	Markers
0	TNFR signaling	TLR signaling (7/8/9)	<i>Srgn</i>
	INFalpha/beta		
1	Rho GTPase signaling	formyl-peptide signaling	<i>Prok2</i>
		TLR signaling	<i>Srgn</i>
2	Rho GTPase signaling	Chemokine signaling	<i>Prok2</i>
		Cell surface interaction at vascular wall	<i>Cd177</i>
3	Cell division	formyl-peptide signaling	<i>Srgn</i>
			<i>Il1b</i>
4	Rho GTPase signaling	TLR signaling	<i>Prok2</i>
		Complement activators	
5	Metabolism	Complement activators	<i>Prok2</i>
			<i>Mmp8</i>
6	Death receptor signaling	TLR signaling (4)	<i>Prok2</i>
	Rho GTPase signaling	Complement cascade	<i>Srgn</i>
7	Rho GTPase signaling	TLR signaling (4)	<i>Gm5483</i>
	Integrin signaling	TLR signaling (7/8/9)	<i>BC100530</i>
8	Rho GTPase signaling	TLR signaling	<i>Cd74</i>
	Cell division		
9	TGFβ	Detoxification of reactive oxygen	<i>Cxcl2</i>
	Integrin signaling	formyl-peptide signaling	<i>Cxcl3</i>
10	MAPK signaling	Detoxification of reactive oxygen	<i>mt-Atp6</i>
	IL-3, IL-5 signaling		
11	Rho GTPase signaling	Complement cascade	<i>H2-T23</i>
		Detoxification of reactive oxygen	<i>Isg15</i>
12	NS	Complement cascade	<i>Hbb-ba</i>
13	Autophagy	Peptide ligand-binding receptors	<i>Ltf</i>
			<i>Ly6c2</i>

Chapter 4. Animal use and experimentation

Animal protocols

All protocols and procedures were under Indiana University IACUC review. All protocol used for the proposed experiment was fully vetted, reviewed and approved by the Indiana University IACUC.

Protocol 1. Ischemia reperfusion injury surgery (adapted from T. Ashkar).

1. Before and throughout the surgery, animals will be maintained under anesthesia using isoflurane.
2. After preparation, setup and anesthesia, and under sterile conditions, the abdomen will be entered through a small incision.
3. The renal pedicles will be identified, and bilateral clamps will be applied to both pedicles for 22 or 30 minutes.
4. Clamps will be removed, and reperfusion of the kidneys verified visually. The abdominal incision will be closed in 2 layers.
5. An analgesic (Buprenorphine 0.1mg/kg) in addition to 1-2 cc of warm saline will be administered subcutaneously at the end of surgery.
6. Animals will be carefully monitored after surgery. A clinical assessment of each animal, noting general appearance, activity level, food intake and skin turgor will be performed daily.
7. After 6 hours of reperfusion the kidneys will be harvested. Animals will be anesthetized with pentobarbital 130mg/kg IP, a blood specimen will be drawn, kidneys will be removed, and the animals sacrificed.

Protocol 2: Sham surgery, control for surgery and is outlined below.

1. Before and throughout the surgery, animals will be maintained under anesthesia using isoflurane.
2. After preparation, setup and anesthesia, and under sterile conditions, the abdomen will be entered through a small incision.
3. The abdomen will remain open for 22 or 30 minutes.
4. The abdominal incision will be closed in 2 layers.
5. An analgesic (Buprenorphine 0.1mg/kg) in addition to 1-2 cc of warm saline will be administered subcutaneously at the end of surgery.
6. Animals will be carefully monitored after surgery. A clinical assessment of each animal, noting general appearance, activity level, food intake and skin turgor will be performed daily.
7. After 6 hours of reperfusion the kidneys will be harvested. Animals will be anesthetized with pentobarbital 130mg/kg IP, a blood specimen will be drawn, kidneys will be removed, and the animals sacrificed.

Animal use

Justification

Previous work was performed in wild-type male 129Sv/Ev (Taconic) mice at 8-10 weeks. Ischemia reperfusion injury (IRI) of the kidney was performed in the male mice exclusively because female mice are resistant to IRI (64). Furthermore, in this work all IRI was performed in males to extend existing data and, for reasons that have yet to be elucidated, there is a sex dependent difference in susceptibility to AKI in mice. As such, the experiments are intentionally performed in males only as females appear to be more resistant to AKI following IRI.

Veterinary care

All animals were housed in the Indiana University animal facility-Laboratory Animal Resource Center (LARC). The LARC is an AALAC accredited facility that is connected to our laboratory building. The LARC employs 5 fulltime veterinarians and additional staff that carryout routine animal care and monitoring at least twice daily. Mice had access to water *ad libitum* and standard chow.

Limiting discomfort of animals

All surgeries are survival surgeries following ischemia reperfusion injury of the kidney or a sham surgery. Discomfort was managed before, during and after surgery. Prior to the surgery anesthesia with 5% isoflurane and low flow oxygen was used. The depth of anesthesia was monitored by response to tail or toe pinch, spontaneous movements, and the animals' respiratory rate. Animals were monitored continuously before and during surgery. To maintain anesthesia the isoflurane was be reduced to 1-2%. Periodically, every 3-4 minutes, responsiveness was tested to tail or toe pinch, and assess spontaneous movements and the animals' respiratory rate. Following all surgeries and twice daily until euthanasia, each animal was given a subcutaneous dose of analgesic (Buprenorphine HCl, 0.1 mg/Kg) to minimize post-operative discomfort. After surgery, all animals were monitored every hour for 12 hours and then every 4 hours until euthanasia. To limit discomfort mice were monitored for not taking food for more than one day or minimal movement in response to stimulation on two occasions.

Euthanasia

In surgeries, mice under sedation were exsanguinated following harvesting of tissue and cervical dislocation to ensure death. This method of euthanasia is consistent with the

recommendations of the Panel on Euthanasia of the American Veterinary Medical Association and approved by Indiana University institutional animal use committee.

Summary and Conclusions

Neutrophil diversity has been examined in specific disease and pathologies. These accounts have been limited by available techniques (e.g. microscopy and flow cytometry), a reliance on validated markers and the ad hoc hierarchical trees based on these markers and techniques. The use of single-cell RNASeq has revolutionized our ability to resolve and holistically redefine populations of cells in an unbiased manner. Here it is demonstrated that there is neutrophil diversity in the mouse kidney and that neutrophil populations respond specifically to their environment and a disease state. The added complexity in neutrophil biology revealed through the novel application of these approaches requires a reevaluation of existing assumptions about mechanism and the role of neutrophils in health and disease.

Neutrophils are more nuanced than previously appreciated. Six transcriptionally distinct populations have been described in this work. Furthermore, their putative behaviors, imputed by pathway analysis, were more varied than expected. They included distinct immunomodulatory populations via either MHC I or MHC II mechanisms, a presumptively motile population, a CXCR2 signaling population and a classically activated population. Two of these, the signaling and the activated populations, may be further subdivided (**Table 2.1** and **Figure 2.12**). Furthermore, specific neutrophil populations are uniquely sensitive to the severity of AKI (**Figure 2.14** and **Figures 3.4-3.5**). For instance, the proportion of neutrophil cluster 8 (MHC II antigen presentation) in the kidney increases in moderate injury and not in severe injury versus a sham surgery (**Figure 2.16** and **3.5**). These populations are not limited to AKI or the kidney. Neutrophils like the motile and MHC II antigen presenting populations can be found in a mouse model of metastasizing cancer in the spleen (**Figure 2.17**). Thus, the neutrophil diversity described here has

captured subpopulations of neutrophils associated with AKI and begun to define the landscape of common neutrophil types across tissues and disease.

CXCR2 signaling is central to AKI. The CXCR2 ligand *Cxcl2* has been shown to be a major instigator of neutrophil chemotaxis in AKI and poor recovery of kidney function. In this work, *Cxcl3*, also a ligand of CXCR2, is shown to be uniquely expressed after severe injury in a specific set of neutrophils. This specificity suggests a tightly regulated chemokine that may act in addition to *Cxcl2* in severe injury. Models of CXCR2 axis activity on neutrophils during AKI are given in Appendix A (**Figures A.1-A.3**).

The role of THP in modulating neutrophil diversity is both nonspecific *and* finetuned. For instance, the upregulated pathways in neutrophils were nearly uniform in the THP^{-/-} mice (**Table 3.2**) yet there appears to be specific modulation neutrophil populations (**Figure 3.3**). This conundrum is not new to THP. THP has a specific role modulating the immune system in the kidney(83) while also having a systemic impact(87, 88). Furthermore, the increase in CXCR2 ligand expression in specific cell types following injury of THP^{-/-} mice may be explained by THPs role in modulation of the IL17/IL23 axis. IL17 is known to induce upregulation of CXCR2 ligands(91). Thus, the S1 segment of the proximal tubule and granular cells of the juxtaglomerular apparatus may be targets of THPs modulation of the cytokine milieu through the IL17/IL23 axis.

Future directions

The diversity and complexity of neutrophils proposed by this work argues for an in-depth investigation of neutrophil biology in tissue injury. The kidney is well suited for studying neutrophil diversity in normal physiology and pathophysiology as demonstrated by complexity of neutrophil biology during ischemic AKI. Furthermore, neutrophils have been implicated in repair after tissue damage in several organs but not in the kidney.

Thus, there is an opportunity to expand our mechanistic understanding of a central actor in immunology in the complex pathologies of the kidney.

CXCL3 is a new ligand for neutrophil recruitment that may be involved in the mechanistic differences between severe and moderate AKI. Whether CXCL3 and CXCL2 act on CXCR2 in concert, in opposition or independently to drive neutrophil recruitment warrants additional investigation. First, it needs to be demonstrated that CXCL3 plays a significant role, like CXCL2, in the progression of AKI. These data suggest that both CXCL2 and CXCL3 may act on CXCR2 to drive the severe injury seen in 30-minute IRI. To test for this an antibody based CXCL3 neutralization experiment could be done on 30-minute IRI. Presumably, following CXCL3 neutralization, only CXCL2 signaling would remain and phenotypically the neutralized 30-minute IRI would resemble 22-minute IRI. Beyond this study the next avenue to pursue could include genetic testing of the origin and timing of both CXCL3 and CXCL2. For instance, inducible cell-type specific knockouts of both CXCL3 and CXCL2 would be a malleable and powerful system for elucidating cytokine signaling in AKI.

The role of atypical antigen presenting neutrophils in renal pathology is unknown. The putative MHC-II antigen presenting neutrophils were detected more frequently in moderate injury. It is possible that they are involved in modulating the response of T-cells and NK cells in injured tissue. Further elucidation of their role in AKI may provide insight into how severity of injury impacts recovery of kidney function. Genetic models could provide a framework to selectively track (reporter strains), remove and induce behaviors in neutrophils. For instance, the selective and inducible removal of neutrophil population 8 would allow for testing of the specific requirement for these actors in AKI.

The shifts in cytokines and distribution of differentially regulated neutrophil clusters with the severity of injury suggests a “one-size fits all” approach to AKI is inadequate (**Figures A.1-2**). Thus, it is timely to explore the impact of changing both ischemia and

reperfusion times on injury and assaying the response of the parenchyma and infiltrating immune cells with single-cell sequencing, high-resolution large-scale imaging and multiplexed ELISAs. This will benefit our understanding of ischemic AKI in two ways: 1) improve our mechanistic understanding of ischemic AKI by manipulating its two fundamental variables and 2) develop better models for the range of clinical ischemic AKI.

The role of etiologies of AKI on neutrophil diversity needs to be investigated as well. Experimentally, models of drug-induced AKI (cisplatin) and septic-AKI should be used to investigate the impact of these etiologies on neutrophil diversity and possibly CXCR2 signaling. A comparative approach between ischemic, septic and drug induced AKI would help highlight common and unique neutrophil types and behaviors and develop better models of the role of neutrophil biology in AKI which, in turn, might allow for improved theragnostic approaches.

This work will hopefully be a starting point for a plenitude of research projects. This work provides a foundation for exploring the fundamental nature of neutrophil biology, the orchestration of chemokines on the CXCR2 axis and has uncovered complexity in the immunology of ischemic injury which may untangle the complex etiology of acute kidney injury.

Appendix A

Models for neutrophil involvement in AKI with changes in the severity of injury and the absence of THP.

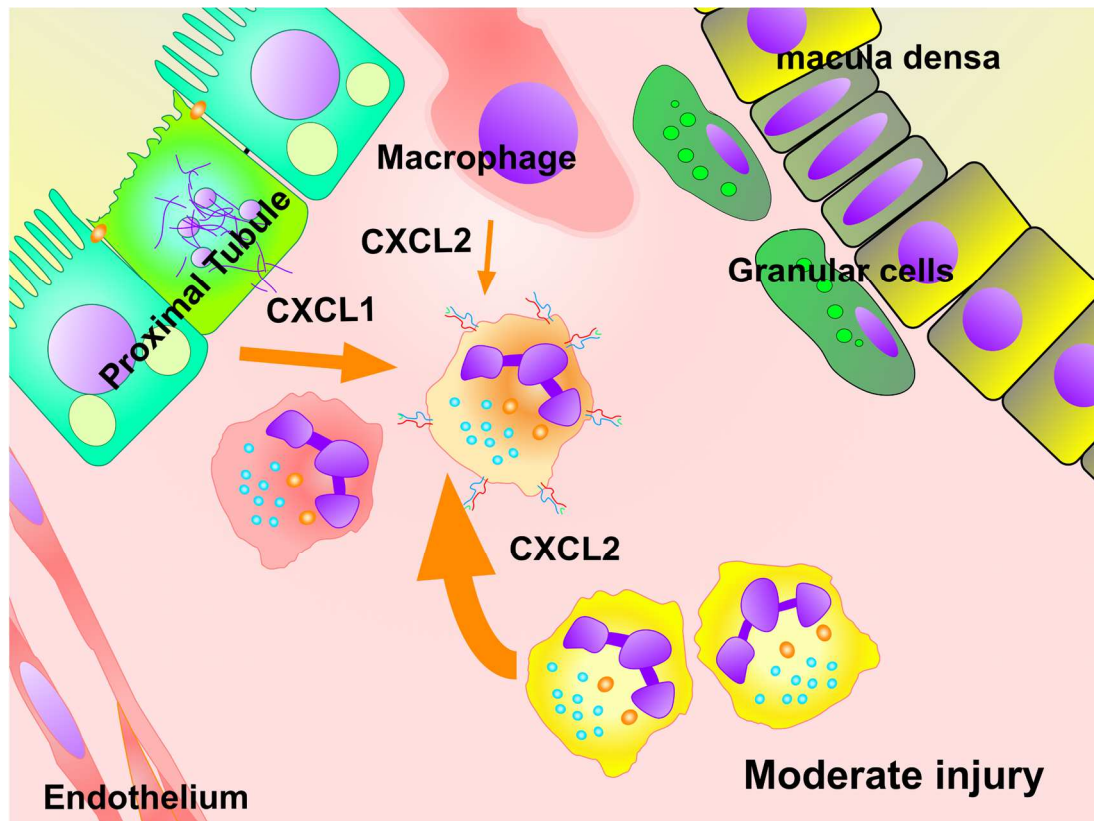


Figure A.1. Model of cytokine activity on neutrophils with moderate injury. CXCR2 signaling in moderate injury is primarily from other neutrophils via CXCL2 with additional CXCL2 from macrophages and CXCL1 from proximal tubule epithelial cells.

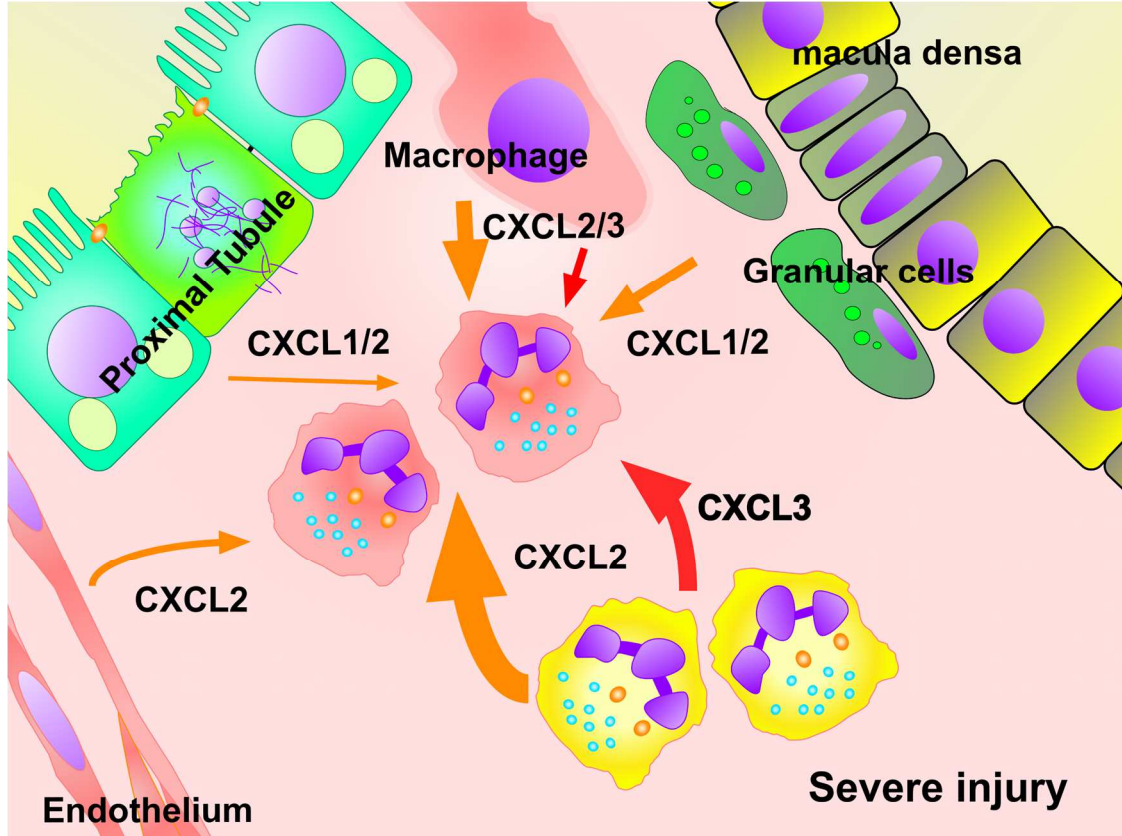


Figure A.2. Model of cytokine activity on neutrophils with severe injury. CXCR2 signaling in severe injury is significantly from other neutrophils via CXCL2 and CXCL3 and additional CXCL2 and CXCL3 from macrophages and CXCL2 from the endothelium, and CXCL1/2 from proximal tubule epithelium and the granular cells of the juxtaglomerular apparatus.

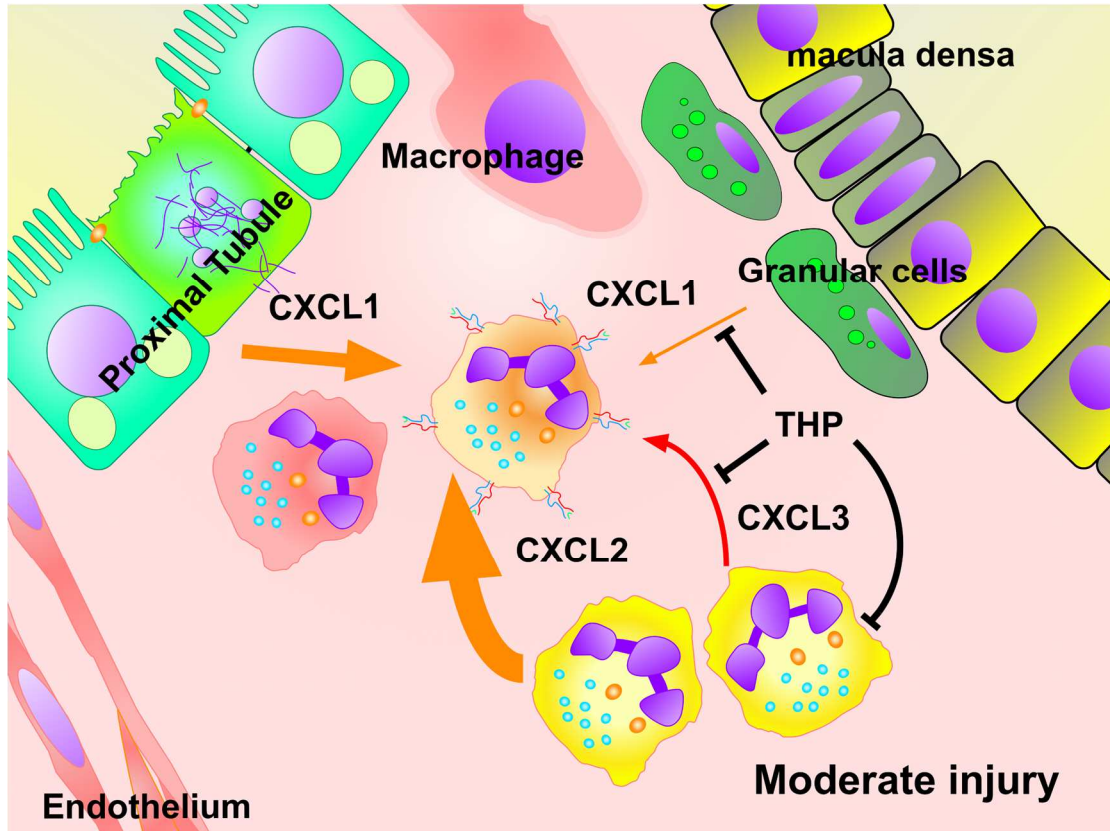


Figure A.3. Model of cytokine activity on neutrophils with moderate injury in THP-/- mice. CXCR2 signaling in THP-/- mice with moderate injury is primarily from other neutrophils via CXCL2 and CXCL3 and CXCL1 from proximal tubule epithelium. The proposed role of THP in suppressing expression of CXCL3 and CXCL1 and in shaping neutrophil proportions is indicated.

References

1. Mehta RL, Cerda J, Burdmann EA, Tonelli M, Garcia-Garcia G, Jha V, et al. International Society of Nephrology's Oby25 initiative for acute kidney injury (zero preventable deaths by 2025): a human rights case for nephrology. *Lancet*. 2015;385(9987):2616-43. Epub 2015/03/18. doi: 10.1016/S0140-6736(15)60126-X. PubMed PMID: 25777661.
2. Kellum JA, Hoste EA. Acute kidney injury: epidemiology and assessment. *Scand J Clin Lab Invest Suppl*. 2008;241:6-11. Epub 2008/08/21. doi: 10.1080/00365510802144813. PubMed PMID: 18569958.
3. Zuk A, Bonventre JV. Acute Kidney Injury. *Annu Rev Med*. 2016;67:293-307. doi: 10.1146/annurev-med-050214-013407. PubMed PMID: 26768243; PubMed Central PMCID: PMC4845743.
4. Silver SA, Long J, Zheng Y, Chertow GM. Cost of Acute Kidney Injury in Hospitalized Patients. *J Hosp Med*. 2017;12(2):70-6. Epub 2017/02/10. doi: 10.12788/jhm.2683. PubMed PMID: 28182800.
5. Silver SA, Chertow GM. The Economic Consequences of Acute Kidney Injury. *Nephron*. 2017;137(4):297-301. Epub 2017/06/09. doi: 10.1159/000475607. PubMed PMID: 28595193; PubMed Central PMCID: PMC5743773.
6. Hoste EA, Schurgers M. Epidemiology of acute kidney injury: how big is the problem? *Crit Care Med*. 2008;36(4 Suppl):S146-51. Epub 2008/04/11. doi: 10.1097/CCM.0b013e318168c590. PubMed PMID: 18382186.
7. Collister D, Pannu N, Ye F, James M, Hemmelgarn B, Chui B, et al. Health Care Costs Associated with AKI. *Clin J Am Soc Nephrol*. 2017;12(11):1733-43. Epub 2017/10/21. doi: 10.2215/CJN.00950117. PubMed PMID: 29051143; PubMed Central PMCID: PMC5672961.

8. Zappitelli M, Parikh CR, Akcan-Arikan A, Washburn KK, Moffett BS, Goldstein SL. Ascertainment and epidemiology of acute kidney injury varies with definition interpretation. *Clin J Am Soc Nephrol.* 2008;3(4):948-54. Epub 2008/04/18. doi: 10.2215/CJN.05431207. PubMed PMID: 18417742; PubMed Central PMCID: PMCPMC2440279.
9. Zappitelli M. Epidemiology and diagnosis of acute kidney injury. *Seminars in nephrology.* 2008;28(5):436-46. Epub 2008/09/16. doi: 10.1016/j.semnephrol.2008.05.003. PubMed PMID: 18790363.
10. Schetz M, Dasta J, Goldstein S, Golper T. Drug-induced acute kidney injury. *Curr Opin Crit Care.* 2005;11(6):555-65. Epub 2005/11/18. doi: 10.1097/01.ccx.0000184300.68383.95. PubMed PMID: 16292059.
11. Waikar SS, Liu KD, Chertow GM. Diagnosis, epidemiology and outcomes of acute kidney injury. *Clin J Am Soc Nephrol.* 2008;3(3):844-61. Epub 2008/03/14. doi: 10.2215/CJN.05191107. PubMed PMID: 18337550.
12. Izzedine H, Perazella MA. Anticancer Drug-Induced Acute Kidney Injury. *Kidney Int Rep.* 2017;2(4):504-14. Epub 2018/01/11. doi: 10.1016/j.ekir.2017.02.008. PubMed PMID: 29318217; PubMed Central PMCID: PMCPMC5720534.
13. Mehta RL, Kellum JA, Shah SV, Molitoris BA, Ronco C, Warnock DG, et al. Acute Kidney Injury Network: report of an initiative to improve outcomes in acute kidney injury. *Crit Care.* 2007;11(2):R31. Epub 2007/03/03. doi: 10.1186/cc5713. PubMed PMID: 17331245; PubMed Central PMCID: PMCPMC2206446.
14. Ftouh S, Lewington A, Acute Kidney Injury Guideline Development Group convened by the National Clinical Guidelines C, commissioned by the National Institute for Health Care Excellence iawTRCoPC. Prevention, detection and management of acute kidney injury: concise guideline. *Clin Med (Lond).* 2014;14(1):61-5. Epub 2014/02/18. doi: 10.7861/clinmedicine.14-1-61. PubMed PMID: 24532748.

15. Khwaja A. KDIGO clinical practice guidelines for acute kidney injury. *Nephron Clin Pract.* 2012;120(4):c179-84. Epub 2012/08/15. doi: 10.1159/000339789. PubMed PMID: 22890468.
16. Basile DP, Anderson MD, Sutton TA. Pathophysiology of acute kidney injury. *Compr Physiol.* 2012;2(2):1303-53. Epub 2012/04/01. doi: 10.1002/cphy.c110041. PubMed PMID: 23798302; PubMed Central PMCID: PMC3919808.
17. Rabb H, Griffin MD, McKay DB, Swaminathan S, Pickkers P, Rosner MH, et al. Inflammation in AKI: Current Understanding, Key Questions, and Knowledge Gaps. *Journal of the American Society of Nephrology : JASN.* 2016;27(2):371-9. Epub 2015/11/13. doi: 10.1681/ASN.2015030261. PubMed PMID: 26561643; PubMed Central PMCID: PMC4731128.
18. Mulay SR, Holderied A, Kumar SV, Anders HJ. Targeting Inflammation in So-Called Acute Kidney Injury. *Seminars in nephrology.* 2016;36(1):17-30. Epub 2016/04/18. doi: 10.1016/j.semnephrol.2016.01.006. PubMed PMID: 27085732.
19. Lee SA, Noel S, Sadasivam M, Hamad ARA, Rabb H. Role of Immune Cells in Acute Kidney Injury and Repair. *Nephron.* 2017;137(4):282-6. Epub 2017/06/12. doi: 10.1159/000477181. PubMed PMID: 28601878; PubMed Central PMCID: PMC5723562.
20. Makris K, Spanou L. Acute Kidney Injury: Definition, Pathophysiology and Clinical Phenotypes. *Clin Biochem Rev.* 2016;37(2):85-98. Epub 2017/03/18. PubMed PMID: 28303073; PubMed Central PMCID: PMC5198510.
21. Wei Q, Dong Z. Mouse model of ischemic acute kidney injury: technical notes and tricks. *American journal of physiology Renal physiology.* 2012;303(11):F1487-94. Epub 2012/09/21. doi: 10.1152/ajprenal.00352.2012. PubMed PMID: 22993069; PubMed Central PMCID: PMC3532486.

22. Rosales C. Neutrophil: A Cell with Many Roles in Inflammation or Several Cell Types? *Front Physiol.* 2018;9:113. Epub 2018/03/09. doi: 10.3389/fphys.2018.00113. PubMed PMID: 29515456; PubMed Central PMCID: PMC5826082.
23. Scapini P, Marini O, Tecchio C, Cassatella MA. Human neutrophils in the saga of cellular heterogeneity: insights and open questions. *Immunol Rev.* 2016;273(1):48-60. Epub 2016/08/26. doi: 10.1111/imr.12448. PubMed PMID: 27558327.
24. Garley M, Jablonska E. Heterogeneity Among Neutrophils. *Arch Immunol Ther Exp (Warsz).* 2018;66(1):21-30. Epub 2017/06/01. doi: 10.1007/s00005-017-0476-4. PubMed PMID: 28560557; PubMed Central PMCID: PMC5767199.
25. Ng LG, Ostuni R, Hidalgo A. Heterogeneity of neutrophils. *Nature reviews Immunology.* 2019;19(4):255-65. Epub 2019/03/01. doi: 10.1038/s41577-019-0141-8. PubMed PMID: 30816340.
26. Wright HL, Moots RJ, Bucknall RC, Edwards SW. Neutrophil function in inflammation and inflammatory diseases. *Rheumatology (Oxford).* 2010;49(9):1618-31. Epub 2010/03/27. doi: 10.1093/rheumatology/keq045. PubMed PMID: 20338884.
27. Lawrence SM, Corriden R, Nizet V. The Ontogeny of a Neutrophil: Mechanisms of Granulopoiesis and Homeostasis. *Microbiol Mol Biol Rev.* 2018;82(1). Epub 2018/02/14. doi: 10.1128/MMBR.00057-17. PubMed PMID: 29436479; PubMed Central PMCID: PMC5813886.
28. Christoffersson G, Phillipson M. The neutrophil: one cell on many missions or many cells with different agendas? *Cell Tissue Res.* 2018;371(3):415-23. Epub 2018/02/13. doi: 10.1007/s00441-017-2780-z. PubMed PMID: 29435651; PubMed Central PMCID: PMC5820408.
29. Zhang X, Kluger Y, Nakayama Y, Poddar R, Whitney C, DeTora A, et al. Gene expression in mature neutrophils: early responses to inflammatory stimuli. *J Leukoc Biol.*

2004;75(2):358-72. Epub 2003/11/25. doi: 10.1189/jlb.0903412. PubMed PMID: 14634056.

30. de Oliveira S, Rosowski EE, Huttenlocher A. Neutrophil migration in infection and wound repair: going forward in reverse. *Nat Rev Immunol.* 2016;16(6):378-91. Epub 2016/05/28. doi: 10.1038/nri.2016.49. PubMed PMID: 27231052; PubMed Central PMCID: PMC5367630.

31. Papayannopoulos V. Neutrophil extracellular traps in immunity and disease. *Nature reviews Immunology.* 2018;18(2):134-47. Epub 2017/10/11. doi: 10.1038/nri.2017.105. PubMed PMID: 28990587.

32. Raup-Konsavage WM, Wang Y, Wang WW, Feliars D, Ruan H, Reeves WB. Neutrophil peptidyl arginine deiminase-4 has a pivotal role in ischemia/reperfusion-induced acute kidney injury. *Kidney Int.* 2018;93(2):365-74. Epub 2017/10/25. doi: 10.1016/j.kint.2017.08.014. PubMed PMID: 29061334; PubMed Central PMCID: PMC5794573.

33. Nakazawa D, Kumar SV, Marschner J, Desai J, Holderied A, Rath L, et al. Histones and Neutrophil Extracellular Traps Enhance Tubular Necrosis and Remote Organ Injury in Ischemic AKI. *Journal of the American Society of Nephrology : JASN.* 2017;28(6):1753-68. Epub 2017/01/12. doi: 10.1681/ASN.2016080925. PubMed PMID: 28073931; PubMed Central PMCID: PMC5461800.

34. Fridlender ZG, Sun J, Kim S, Kapoor V, Cheng G, Ling L, et al. Polarization of tumor-associated neutrophil phenotype by TGF-beta: "N1" versus "N2" TAN. *Cancer Cell.* 2009;16(3):183-94. Epub 2009/09/08. doi: 10.1016/j.ccr.2009.06.017. PubMed PMID: 19732719; PubMed Central PMCID: PMC2754404.

35. Bird L. TUMOUR IMMUNOLOGY Neutrophil plasticity. *Nature Reviews Immunology.* 2009;9(10). doi: 10.1038/nri2649. PubMed PMID: WOS:000270133000004.

36. Shaul ME, Levy L, Sun J, Mishalian I, Singhal S, Kapoor V, et al. Tumor-associated neutrophils display a distinct N1 profile following TGFbeta modulation: A transcriptomics analysis of pro- vs. antitumor TANs. *Oncoimmunology*. 2016;5(11):e1232221. Epub 2016/12/22. doi: 10.1080/2162402X.2016.1232221. PubMed PMID: 27999744; PubMed Central PMCID: PMC5139653.
37. Singhal S, Bhojnagarwala PS, O'Brien S, Moon EK, Garfall AL, Rao AS, et al. Origin and Role of a Subset of Tumor-Associated Neutrophils with Antigen-Presenting Cell Features in Early-Stage Human Lung Cancer. *Cancer Cell*. 2016;30(1):120-35. Epub 2016/07/05. doi: 10.1016/j.ccell.2016.06.001. PubMed PMID: 27374224; PubMed Central PMCID: PMC4945447.
38. Powell DR, Huttenlocher A. Neutrophils in the Tumor Microenvironment. *Trends Immunol*. 2016;37(1):41-52. Epub 2015/12/25. doi: 10.1016/j.it.2015.11.008. PubMed PMID: 26700397; PubMed Central PMCID: PMC4707100.
39. Shimada Y, Saji H, Kakihana M, Honda H, Usuda J, Kajiwara N, et al. Retrospective analysis of nodal spread patterns according to tumor location in pathological N2 non-small cell lung cancer. *World J Surg*. 2012;36(12):2865-71. Epub 2012/09/06. doi: 10.1007/s00268-012-1743-5. PubMed PMID: 22948194; PubMed Central PMCID: PMC3501158.
40. Ma Y, Yabluchanskiy A, Iyer RP, Cannon PL, Flynn ER, Jung M, et al. Temporal neutrophil polarization following myocardial infarction. *Cardiovasc Res*. 2016;110(1):51-61. Epub 2016/01/31. doi: 10.1093/cvr/cvw024. PubMed PMID: 26825554; PubMed Central PMCID: PMC4798046.
41. Cuartero MI, Ballesteros I, Moraga A, Nombela F, Vivancos J, Hamilton JA, et al. N2 neutrophils, novel players in brain inflammation after stroke: modulation by the PPARgamma agonist rosiglitazone. *Stroke*. 2013;44(12):3498-508. Epub 2013/10/19. doi: 10.1161/STROKEAHA.113.002470. PubMed PMID: 24135932.

42. Baban B, Marchetti C, Khodadadi H, Malik A, Emami G, Lin PC, et al. Glucocorticoid-Induced Leucine Zipper Promotes Neutrophil and T-Cell Polarization with Protective Effects in Acute Kidney Injury. *J Pharmacol Exp Ther.* 2018;367(3):483-93. Epub 2018/10/12. doi: 10.1124/jpet.118.251371. PubMed PMID: 30301736.
43. Baban B, Hoda N, Malik A, Khodadadi H, Simmerman E, Vaibhav K, et al. Impact of cannabidiol treatment on regulatory T-17 cells and neutrophil polarization in acute kidney injury. *American journal of physiology Renal physiology.* 2018;315(4):F1149-F58. Epub 2018/06/14. doi: 10.1152/ajprenal.00112.2018. PubMed PMID: 29897289.
44. Akcay A, Nguyen Q, Edelstein CL. Mediators of inflammation in acute kidney injury. *Mediators Inflamm.* 2009;2009:137072. Epub 2010/02/26. doi: 10.1155/2009/137072. PubMed PMID: 20182538; PubMed Central PMCID: PMC2825552.
45. Awad AS, Rouse M, Huang L, Vergis AL, Reutershan J, Cathro HP, et al. Compartmentalization of neutrophils in the kidney and lung following acute ischemic kidney injury. *Kidney Int.* 2009;75(7):689-98. Epub 2009/01/09. doi: 10.1038/ki.2008.648. PubMed PMID: 19129795; PubMed Central PMCID: PMC2656389.
46. El-Achkar TM, McCracken R, Liu Y, Heitmeier MR, Bourgeois S, Ryerse J, et al. Tamm-Horsfall protein translocates to the basolateral domain of thick ascending limbs, interstitium, and circulation during recovery from acute kidney injury. *American journal of physiology Renal physiology.* 2013;304(8):F1066-75. Epub 2013/02/08. doi: 10.1152/ajprenal.00543.2012. PubMed PMID: 23389456; PubMed Central PMCID: PMC3625838.
47. Kelly KJ, Williams WW, Jr., Colvin RB, Meehan SM, Springer TA, Gutierrez-Ramos JC, et al. Intercellular adhesion molecule-1-deficient mice are protected against ischemic renal injury. *J Clin Invest.* 1996;97(4):1056-63. Epub 1996/02/15. doi:

10.1172/JCI118498. PubMed PMID: 8613529; PubMed Central PMCID: PMCPMC507153.

48. El-Achkar TM, McCracken R, Rauchman M, Heitmeier MR, Al-Aly Z, Dagher PC, et al. Tamm-Horsfall protein-deficient thick ascending limbs promote injury to neighboring S3 segments in an MIP-2-dependent mechanism. *American journal of physiology Renal physiology*. 2011;300(4):F999-1007. Epub 2011/01/14. doi: 10.1152/ajprenal.00621.2010. PubMed PMID: 21228114.

49. Micanovic R, Khan S, El-Achkar TM. Immunofluorescence laser micro-dissection of specific nephron segments in the mouse kidney allows targeted downstream proteomic analysis. *Physiol Rep*. 2015;3(2). Epub 2015/02/14. doi: 10.14814/phy2.12306. PubMed PMID: 25677553; PubMed Central PMCID: PMCPMC4393212.

50. Barwinska D, Ferkowicz MJ, Cheng YH, Winfree S, Dunn KW, Kelly KJ, et al. Application of Laser Microdissection to Uncover Regional Transcriptomics in Human Kidney Tissue. *J Vis Exp*. 2020(160). Epub 2020/07/01. doi: 10.3791/61371. PubMed PMID: 32597856.

51. See P, Lum J, Chen J, Ginhoux F. A Single-Cell Sequencing Guide for Immunologists. *Front Immunol*. 2018;9:2425. Epub 2018/11/09. doi: 10.3389/fimmu.2018.02425. PubMed PMID: 30405621; PubMed Central PMCID: PMCPMC6205970.

52. Williams EJ, Green J, Beckingham I, Parks R, Martin D, Lombard M, et al. Guidelines on the management of common bile duct stones (CBDS). *Gut*. 2008;57(7):1004-21. Epub 2008/03/07. doi: 10.1136/gut.2007.121657. PubMed PMID: 18321943.

53. Kirita Y, Wu H, Uchimura K, Wilson PC, Humphreys BD. Cell profiling of mouse acute kidney injury reveals conserved cellular responses to injury. *Proc Natl Acad Sci U S A*. 2020. Epub 2020/06/24. doi: 10.1073/pnas.2005477117. PubMed PMID: 32571916.

54. Kumar P, Tan Y, Cahan P. Understanding development and stem cells using single cell-based analyses of gene expression. *Development*. 2017;144(1):17-32. Epub 2017/01/05. doi: 10.1242/dev.133058. PubMed PMID: 28049689; PubMed Central PMCID: PMC5278625.
55. Papalexi E, Satija R. Single-cell RNA sequencing to explore immune cell heterogeneity. *Nature reviews Immunology*. 2018;18(1):35-45. Epub 2017/08/09. doi: 10.1038/nri.2017.76. PubMed PMID: 28787399.
56. Wu H, Uchimura K, Donnelly EL, Kirita Y, Morris SA, Humphreys BD. Comparative Analysis and Refinement of Human PSC-Derived Kidney Organoid Differentiation with Single-Cell Transcriptomics. *Cell Stem Cell*. 2018;23(6):869-81 e8. Epub 2018/11/20. doi: 10.1016/j.stem.2018.10.010. PubMed PMID: 30449713; PubMed Central PMCID: PMC6324730.
57. Fu J, Akat KM, Sun Z, Zhang W, Schlondorff D, Liu Z, et al. Single-Cell RNA Profiling of Glomerular Cells Shows Dynamic Changes in Experimental Diabetic Kidney Disease. *Journal of the American Society of Nephrology : JASN*. 2019;30(4):533-45. Epub 2019/03/09. doi: 10.1681/ASN.2018090896. PubMed PMID: 30846559; PubMed Central PMCID: PMC6442341.
58. Alshetaiwi H, Pervolarakis N, McIntyre LL, Ma D, Nguyen Q, Rath JA, et al. Defining the emergence of myeloid-derived suppressor cells in breast cancer using single-cell transcriptomics. *Sci Immunol*. 2020;5(44). Epub 2020/02/23. doi: 10.1126/sciimmunol.aay6017. PubMed PMID: 32086381; PubMed Central PMCID: PMC7219211.
59. Park J, Shrestha R, Qiu C, Kondo A, Huang S, Werth M, et al. Single-cell transcriptomics of the mouse kidney reveals potential cellular targets of kidney disease. *Science*. 2018;360(6390):758-63. Epub 2018/04/07. doi: 10.1126/science.aar2131. PubMed PMID: 29622724; PubMed Central PMCID: PMC6188645.

60. Zimmerman KA, Bentley MR, Lever JM, Li Z, Crossman DK, Song CJ, et al. Single-Cell RNA Sequencing Identifies Candidate Renal Resident Macrophage Gene Expression Signatures across Species. *Journal of the American Society of Nephrology : JASN*. 2019;30(5):767-81. Epub 2019/04/06. doi: 10.1681/ASN.2018090931. PubMed PMID: 30948627; PubMed Central PMCID: PMC6493978.
61. Stuart T, Butler A, Hoffman P, Hafemeister C, Papalexi E, Mauck WM, 3rd, et al. Comprehensive Integration of Single-Cell Data. *Cell*. 2019;177(7):1888-902 e21. Epub 2019/06/11. doi: 10.1016/j.cell.2019.05.031. PubMed PMID: 31178118; PubMed Central PMCID: PMC6687398.
62. Satija R, Farrell JA, Gennert D, Schier AF, Regev A. Spatial reconstruction of single-cell gene expression data. *Nat Biotechnol*. 2015;33(5):495-502. Epub 2015/04/14. doi: 10.1038/nbt.3192. PubMed PMID: 25867923; PubMed Central PMCID: PMC4430369.
63. Aran D, Looney AP, Liu L, Wu E, Fong V, Hsu A, et al. Reference-based analysis of lung single-cell sequencing reveals a transitional profibrotic macrophage. *Nat Immunol*. 2019;20(2):163-72. Epub 2019/01/16. doi: 10.1038/s41590-018-0276-y. PubMed PMID: 30643263; PubMed Central PMCID: PMC6340744.
64. Lee SJ, Borsting E, Decleves AE, Singh P, Cunard R. Podocytes express IL-6 and lipocalin 2/ neutrophil gelatinase-associated lipocalin in lipopolysaccharide-induced acute glomerular injury. *Nephron Exp Nephrol*. 2012;121(3-4):e86-96. Epub 2012/12/14. doi: 10.1159/000345151. PubMed PMID: 23234871; PubMed Central PMCID: PMC4012854.
65. Swamydas M, Luo Y, Dorf ME, Lionakis MS. Isolation of Mouse Neutrophils. *Curr Protoc Immunol*. 2015;110:3 20 1-3 15. Epub 2015/08/04. doi: 10.1002/0471142735.im0320s110. PubMed PMID: 26237011; PubMed Central PMCID: PMC4574512.

66. Leung-Tack J, Tavera C, Martinez J, Colle A. Neutrophil chemotactic activity is modulated by human cystatin C, an inhibitor of cysteine proteases. *Inflammation*. 1990;14(3):247-58. Epub 1990/06/01. doi: 10.1007/BF00915809. PubMed PMID: 2361732.
67. Sundqvist M, Welin A, Elmwall J, Osla V, Nilsson UJ, Leffler H, et al. Galectin-3 type-C self-association on neutrophil surfaces; The carbohydrate recognition domain regulates cell function. *Journal of leukocyte biology*. 2018;103(2):341-53. Epub 2018/01/19. doi: 10.1002/JLB.3A0317-110R. PubMed PMID: 29345346.
68. Vono M, Lin A, Norrby-Teglund A, Koup RA, Liang F, Lore K. Neutrophils acquire the capacity for antigen presentation to memory CD4(+) T cells in vitro and ex vivo. *Blood*. 2017;129(14):1991-2001. Epub 2017/02/02. doi: 10.1182/blood-2016-10-744441. PubMed PMID: 28143882; PubMed Central PMCID: PMC5383872.
69. Takashima A, Yao Y. Neutrophil plasticity: acquisition of phenotype and functionality of antigen-presenting cell. *Journal of leukocyte biology*. 2015;98(4):489-96. doi: 10.1189/jlb.1MR1014-502R. PubMed PMID: WOS:000362832700006.
70. Danielle Janosevic JM, Thomas McCarthy, Amy Zollman, Farooq Syed, Xiaoling Xuei, Hongyu Gao, ProfileYunlong Liu, Kimberly S. Collins, Ying-Hua Cheng, Seth Winfree, Tarek M. El-Achkar, Bernhard Maier, Ricardo Melo Ferreira, Michael T. Eadon, View Takashi Hato, Pierre C. Dagher. The orchestrated cellular and molecular responses of the kidney to endotoxin define the sepsis timeline. 2020. doi: <https://doi.org/10.1101/2020.05.27.118620>.
71. Schindelin J, Arganda-Carreras I, Frise E, Kaynig V, Longair M, Pietzsch T, et al. Fiji: an open-source platform for biological-image analysis. *Nat Methods*. 2012;9(7):676-82. Epub 2012/06/30. doi: 10.1038/nmeth.2019. PubMed PMID: 22743772; PubMed Central PMCID: PMC3855844.

72. Pietzsch T, Preibisch S, Tomancak P, Saalfeld S. ImgLib2--generic image processing in Java. *Bioinformatics* (Oxford, England). 2012;28(22):3009-11. Epub 2012/09/11. doi: 10.1093/bioinformatics/bts543. PubMed PMID: 22962343; PubMed Central PMCID: PMC3496339.
73. Franck G, Mawson TL, Folco EJ, Molinaro R, Ruvkun V, Engelbertsen D, et al. Roles of PAD4 and NETosis in Experimental Atherosclerosis and Arterial Injury: Implications for Superficial Erosion. *Circ Res*. 2018;123(1):33-42. Epub 2018/03/25. doi: 10.1161/CIRCRESAHA.117.312494. PubMed PMID: 29572206; PubMed Central PMCID: PMC6014872.
74. Pittman K, Kubes P. Damage-associated molecular patterns control neutrophil recruitment. *J Innate Immun*. 2013;5(4):315-23. Epub 2013/03/15. doi: 10.1159/000347132. PubMed PMID: 23486162.
75. El-Achkar TM, Wu XR, Rauchman M, McCracken R, Kiefer S, Dagher PC. Tamm-Horsfall protein protects the kidney from ischemic injury by decreasing inflammation and altering TLR4 expression. *American journal of physiology Renal physiology*. 2008;295(2):F534-44. Epub 2008/05/23. doi: 10.1152/ajprenal.00083.2008. PubMed PMID: 18495803; PubMed Central PMCID: PMC5504389.
76. Muller WA. Mechanisms of leukocyte transendothelial migration. *Annu Rev Pathol*. 2011;6:323-44. Epub 2010/11/16. doi: 10.1146/annurev-pathol-011110-130224. PubMed PMID: 21073340; PubMed Central PMCID: PMC3628537.
77. Tecchio C, Micheletti A, Cassatella MA. Neutrophil-derived cytokines: facts beyond expression. *Front Immunol*. 2014;5:508. Epub 2014/11/07. doi: 10.3389/fimmu.2014.00508. PubMed PMID: 25374568; PubMed Central PMCID: PMC4204637.
78. Paragas N, Qiu A, Zhang Q, Samstein B, Deng SX, Schmidt-Ott KM, et al. The Ngal reporter mouse detects the response of the kidney to injury in real time. *Nat Med*.

2011;17(2):216-22. Epub 2011/01/18. doi: 10.1038/nm.2290. PubMed PMID: 21240264; PubMed Central PMCID: PMCPMC3059503.

79. Yu G, He QY. ReactomePA: an R/Bioconductor package for reactome pathway analysis and visualization. *Mol Biosyst*. 2016;12(2):477-9. Epub 2015/12/15. doi: 10.1039/c5mb00663e. PubMed PMID: 26661513.

80. Miura M, Fu X, Zhang QW, Remick DG, Fairchild RL. Neutralization of Gro alpha and macrophage inflammatory protein-2 attenuates renal ischemia/reperfusion injury. *Am J Pathol*. 2001;159(6):2137-45. Epub 2001/12/06. doi: 10.1016/s0002-9440(10)63065-9. PubMed PMID: 11733364; PubMed Central PMCID: PMCPMC1850606.

81. Furuichi K, Wada T, Kaneko S, Murphy PM. Roles of chemokines in renal ischemia/reperfusion injury. *Front Biosci*. 2008;13:4021-8. Epub 2008/05/30. PubMed PMID: 18508496.

82. Chung AC, Lan HY. Chemokines in renal injury. *Journal of the American Society of Nephrology : JASN*. 2011;22(5):802-9. Epub 2011/04/09. doi: 10.1681/ASN.2010050510. PubMed PMID: 21474561.

83. Micanovic R, Khan S, Janosevic D, Lee ME, Hato T, Srour EF, et al. Tamm-Horsfall Protein Regulates Mononuclear Phagocytes in the Kidney. *Journal of the American Society of Nephrology : JASN*. 2018;29(3):841-56. Epub 2017/11/29. doi: 10.1681/ASN.2017040409. PubMed PMID: 29180395; PubMed Central PMCID: PMCPMC5827593.

84. Shi C, Pamer EG. Monocyte recruitment during infection and inflammation. *Nature reviews Immunology*. 2011;11(11):762-74. Epub 2011/10/11. doi: 10.1038/nri3070. PubMed PMID: 21984070; PubMed Central PMCID: PMCPMC3947780.

85. Micanovic R, LaFavers K, Garimella PS, Wu XR, El-Achkar TM. Uromodulin (Tamm-Horsfall protein): guardian of urinary and systemic homeostasis. *Nephrol Dial Transplant*. 2019. Epub 2019/01/17. doi: 10.1093/ndt/gfy394. PubMed PMID: 30649494.

86. Serafini-Cessi F, Malagolini N, Cavallone D. Tamm-Horsfall glycoprotein: biology and clinical relevance. *Am J Kidney Dis.* 2003;42(4):658-76. Epub 2003/10/02. PubMed PMID: 14520616.
87. Micanovic R, Chitteti BR, Dagher PC, Srour EF, Khan S, Hato T, et al. Tamm-Horsfall Protein Regulates Granulopoiesis and Systemic Neutrophil Homeostasis. *Journal of the American Society of Nephrology : JASN.* 2015. Epub 2015/01/04. doi: 10.1681/asn.2014070664. PubMed PMID: 25556169.
88. LaFavers KA, Macedo E, Garimella PS, Lima C, Khan S, Myslinski J, et al. Circulating uromodulin inhibits systemic oxidative stress by inactivating the TRPM2 channel. *Sci Transl Med.* 2019;11(512). Epub 2019/10/04. doi: 10.1126/scitranslmed.aaw3639. PubMed PMID: 31578243; PubMed Central PMCID: PMC7034444.
89. Wu H, Ma J, Wang P, Corpuz TM, Panchapakesan U, Wyburn KR, et al. HMGB1 contributes to kidney ischemia reperfusion injury. *Journal of the American Society of Nephrology : JASN.* 2010;21(11):1878-90. Epub 2010/09/18. doi: 10.1681/ASN.2009101048. PubMed PMID: 20847143; PubMed Central PMCID: PMC3014003.
90. Micanovic R, Chitteti BR, Dagher PC, Srour EF, Khan S, Hato T, et al. Tamm-Horsfall Protein Regulates Granulopoiesis and Systemic Neutrophil Homeostasis. *J Am Soc Nephrol.* 2015;26(9):2172-82. Epub 2015/01/04. doi: ASN.2014070664 [pii] 10.1681/ASN.2014070664. PubMed PMID: 25556169.
91. Onishi RM, Gaffen SL. Interleukin-17 and its target genes: mechanisms of interleukin-17 function in disease. *Immunology.* 2010;129(3):311-21. Epub 2010/04/23. doi: 10.1111/j.1365-2567.2009.03240.x. PubMed PMID: 20409152; PubMed Central PMCID: PMC2826676.

Curriculum vitae

Seth Winfree

POSITIONS

- 2015-2017 Director of New Technologies, Indiana Center for Biological Microscopy, Department of Medicine, Division of Nephrology, Indiana University School of Medicine, Indianapolis, IN
- 2013-2015 Microscopy Technologist, Indiana Center for Biological Microscopy, Department of Medicine, Division of Nephrology, Indiana University School of Medicine, Indianapolis, IN
- 2007-2012 Biologist (GS12), Salmonella-Host Cell Interactions Section, Rocky Mountain Laboratories, National Institutes of Health, Hamilton, MT
- 2000-2003 Scientist (contracted to NASA at Ames Research Center), Lockheed Martin, Moffett Field, CA
- 1999-2000 Information Technologies Assistant, Santa Cruz Biotechnology, Santa Cruz, CA

EDUCATION

- 2017-2020 PhD, Cellular and Integrative Physiology, Indiana University, Indianapolis, IN
Laboratory of Tarek El-Achkar
Neutrophil diversity in ischemic acute kidney injury

- 2003-2007 MS, Biological Sciences, Stanford University, Palo Alto, CA
Laboratory of Ron R. Kopito
Characterization and transport of an aggresome substrate
- 1999 BS, Biochemistry and Molecular Biology, University of California,
Santa Cruz, CA
Laboratory of Anthony Fink
*The role of DnaJ in the DnaK reaction cycle: initial chaperone for
a permanently unfolded polypeptide substrate*

TEACHING AND MENTORING

Teaching

- 2018-2019 Course manager, Optical Microscopy and Imaging in Biomedical Sciences,
Marine Biology Laboratory, Woods Hole, MA
- 2014-2017 Teaching Assistant, Optical Microscopy and Imaging in Biomedical
Sciences, Marine Biology Laboratory, Woods Hole, MA
- 2013, 15, 17 Instructor and Teaching Assistant, O'Brien Intravital Microscopy Course,
Indiana University School of Medicine, Indianapolis, IN
- 2003, 2006 Teaching Assistant, Biology, Stanford University, Stanford, CA

Mentoring

- 2019 Medical student, Indiana University
- 2018 Research intern, Indiana University

O'Brien Center intern, Indiana University
2017 O'Brien Center intern, Indiana University
2005 Rotation student, Stanford University

INVITED SPEAKER

2019 HubMAP symposium, Common Coordinate Framework Workshop, Indiana University, Bloomington, IN

2017 Department of Cellular and Integrative Physiology, Indiana University School of Medicine, Indianapolis, IN

2017 Regenerative Medicine Seminar, Vascular and Cardiac Adult Stem Cell Therapy Center, Indiana University School of Medicine, Indianapolis, IN

2015 Pathology Grand Rounds, Indiana University Health, Indianapolis, IN

AWARDS

2018 Stier Award for Research Excellence, Department of Cellular and Integrative Physiology, Indiana University School of Medicine

2018, 2020 Opportunity Pool Travel Grant, Kidney Precision Medicine Project, NIDDK/NIH.

1999 Academic Honors for Undergraduate Thesis, University of California, Santa Cruz, CA

PUBLICATIONS

In-press

* Co-first authorship.

1. A Precision Medicine Approach Uncovers a Unique Signature of Neutrophils in Patients With Brushite Kidney Stones. Makki MS, **Winfree S**, Lingeman JE, Witzmann FA, Worcester EM, Krambeck AE, Coe FL, Evan AP, Bledsoe S, Bergsland KJ, Khochare S, Barwinska D, Williams JC Jr, El-Achkar TM. *Kidney Int Rep.* 2020 Feb 20;5(5):663-677. doi: 10.1016/j.ekir.2020.02.1025. eCollection 2020 May.
2. Circulating uromodulin inhibits systemic oxidative stress by inactivating the TRPM2 channel. LaFavers KA, Macedo E, Garimella PS, Lima C, Khan S, Myslinski J, McClintick J, Witzmann FA, **Winfree S**, Phillips CL, Hato T, Dagher PC, Wu XR, El-Achkar TM, Micanovic R. *Sci Transl Med.* 2019 Oct 2;11(512):eaaw3639. doi: 10.1126/scitranslmed.aaw3639.
3. Clendenon SG, Fu X, Von Hoene RA, Clendenon JL, Sluka JP, **Winfree S**, Mang H, Martinez M, Filson AJ, Klaunig JE, Glazier JA, Dunn KW. 2019. A simple automated method for continuous fieldwise measurement of microvascular hemodynamics. *Microvasc Res.* May;123:7-13. doi: 10.1016/j.mvr.2018.11.010. Epub 2018 Nov 28.
4. Brandt SL, Wang S, DeJani NN, Klopfenstein N, **Winfree S**, Filgueiras L, McCarthy BP, Territo PR, Serezani CH. 2018. Excessive localized leukotriene B4 levels dictate poor skin host defense in diabetic mice. *JCI Insight.* Sep 6;3(17).pii: 120220. doi: 10.1172/jci.insight.120220.

5. Brandt SL, Klopfenstein N, Wang S, **Winfree S**, McCarthy BP, Territo PR, Miller L, Serezani CH. 2018. Macrophage-derived LTB4 promotes abscess formation and clearance of *Staphylococcus aureus* skin infection in mice. *PLoS Pathog.* Aug13;14(8):e1007244. doi: 10.1371/journal.ppat.1007244.
6. Swallow EA, Aref MW, Chen N, Byiringiro I, Hammond MA, McCarthy BP, Territo PR, Kamocka MM, **Winfree S**, Dunn KW, Moe SM, Allen MR. 2018. Skeletal accumulation of fluorescently tagged zoledronate is higher in animals with early stage chronic kidney disease. *Osteoporos Int.* Sep;29(9):2139-2146. doi: 10.1007/s00198-018-4589-3.
7. **Winfree S**, Dagher PC, Dunn KW, Eadon MT, Ferkowicz M, Barwinska D, Kelly KJ, Sutton TA, El-Achkar TM. 2018. Quantitative Large-Scale Three-Dimensional Imaging of Human Kidney Biopsies: A Bridge to Precision Medicine in Kidney Disease. *Nephron.* 140(2):134-139. doi: 10.1159/000490006.
8. Hato T, **Winfree S**, Dagher PC. 2018. Kidney Imaging: Intravital Microscopy. *Methods Mol Biol.* 1763:129-136. doi: 10.1007/978-1-4939-7762-8_12.
9. Varberg KM, **Winfree S**, Dunn KW, Haneline LS. 2018. Kinetic Analysis of Vasculogenesis Quantifies Dynamics of Vasculogenesis and Angiogenesis *In Vitro*. *J Vis Exp.* Jan 31;(131). doi: 10.3791/57044.
10. Kolb AL, Corridon PR, Zhang S, Xu W, Witzmann FA, Collett JA, Rhodes GJ, **Winfree S**, Bready D, Pfeffenberger ZJ, Pomerantz JM, Hato T, Nagami GT, Molitoris BA, Basile DP, Atkinson SJ, Bacallao RL. 2018. Exogenous Gene Transmission of Isocitrate

Dehydrogenase 2 Mimics Ischemic Preconditioning Protection. *J Am Soc Nephrol.* Apr;29(4):1154-1164. doi: 10.1681/ASN.2017060675.

11. Micanovic R, Khan S, Janosevic D, Lee ME, Hato T, Srour EF, **Winfree S**, Ghosh J, Tong Y, Rice SE, Dagher PC, Wu XR, El-Achkar TM. 2018. Tamm-Horsfall Protein Regulates Mononuclear Phagocytes in the Kidney. *J Am Soc Nephrol.* Mar;29(3):841-856. doi: 10.1681/ASN.2017040409.

12. **Winfree S**, Gilk SD. 2017. Quantitative Dextran Trafficking to the *Coxiella burnetii* Parasitophorous Vacuole. *Curr Protoc Microbiol.* Aug 11;46:6C.2.1-6C.2.12. doi: 10.1002/cpmc.34.

13. **Winfree S**, Ferkowicz MJ, Dagher PC, Kelly KJ, Eadon MT, Sutton TA, Markel TA, Yoder MC, Dunn KW, El-Achkar TM. 2017. Large-scale 3-dimensional quantitative imaging of tissues: state-of-the-art and translational implications. *Transl Res.* Nov;189:1-12. doi: 10.1016/j.trsl.2017.07.006. Epub 2017 Jul 22.

14. **Winfree S**, Hato T, Day RN. 2017. Intravital microscopy of biosensor activities and intrinsic metabolic states. *Methods.* Sep 1;128:95-104. doi: 10.1016/j.ymeth.2017.04.017.

15. Hato T, **Winfree S**, Dagher PC. 2017. Intravital imaging of the kidney. *Methods.* Sep 1;128:33-39. doi: 10.1016/j.ymeth.2017.03.024. Epub 2017 Apr 12.

16. Hato T, **Winfree S***, Day R, Sandoval RM, Molitoris BA, Yoder MC, Wiggins RC, Zheng Y, Dunn KW, Dagher PC. 2017. Two-Photon Intravital Fluorescence Lifetime

Imaging of the Kidney Reveals Cell-Type Specific Metabolic Signatures. *J Am Soc Nephrol*. 2017 Aug;28(8):2420-2430. doi: 10.1681/ASN.2016101153.

17. Mulye M, Samanta D, **Winfree S**, Heinzen RA, Gilk SD. Elevated Cholesterol in the *Coxiella burnetii* Intracellular Niche Is Bacteriolytic. 2017. *MBio*. Feb 28;8(1). pii: e02313-16. doi: 10.1128/mBio.02313-16.

18. **Winfree S**, Khan S, Micanovic R, Eadon MT, Kelly KJ, Sutton TA, Phillips CL, Dunn KW, El-Achkar TM. 2017. Quantitative Three-Dimensional Tissue Cytometry to Study Kidney Tissue and Resident Immune Cells. *J Am Soc Nephrol*. Jul;28(7):2108-2118. doi: 10.1681/ASN.2016091027.

19. Varberg KM, **Winfree S**, Chu C, Tu W, Blue EK, Gohn CR, Dunn KW, Haneline LS. 2017. Kinetic analyses of vasculogenesis inform mechanistic studies. *Am J Physiol Cell Physiol*. Apr 1;312(4):C446-C458. doi: 10.1152/ajpcell.00367.2016.

20. Hato T, **Winfree S**, Kalakeche R, Dube S, Kumar R, Yoshimoto M, Plotkin Z, Dagher PC. 2015. The macrophage mediates the renoprotective effects of endotoxin preconditioning. *J Am Soc Nephrol*. Jun;26(6):1347-62. doi: 10.1681/ASN.2014060561.

21. Banga A, Flaig S, Lewis S, **Winfree S**, Blazer-Yost BL. 2014. Epinephrine stimulation of anion secretion in the Calu-3 serous cell model. *Am J Physiol Lung Cell Mol Physiol*. May 15;306(10):L937-46. doi: 10.1152/ajplung.00190.2013.

22. Spinner JL, **Winfree S**, Starr T, Shannon JG, Nair V, Steele-Mortimer O, Hinnebusch BJ. 2014. *Yersinia pestis* survival and replication within human neutrophil

phagosomes and uptake of infected neutrophils by macrophages. *J Leukoc Biol.* Mar;95(3):389-98. doi: 10.1189/jlb.1112551.

23. Jolly C, **Winfree S**, Hansen B, Steele-Mortimer O. 2014. The Annexin A2/p11 complex is required for efficient invasion of *Salmonella Typhimurium* in epithelial cells. *Cell Microbiol.* Jan;16(1):64-77. doi: 10.1111/cmi.12180.

24. Malik-Kale P, **Winfree S***, Steele-Mortimer O. 2012. The bimodal lifestyle of intracellular *Salmonella* in epithelial cells: replication in the cytosol obscures defects in vacuolar replication. *PLoS One.* 7(6):e38732. doi: 10.1371/journal.pone.0038732.

25. Cooper KG, **Winfree S**, Malik-Kale P, Jolly C, Ireland R, Knodler LA, Steele-Mortimer O. 2011. Activation of Akt by the bacterial inositol phosphatase, SopB, is wortmannin insensitive. *PLoS One.* 6(7):e22260. doi: 10.1371/journal.pone.0022260.

26. Malik-Kale P, Jolly CE, Lathrop S, **Winfree S**, Luterbach C, Steele-Mortimer O. 2011. Salmonella - at home in the host cell. *Front Microbiol.* Jun 3;2:125. doi: 10.3389/fmicb.2011.00125.

27. Knodler LA, Vallance BA, Celli J, **Winfree S**, Hansen B, Montero M, Steele-Mortimer O. 2010. Dissemination of invasive Salmonella via bacterial-induced extrusion of mucosal epithelia. *Proc Natl Acad Sci U S A.* Oct 12;107(41):17733-8. doi: 10.1073/pnas.1006098107.

28. Howe D, Shannon JG, **Winfree S**, Dorward DW, Heinzen RA. 2010. *Coxiella burnetii* phase I and II variants replicate with similar kinetics in degradative

phagolysosome-like compartments of human macrophages. *Infect Immun.* Aug;78(8):3465-74. doi: 10.1128/IAI.00406-10. Epub 2010 Jun 1.

29. Knodler LA, **Winfree S**, Drecktrah D, Ireland R, Steele-Mortimer O. 2009. Ubiquitination of the bacterial inositol phosphatase, SopB, regulates its biological activity at the plasma membrane. *Cell Microbiol.* Nov;11(11):1652-70. doi: 10.1111/j.1462-5822.2009.01356.x.

30. Drecktrah D, Levine-Wilkinson S, Dam T, **Winfree S**, Knodler LA, Schroer TA, Steele-Mortimer O. 2008. Dynamic behavior of *Salmonella*-induced membrane tubules in epithelial cells. *Traffic.* Dec;9(12):2117-29. doi: 10.1111/j.1600-0854.2008.00830.x.

Submitted and in preparation

* Co-first author

† Corresponding author

Andre Woloshuk, Suraj Khochare, Aljohara Fahad Almulhim, Andrew McNutt, Dawson Dean, Daria Barwinska, Michael Ferkowicz, Michael T. Eadon, Katherine J. Kelly, Kenneth W. Dunn, Mohammad A. Hasan, Tarek M. El-Achkar, **Seth Winfree†**, In situ classification of cell types in human kidney tissue using 3D nuclear staining, doi: <https://doi.org/10.1101/2020.06.24.167726> (Biorxiv)

Seth Winfree, James E. Lingeman, Frank Witzmann, Elaine M. Worcester, Amy Krambeck, Fred Coe, Sharon Bledsoe, Kristin Bergsland, James C. Williams, Jr. and Tarek M. El-Achkar, Multimodal imaging reveals a unique autofluorescence signature of Randall's plaque. (Submitted)

Andrew McNutt, Tyler Boogard, Mike Ferkowicz, Tarek M. El-Achkar, **Seth Winfree†**.
Analysis of mesoscale confocal images with supervised and unsupervised 3D cytometry.
(In preparation)

Michael J. Ferkowicz, **Seth Winfree***, Kenneth W. Dunn, Daria Barwinska, Michael Eadon, Pierre Dagher, Tarek M. El-Achkar. Multimodal imaging of human kidney tissue for the Kidney Precision Medicine Project. (Submitted)